NASA Contractor Report 172386

Active Attenuation of Propeller Blade Passage Noise

J. M. Zalas and J. Tichy

Lord Corporation
2000 West Grandview Blvd.
Erie, PA 16514-0038

Contract NAS1-17231
July 1984

National Aeronautics and
Space Administration

Langley Research Center
Hampton, Virginia 23665

TABLE OF CONTENTS

LIST OF FIGURES

SUMMARY

Acoustic measurements are presented to show that active cancellation can be used to achieve significant reduction of blade passage noise in a turboprop cabin. Simultaneous suppression of all blade passage frequencies was attained. The spatial volume over which cancellation occurred, however, is limited. Acoustic intensity maps are presented to show that the acoustic input to the fuselage was sufficiently non-localized so as to require more judicious selection of cancellation speaker location.

INTRODUCTION

The Turboprop Noise Problem

It is anticipated that propeller blade passage noise will be a significant source of interior cabin noise on advanced high-speed turboprop aircraft (Reference 1). With a goal of minimizing these tonal noise components, an active noise cancellation system was used to cancel blade passage spectra below 500 Hz in two different conventional twin engine turboprop aircraft. The interior sound level spectra of these two aircraft are shown in Figures 1 through 3.

Active Noise Cancellation

In this report, the phrase "Active Noise Cancellation" connotes a noise reduction achieved through alteration of the radiation impedance of critical source surfaces thereby reducing the total energy flux into a space. For example, if a cancellation loudspeaker is placed near a compact "monopole" source, a dipole source will be created. The total radiated acoustic power of the dipole will be less than that of the original monopole. The conditions necessary to produce a dipole are that the cancellation speaker be very close to the monopole source, equal in magnitude and 180 degrees out of phase with it.

Advantages of Active Noise Cancellation

Active cancellation has three potential advantages over conventional means for controlling turboprop blade passage noise:

1. Active control works best at low frequencies where passive controls are least effective.

2. Active control requires no aircraft structural design changes.

3. Active control minimizes the weight penalty for noise reduction.

For these reasons, active cancellation appears an attractive alternative to conventional noise control techniques.

DETAILED DISCUSSION OF ACTIVE CANCELLATION

Active noise cancellation involves two primary and necessary tasks:

1. The offending sound source myst be adequately reproduced by a loudspeaker system.

2. A 180 degree phase reversed sound field must be properly distributed at appropriate levels.

In this study, our emphasis was on the second task above. Our goal was to show that active controls could be used to achieve noise reduction at a point in the offending sound field. If this was successful, future work would be done to complete the first task.

The active cancellation system has five major components:

1. Input Sensor
2. Controller
3. Amplifier
4. Loudspeaker
5. Error Sensor

These elements are schematically shown in Figure 4.

The input sensor sends information on the offending noise to the controller. The input sensors investigated in this study were: (1) a synchrophasor signal from the engines, (2) an accelerometer signal from the fuselage wall, (3) an interior microphone signal, and (4) an exterior microphone signal. The controller processes the input signal using a modified Widrow-Hoff Algorithm described in detail in Reference 2. The initial output of the controller is a first estimate of a 180 degree phase reversed cancellation signal. This signal is sent through the amplifier to the loudspeakers. An error sensor, usually a microphone located in the mixed sound field, sends a signal proportional to the residual noise back to the controller. Ideally, the error would be zero, indicating perfect cancellation. In practice, a non-zero error signal is used by the controller to modify the cancellation signal such that the error signal is minimized.

It must be noted here that a zero or minimum error signal only means that cancellation has occurred at the position of the error sensor. Cancellation need not occur at other positions in the volume where cancellation is desired. The key to noise reduction over an extended spatial volume lies in our ability to reproduce the offending sound field with a loudspeaker array. If a sound field can be reproduced, then the active cancellation system can be used to reproduce the sound field 180 degree phase reversed.

There are certain conditions, however, in which reproduction of a sound field would be relatively simple. If a sound source were small relative to its wavelength and approximately the same size as the loud-

speaker to be used, we can say that the sound source is "compact". For such a compact source, one would ideally superimpose a cancellation speaker on the sound source, or, in practice, place the loudspeaker as close as possible to the sound source.

For this study, we made the assumption that the blade passage noise input to the fuselage was localized in the plane of the propeller. If this assumption is valid, then one loudspeaker on each side of the aircraft should be adequate for broad area cancellation. The validity of this assumption, however, would not affect the broad frequency cancellation studies.

EXPERIMENTAL STUDY

Research Goals

The ultimate goal of active noise cancellation for turboprop aircraft is composed of two subgoals:

1. Obtain broad frequency cancellation of propeller blade passage noise.

2. Obtain broad area cancellation of the propeller blade passage noise in the turboprop cabin.

The work reported here was primarily concerned with subgoal (1), broad frequency cancellation. The questions we wanted to answer are:

1. Can active cancellation give broad frequency cancellation of propeller blade passage noise?

2. Which input signals give the best cancellation performance?

3. Over what area does cancellation occur?

4. Is our assumption of compact noise input valid?

The Experimental Set-Up

Three different aircraft were used in this study. They were all modern, high performance, twin-engine turboprop aircraft with pressurized cabins. Planes A and C were Fairchild Metro Aircraft while plane B was a Gulfstream Commander. Planes A and B were "green", that is, they had no interior seats or trim. Plane C was fully outfitted with seats and trim. All planes were operated at approximate cruise conditions with either left engine on, right engine on, or both engines on. When both engines were on, the synchrophasing system was activated under normal operating conditions.

All signals were recorded on a Racal Store 4D FM tape recorder. Interior sound pressure levels were measured with Bruel and Kjaer Type 4165 condenser microphones powered by a Bruel and Kjaer power supply, Type 2804. Frequency spectra were obtained with a Nicolet 660B FFT analyzer.

The cancellation loudspeaker had a 30.5 cm diameter contained in a volume of approximately 0.03 m^3. All equipment was powered from a sine-wave inverter.

Acoustic intensity was measured with a two microphone probe, the microphone separation being 152 mm. Actual acoustic intensity was calculated from the imaginary part of the cross spectrum obtained from the two probe microphones.

EXPERIMENTAL RESULTS

Preliminary Measurements

To assure ourselves that the cabin interior acoustic environment did not significantly vary during various test conditions, loudspeakers and microphones were located at various placed in the cabin of aircraft A. A white noise generator was used to drive the loudspeakers. Transfer functions between speaker-microphone pairs were measured with the FFT analyzer with aircraft A on the ground (engines off) and inflight, cabin pressurized. It was found that the ground transfer functions were very nearly identical to the inflight transfer functions. From these results, it was concluded that the cabin interior was "acoustically constant" over the range of test conditions to be encountered.

Broad Frequency Cancellation

Our goal here was to assess our ability to cancel each blade passage frequency below 500 Hz, both separately and then simultaneously. This was accomplished by means of a signal generator triggered by a synchrophasor signal from the left engine on plane B. The right engine was not operating during these tests.

For this series of tests, all but one blade passage frequency were suppressed by the generator. The remaining single blade passage signal was then input to the controller. Figures 5 through 10 show that the cancellation system was able to attenuate each blade passage

frequency by at least 7 dB. Next, all suppression on the generator was removed and the signal shown in Figure 11 input to the controller. The results shown in Figure 12 indicate a simultaneous reduction of at least 10 dB for the first six blade passage frequencies.

Optimum Input Signal

Having demonstrated that the cancellation system could achieve broad frequency cancellation at a point in space (error microphone position), we next proceeded to evaluate various input signals other than the synchrophasor signal:

1. Interior microphone
2. Accelerometer attached to fuselage wall
3. Exterior microphone

For these tests, the controller operated on all frequencies simultaneously.

Interior Microphone Input

The input microphone was mounted 5 cm from the fuselage, in the plane of the left propeller, at the vertical point of closest propeller approach. Only the left engine was on. An acoustic enclosure was used to separate the interior sound field from the sound incident from the fuselage. This enclosure prevented the cancellation system from interacting with itself. For example, without the enclosure, increasing cancellation would result in decreasing input signal to the controller.

Figure 13 shows the signal input to the controller from the interior microphone. Note that the second and third blade passage frequencies are considerably higher than the other harmonics. Figure 14 shows the resultant noise reduction. Note that significant cancellation was attained only at the second and third blade passage frequencies, where the input signal was highest.

Accelerometer Input

The accelerometer was attached to the fuselage in the plane of the left propeller, at the point of closest propeller approach. The accelerometer signal, shown in Figure 15, indicates that the third and fourth blade passage frequencies are dominant. Figure 16 shows the resultant cancellation. As with the interior microphone case, it appears that the best cancellation occurs shere the input signal is highest.

Exterior Microphone

Finally, a GenRad Model 1971-9605 ceramic microphone was mounted exterior to the left side of the fuselage. The microphone, protected with an aluminum nose cone, was bolted to the fuselage approximately 15 cm aft of the propeller plane along the line of closest propeller approach. The signal input to the controller is shown in Figure 17 with the resultant cancellation in Figure 18. Note the dramatic cancellation attained.

Discussion of Broad Frequency Results

Without doubt, the exterior microphone input gave the best overall noise reduction. Second in performance was the synchrophasor input. The interior microphone and accelerometer inputs were least effective. It is thought that the poor performance of the latter two inputs is related to the large amplitudes of two blade passage frequencies relative to the other harmonics. It appears that the controller cencentrates on the higher amplitude components of the input spectrum.

CANCELLATION AREA

Measured Results

For these measurements, the cancellation system was set up using the left synchrophasor signal of plane C with only the left engine on. The left wall of the fuselage was marked off in a 30.5 cm by 30.5 cm square grid. The horizontal grid positions were numbered sequentially with the plane of the propeller designated zero. Increasing positive numbers refer to positions aft of the prop plane. In the vertical direction, the grid is labeled alphabetically. The floor position is designated A, with the next vertical grid point B, etc.

The cancellation loudspeaker was placed at position 0-A and oriented upward. The error sensor was located half-way between 0-C and 0-D. Another microphone was moved to each grid point and the sound pressure level tape recorded with the canceller on and off. The data was later analyzed using an FFT analyzer to determine the sound levels at the blade passage frequencies. The results in Figure 19 show the difference in sound level with the canceller on versus canceller off for each blade passage frequency. Because of the loudspeaker, no data was taken at position 0-A.

In Figure 19, negative values indicate cancellation and positive values indicate amplification. Note that cancellation falls off rapidly as one moves away from the error sensor location. In addition, the pattern of cancellation varies considerably with blade passage frequency.

Validity of Compact Source Assumption

The limited area over which significant cancellation was obtained suggests that our assumption of localized noise input to the fuselage is questionable. To test this assumption, acoustic intensity maps of the fuselage walls were measured on the aircraft in flight. Figures 20 through 43 show the results of these measurements on aircraft B. In these figures, the horizontal grid points are numbered, with zero being the plane of the propeller. Each horizontal or vertical increment is 30.5 cm in length. Positive numbers refer to positions aft of the prop plane while negative numbers refer to positions forward of the prop plane. Vertical positions are labeled alphabetically, with the floor designated position A.

The two-microphone cross spectral method was used to measure the acoustic intensity vector at each grid point. (References 3-6). All intensity vectors are perpendicular to the fuselage walls. Positive intensity refers to vectors directed to the interior of the fuselage and negative intensity refers to vectors directed to the exterior of the fuselage.

Figures 20 through 31 present data taken when both engines were on. The dark areas of the Figures denote areas having acoustic intensities within the range specified on each figure. The specified ranges are those having the highest measured levels. Figures 32 through 37 give measured intensity levels on the left side of the aircraft with only the left engine on. Finally, Figures 38 through 43 present right side levels with only the right engine on.

Discussion of Intensity Spectra

In general, the data suggests that the acoustic inputs to the fuselage are at best "semi-compact". For most of the cancellation measurements, the cancellation speakers were at position zero (prop plane) and sitting on the floor (position A). The cancellation data shows that this is not always the best speaker location and, in addition, more than one cancellation speaker may be required in some cases. In view of these findings, it is not surprising that our cancellation occurred only over limited areas.

The Effect of Cancellation on Intensity

Figures 44 through 53 show the effects of active cancellation on the acoustic intensity. The intensity measurements were made on the left side of aircraft C with the left engine only on. The cancellation speaker was at location 0-A, while the error microphone was located

half way between positions 0-C and 0-D. For each grid point, acoustic intensity was measured with the cancellation system off and then with the system on.

It is interesting to note that, in Figures 44 through 47, the cancellation system produced the effect of reversing the direction of the acoustic intensity. At higher frequencies, Figures 48 through 53, this was not the case.

Figure 44, the 0-500 Hz case, is very similar to Figure 46, the 100 Hz case. Hence the overall data seems dominated by the 100 Hz blade passage harmonic. If we define a compact source as one whose dimensions do not exceed a quarter wavelength, the radiating area in Figure 46 (positive intensity) is close to "compact" ($\lambda/4$ = 82 cm). Similar results occur for higher frequencies.

In the case of Figure 46, the speaker was located close to the center of the radiating source, while this was less true for higher frequencies.

CONCLUSIONS

The results of this study show that active cancellation can be used to attain a 7-15 dB reduction of blade passage noise in a turbo-prop cabin. The spatial extent over which cancellation occurs, using one cancellation speaker, was usually less than a quarter wavelength around the error sensor. Acoustic intensity measurements suggest that the primary reason for the limited spatial cancellation is that the acoustic inputs from the fuselage were not as anticipated. While the radiating surfaces for each blade passage frequency are close to being adequately compact, their number and location on the fuselage vary with frequency. In light of this information, the key to broad spatial cancellation lies in proper cancellation speaker placement. Work is currently under way to determine and evaluate loudspeaker placement.

REFERENCES

1. Mixon, J.S. et al., "Interior Noise Considerations for Advanced High-Speed Turboprop Aircraft," J. Aircraft, Vol. 20, No. 9, Sept. 1983, pp. 791-97.

2. Poole, Lynn A. et al., "The Implementation of Digital Filters Using a Modified Widrow-Hoff Algorithm for the Adaptive Cancellation of Acoustic Noise," Proceedings of IEEE International Conference on Acoustics, Speech, and Signal Processing, March 19-21, 1984, pp. 21.7.1 - 21.7.4.

3. Krishnappa, G., "Cross-Spectral Method of Measuring Acoustic Intensity by Correcting Phase and Gain Errors by Microphone Calibration", J. Acoust. Soc. Am., 69 (1), Jan. 1981, pp 307-310.

4. Pascal, J. C., and Carles, C., "Systematic Measurement Errors With Two Microphone Sound Intensity Meters," J. Sound Vib., 83 (1), 1982, pp. 53-65.

5. Gadg, S., "Sound Intensity," Bruel and Kjaer Technical Review, No. 3, 1982, pp 3-39.

6. Fahy, F., "Measurement of Acoustic Intensity Using the Cross Spectral Density of Two Microphone Signals," J. Acoust. Soc. Am., 62 (4), 1977, pp. 1057-59.

7. D'Azzo, John J., and Houpis, Constantine H., "Feedback Control System Analysis and Synthesis," McGraw-Hill, New York, 1966.

8. Pope, L.D., Wilis, C. M., Mayes, W. H., "Aircraft Interior Noise Models: Sidewall Trim, Stiffened Structures and Cabin Acoustics with Floor Partition," Journal of Sound and Vibration 89 (1983), pp. 371-417.

9. Morse, Philip M. and Ingard, K. Uno, "Theoretical Acoustics, McGraw-Hill, New York, 1968.

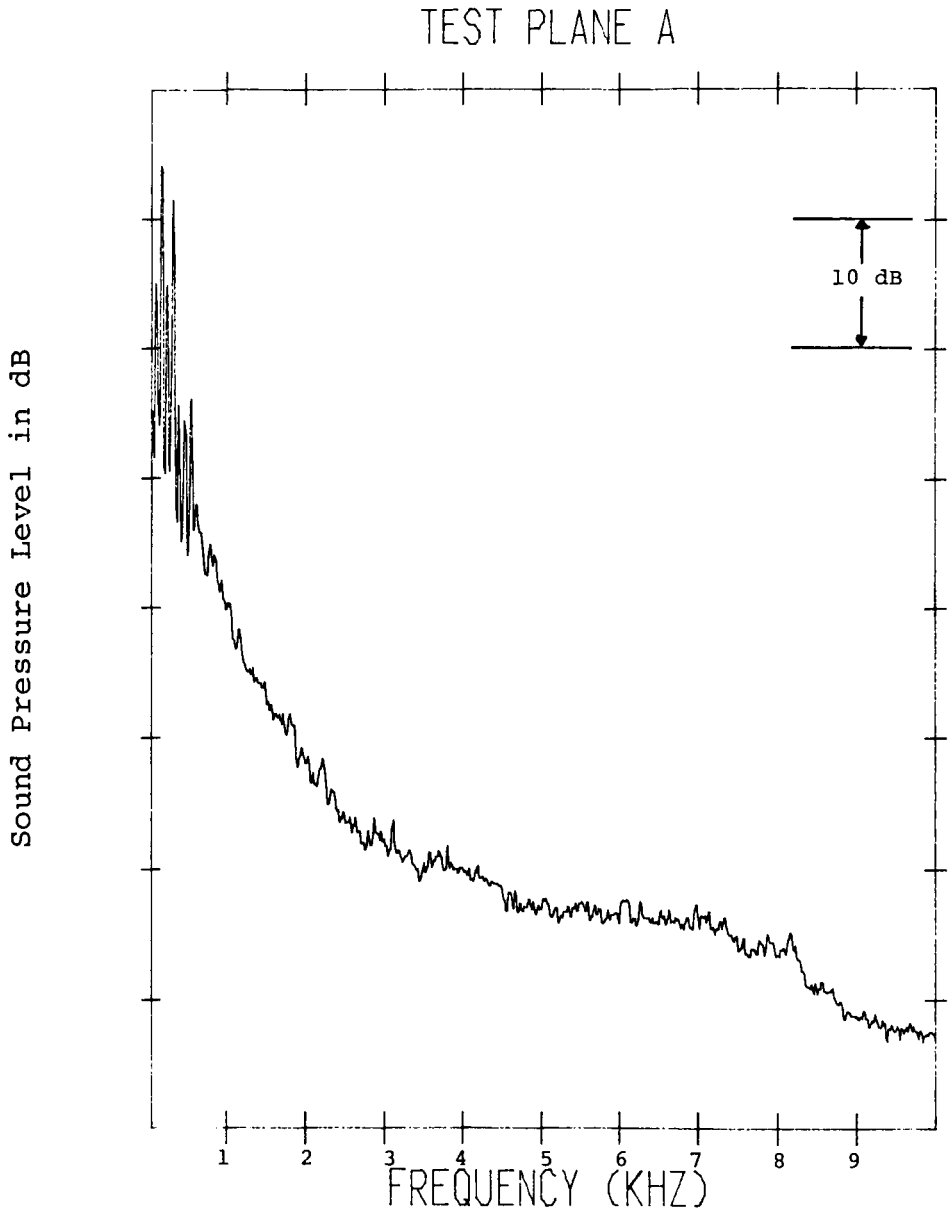
TEST PLANE A
10 dB
Sound Pressure Level in dB
1
2
3
4
5
6
7
8
9
FREQUENCY (KHZ)

Figure 1

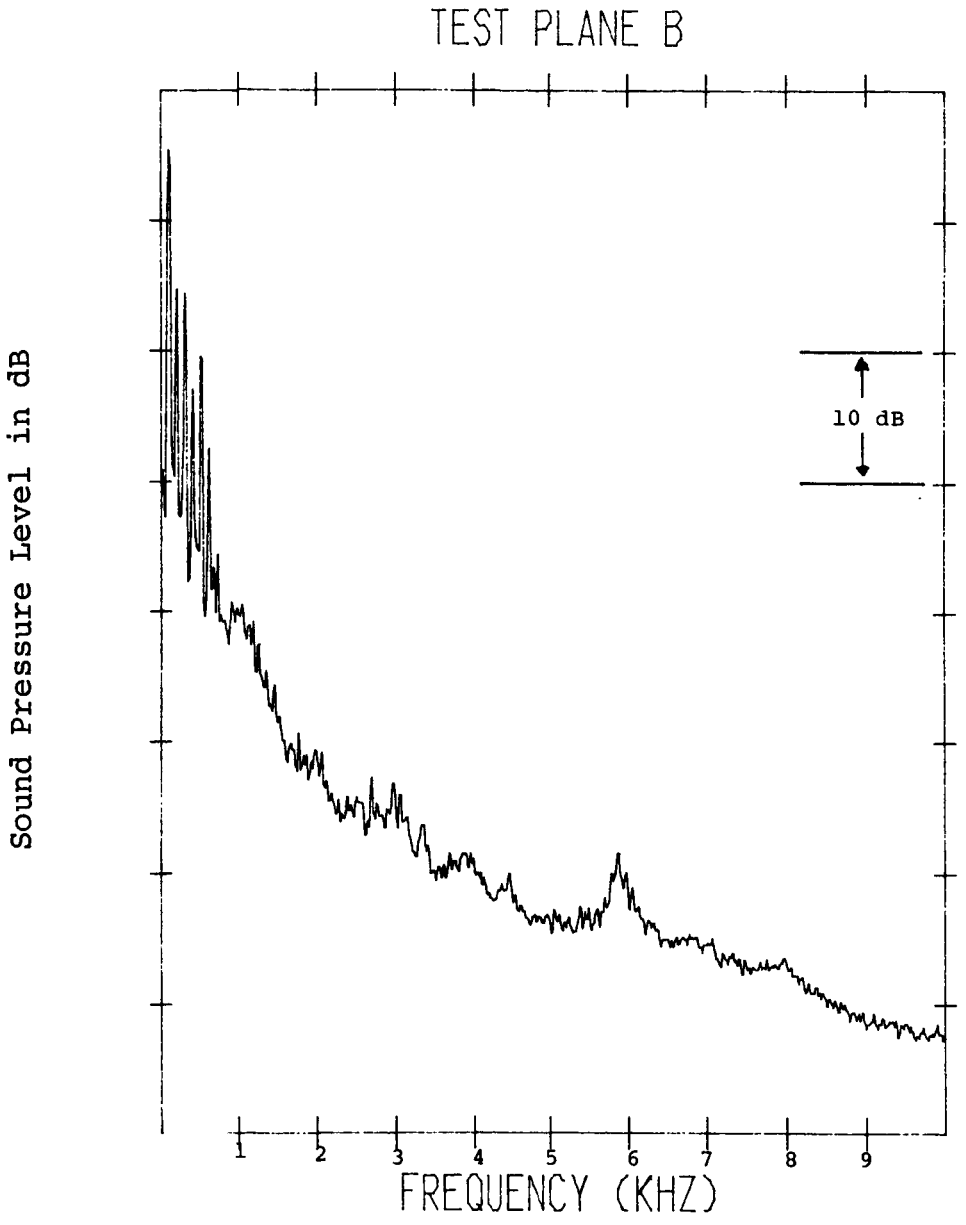
TEST PLANE B
Sound Pressure Level in dB
10 dB
1
2
3
4
5
6
7
8
9
FREQUENCY (KHZ)

Figure 2

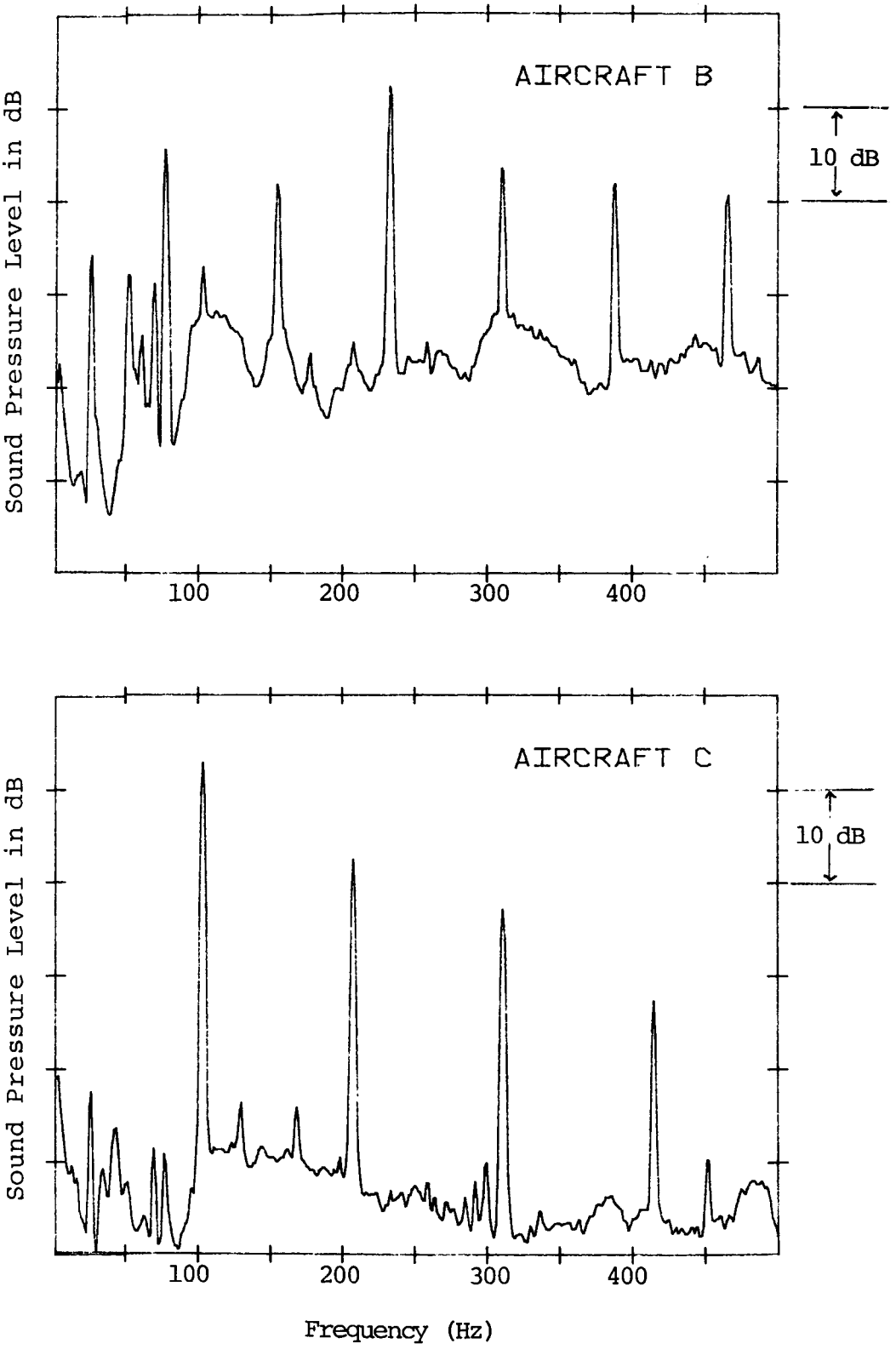

Figure 3: Interior Sound Pressure Level Spectra

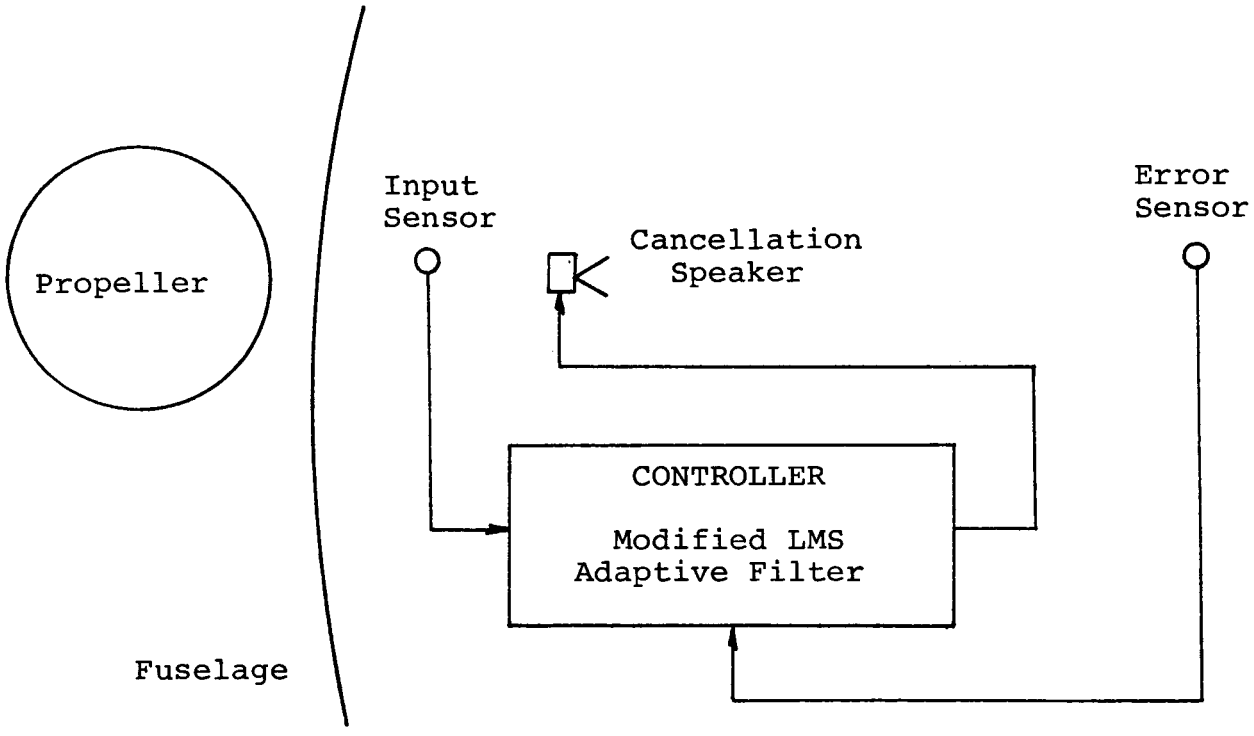

Figure 4: Active Cancellation System

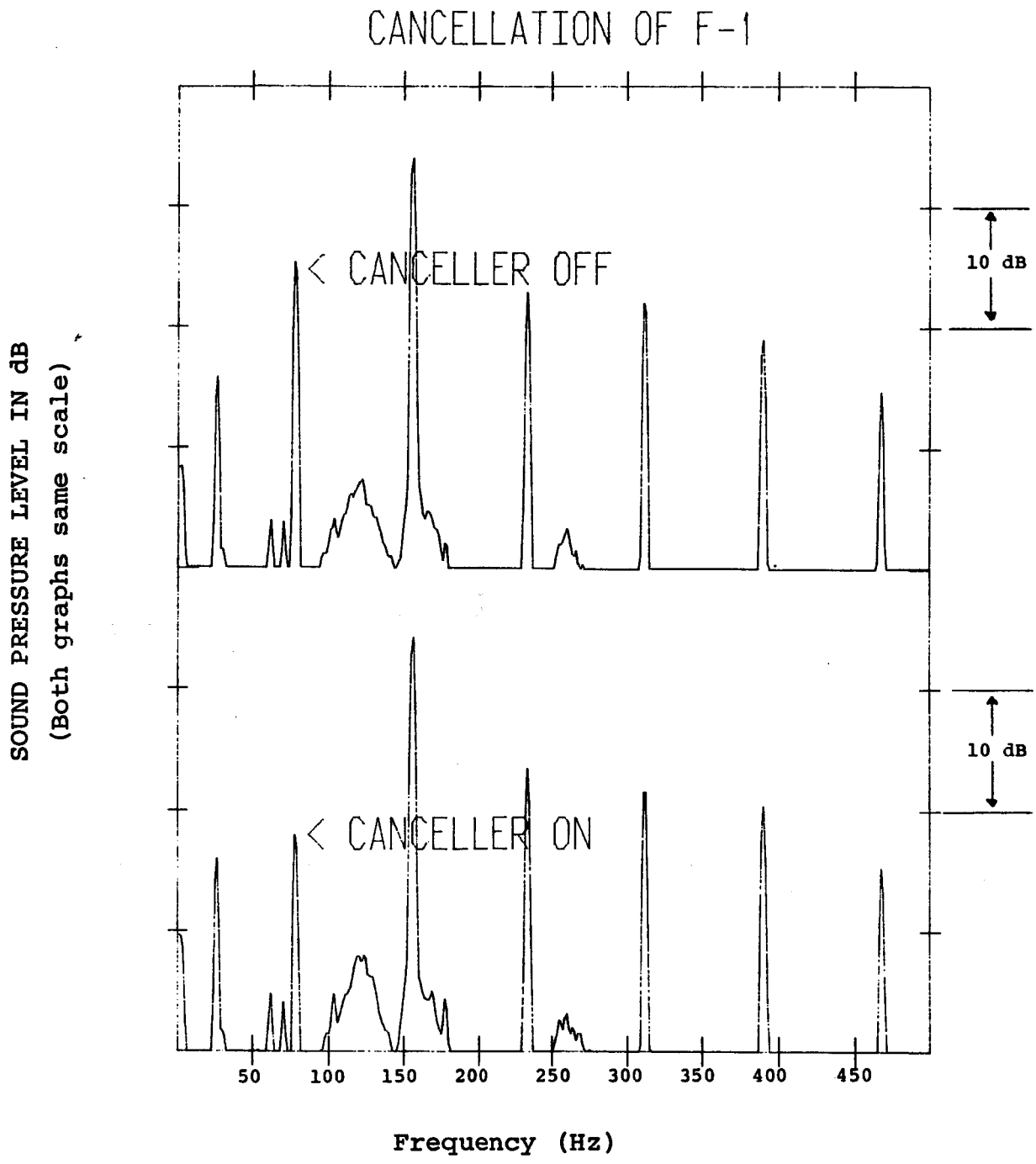

Figure 5: Cancellation of Fundamental Frequency

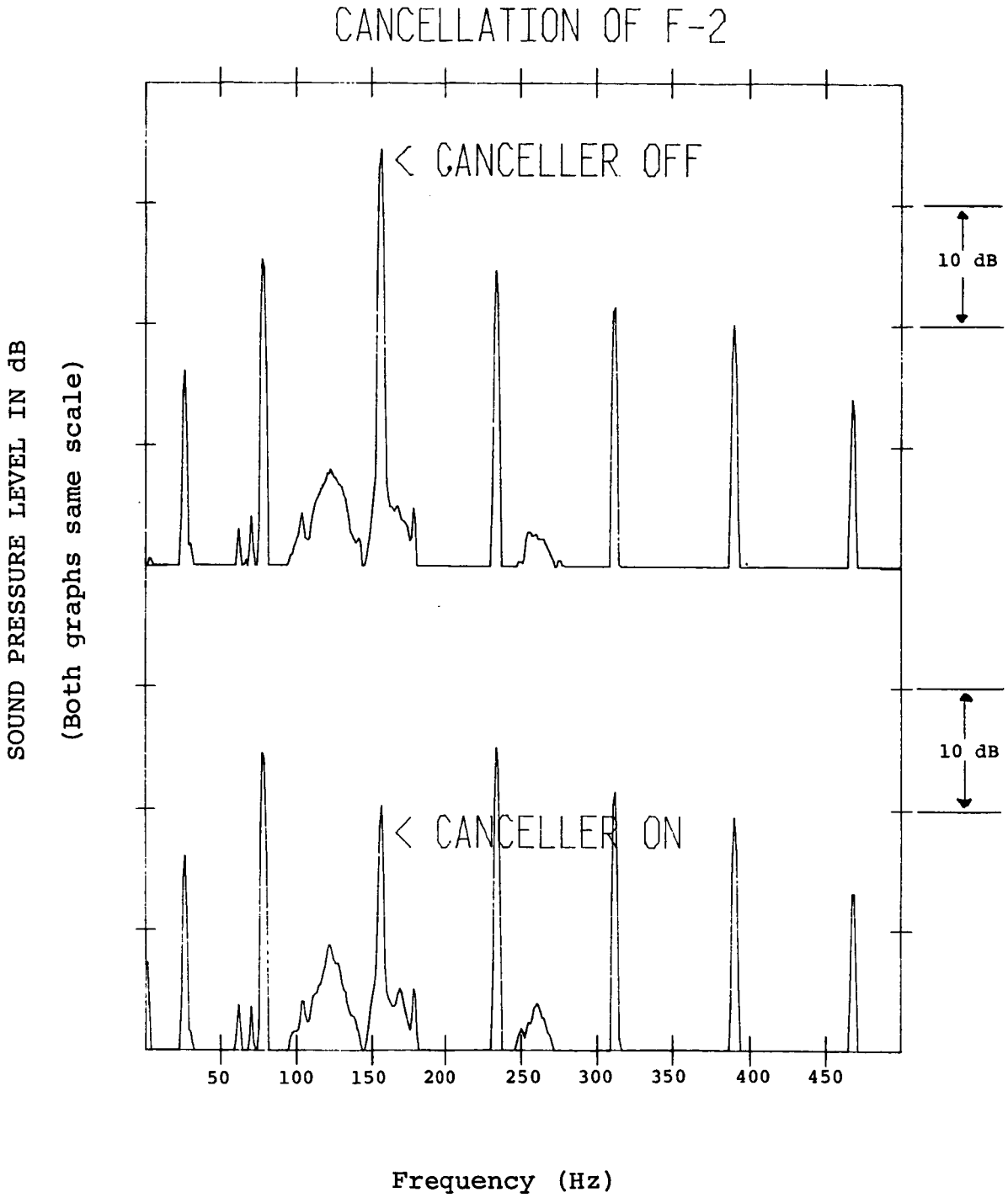

Figure 6: Cancellation of Second Harmonic

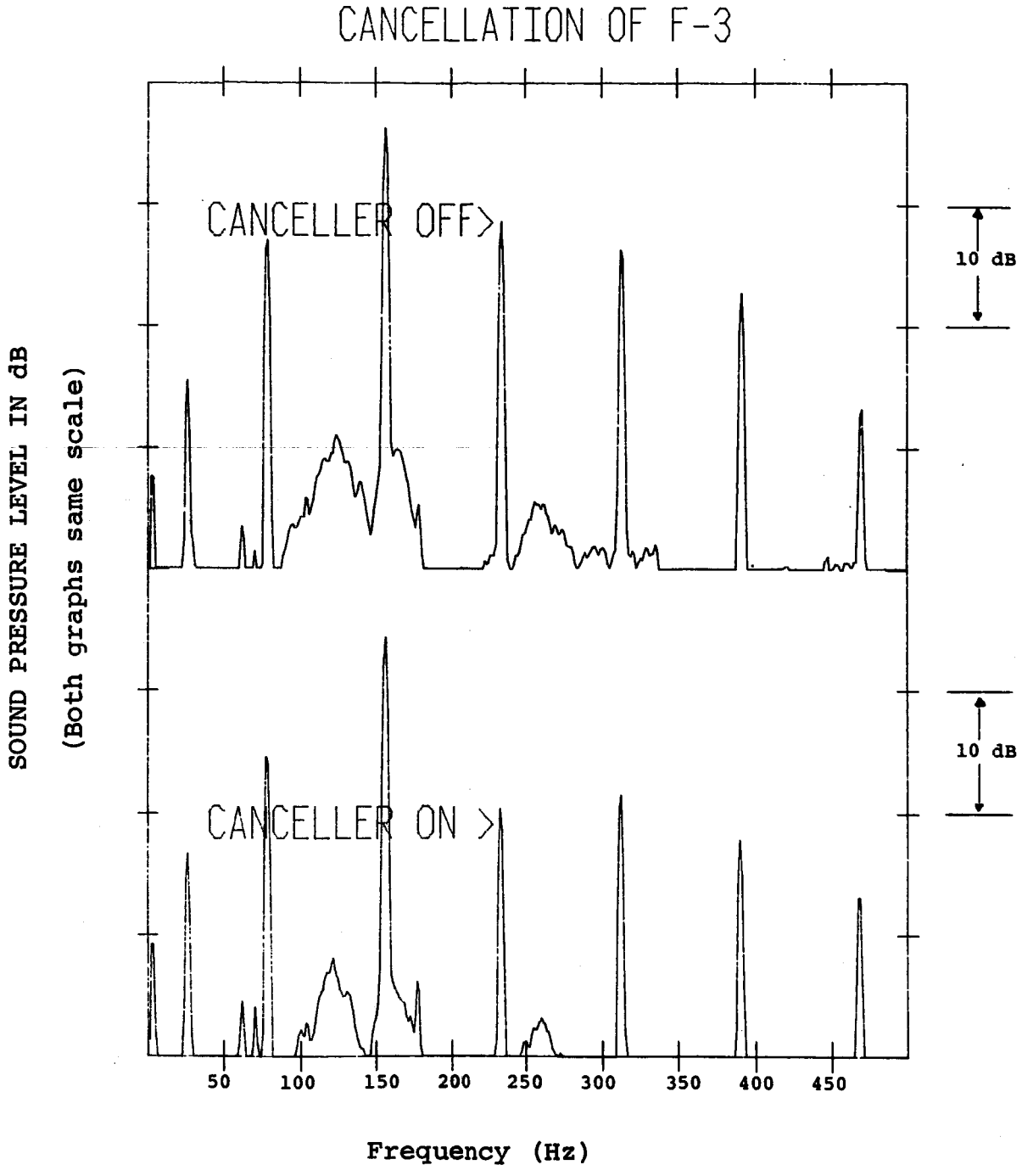

Figure 7: Cancellation of Third Harmonic

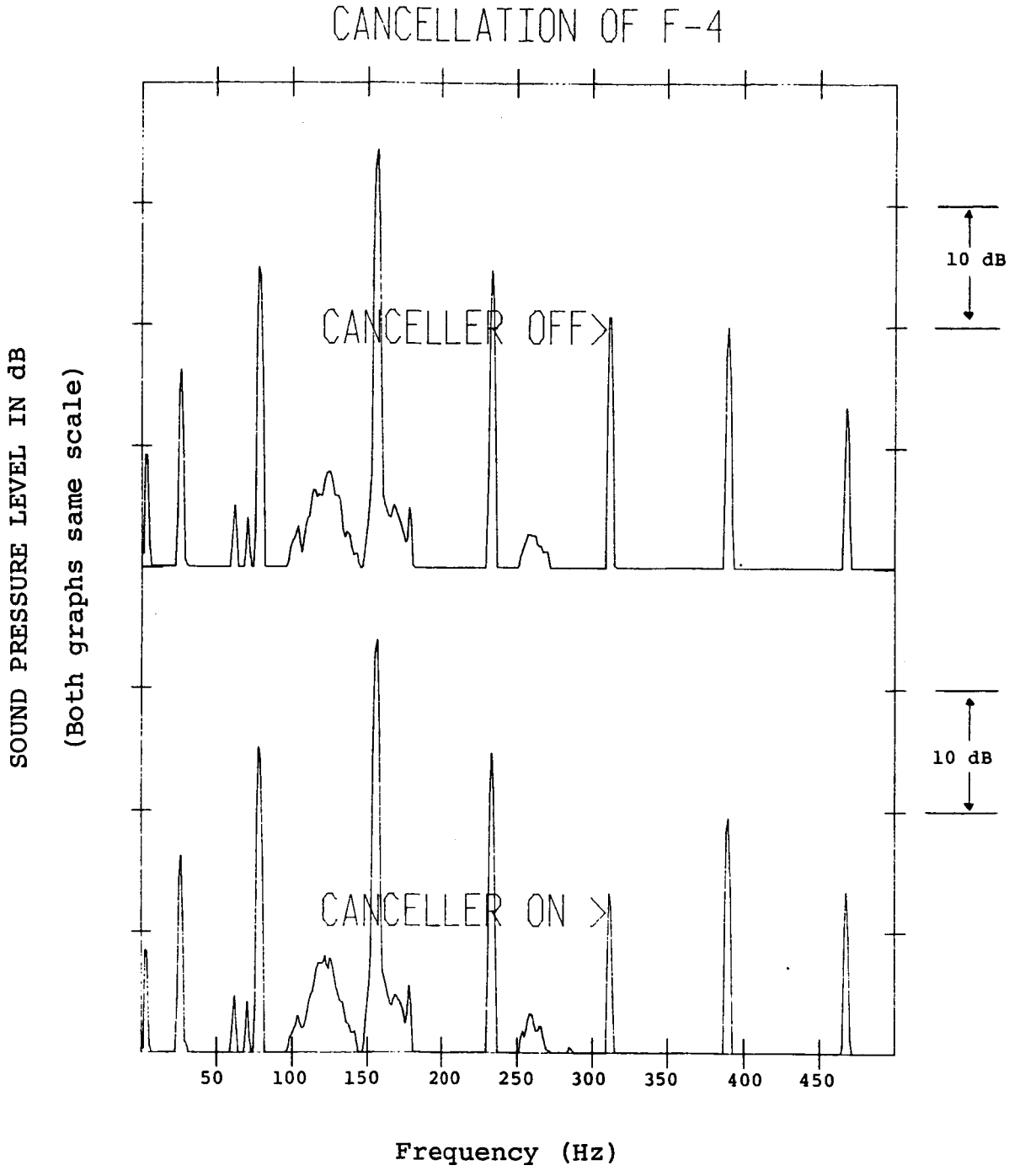

Figure 8: Cancellation of Fourth Harmonic

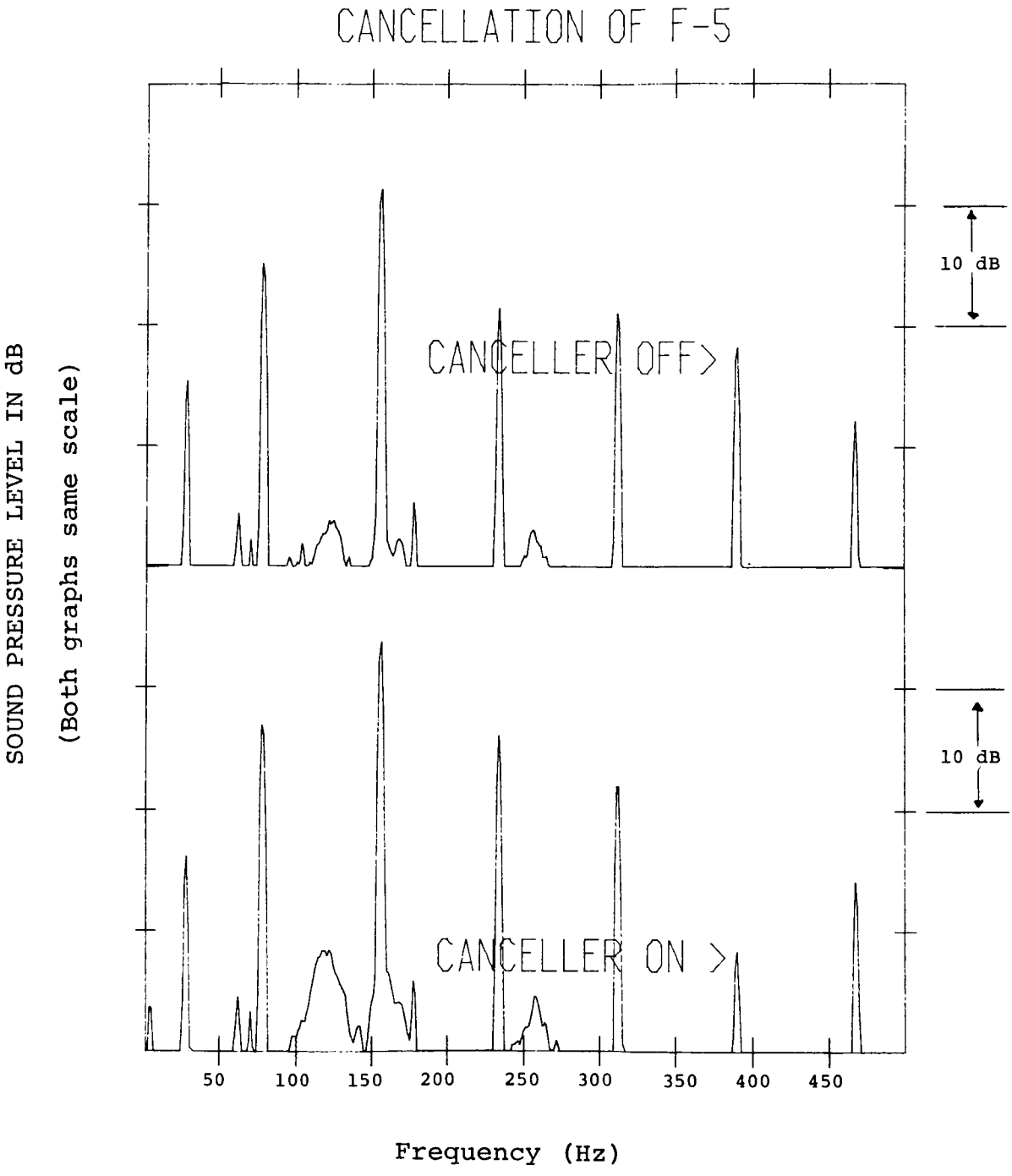

Figure 9: Cancellation of Fifth Harmonic

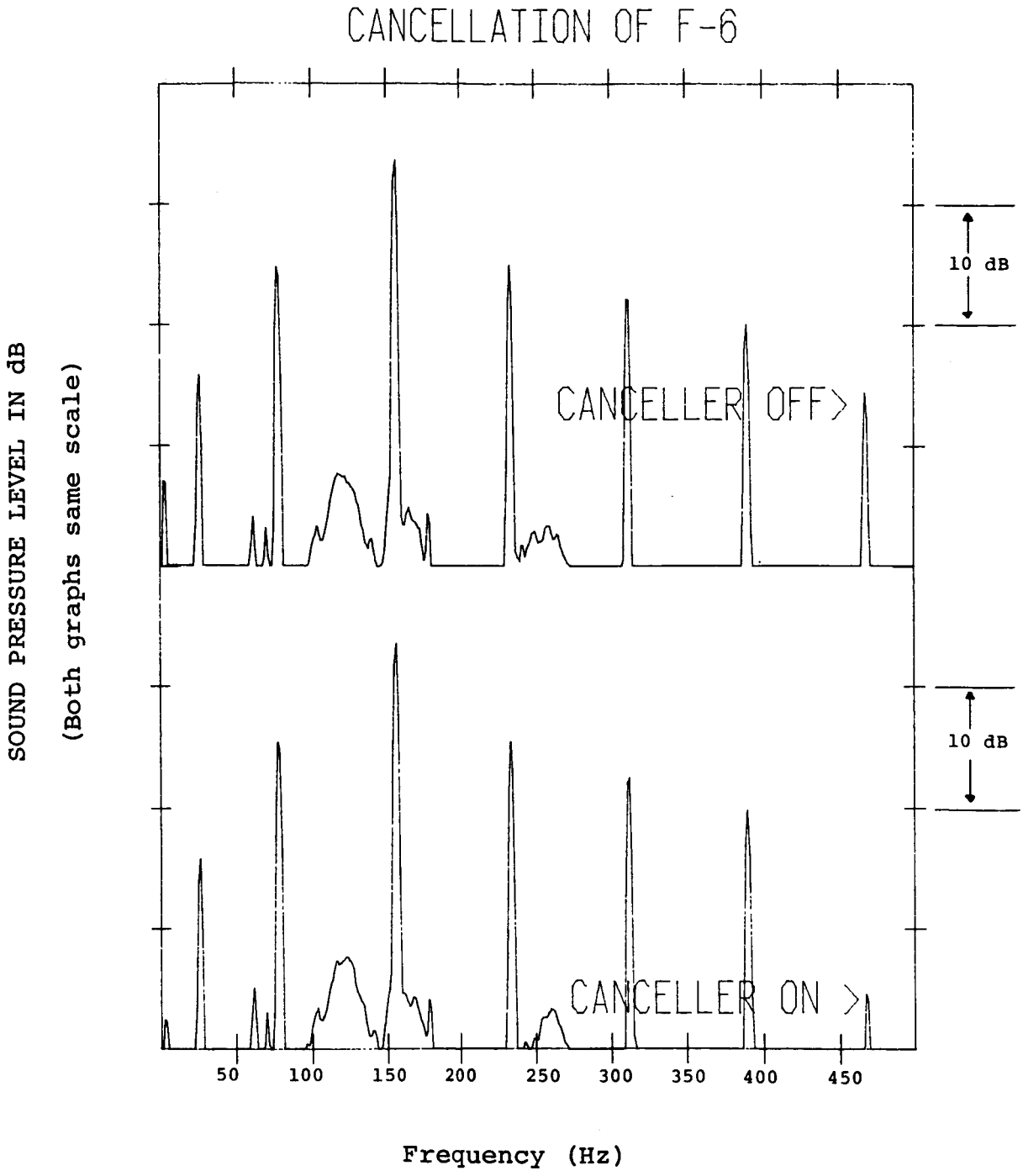

Figure 10: Cancellation of Sixth Harmonic

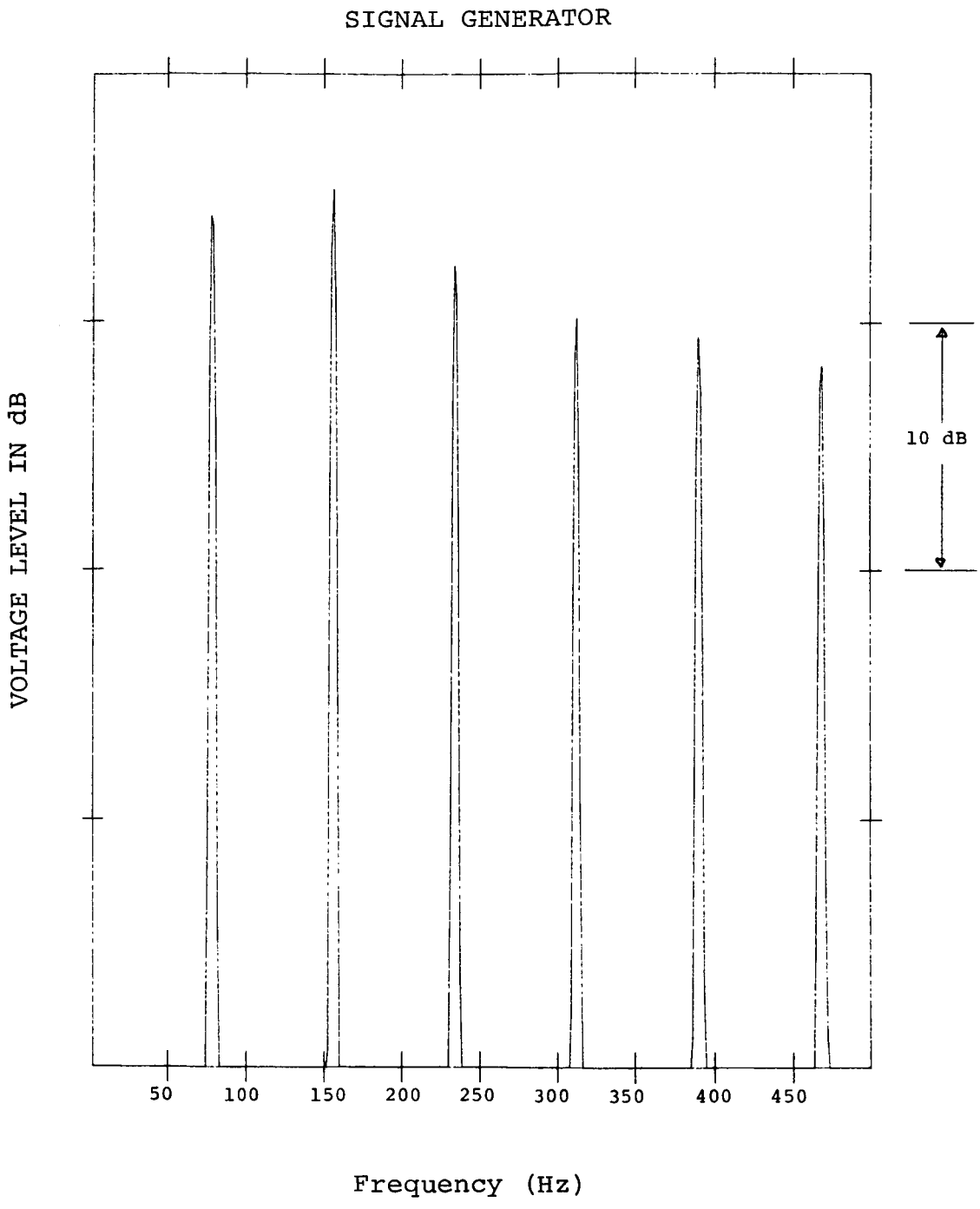

Figure 11: Output of Signal Generator sent to Controller

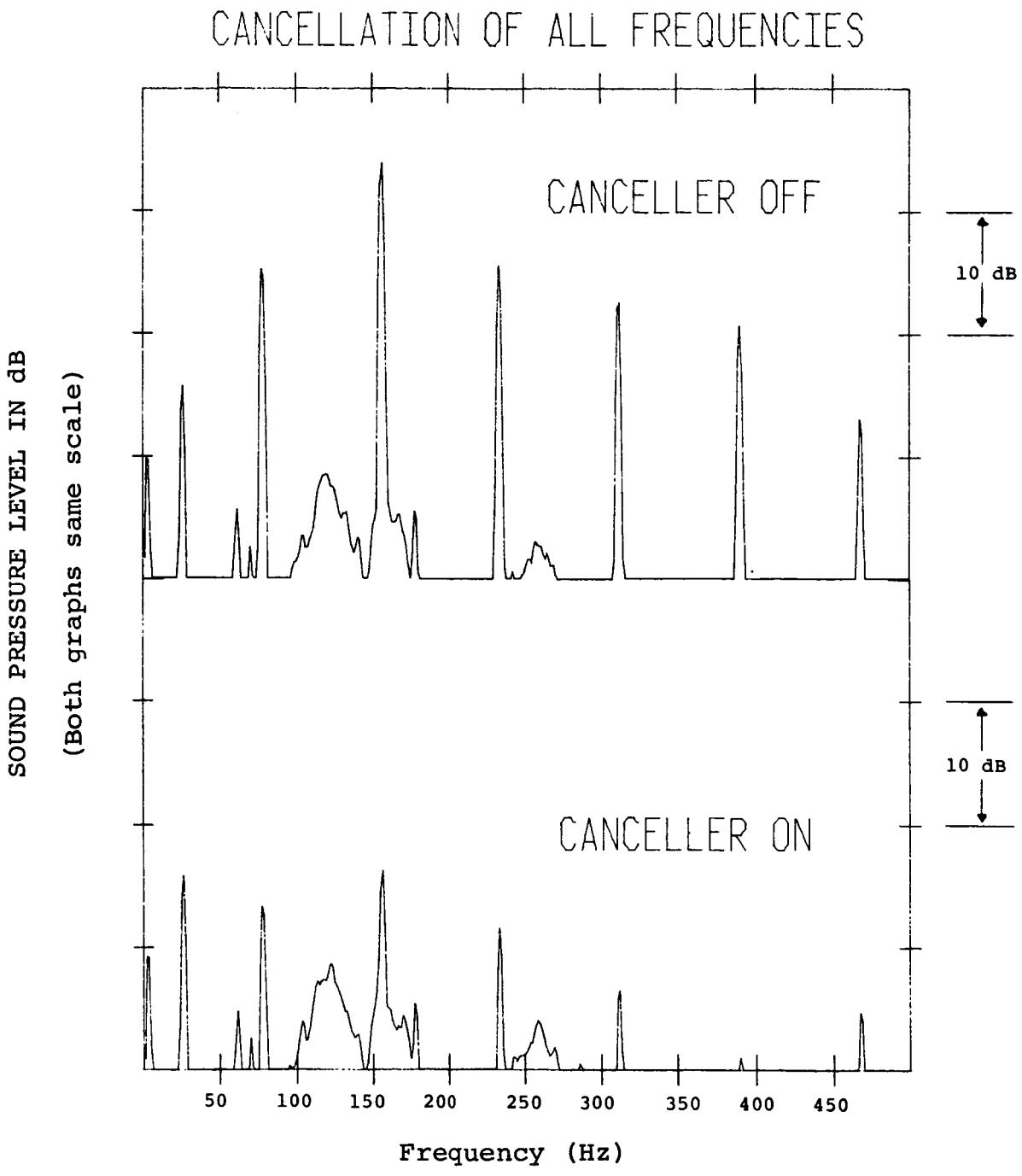

Figure 12: Broad Frequency Cancellation

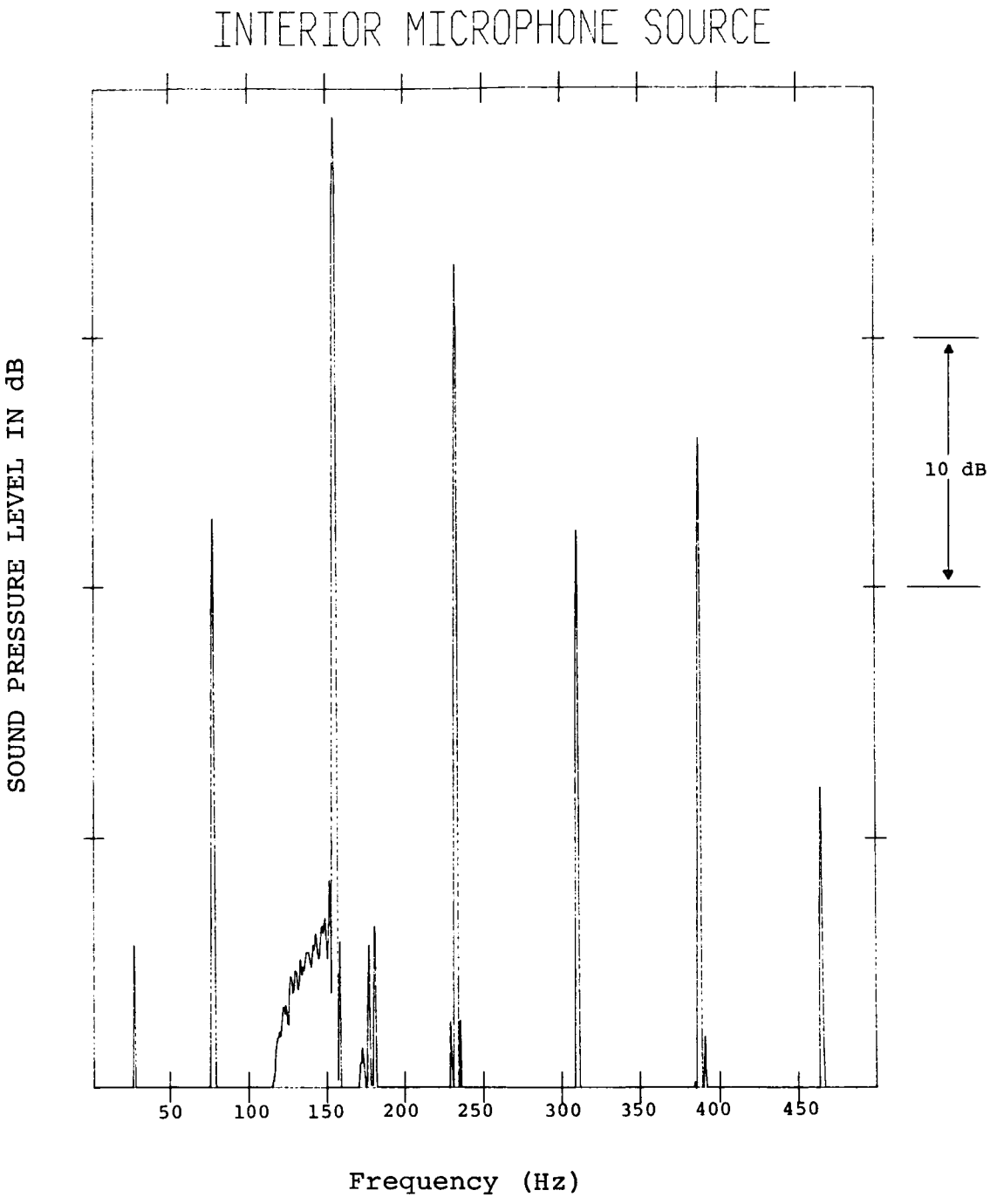

Figure 13: Interior Microphone Source Spectrum

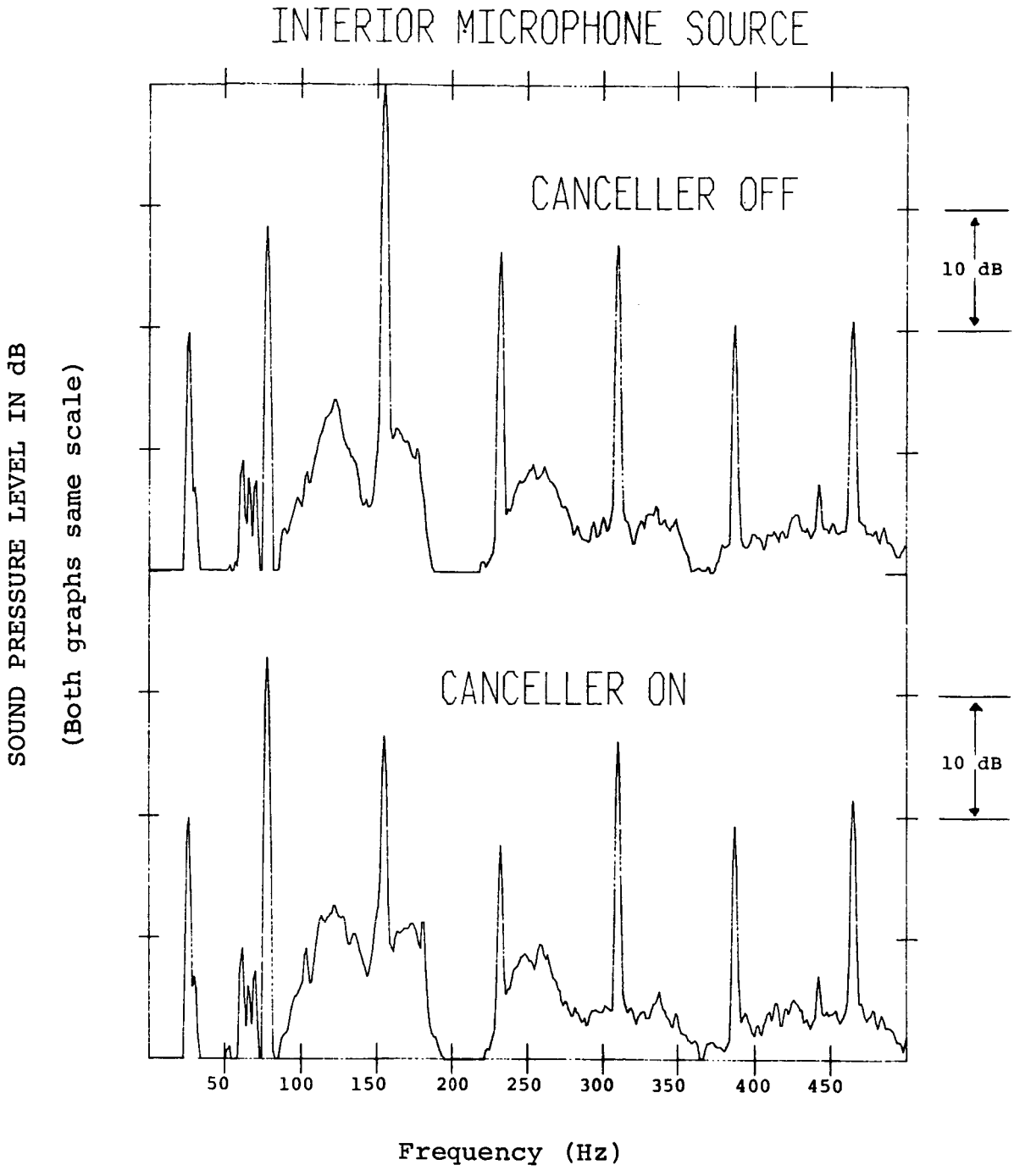

Figure 14: Cancellation Using Interior Microphone Source

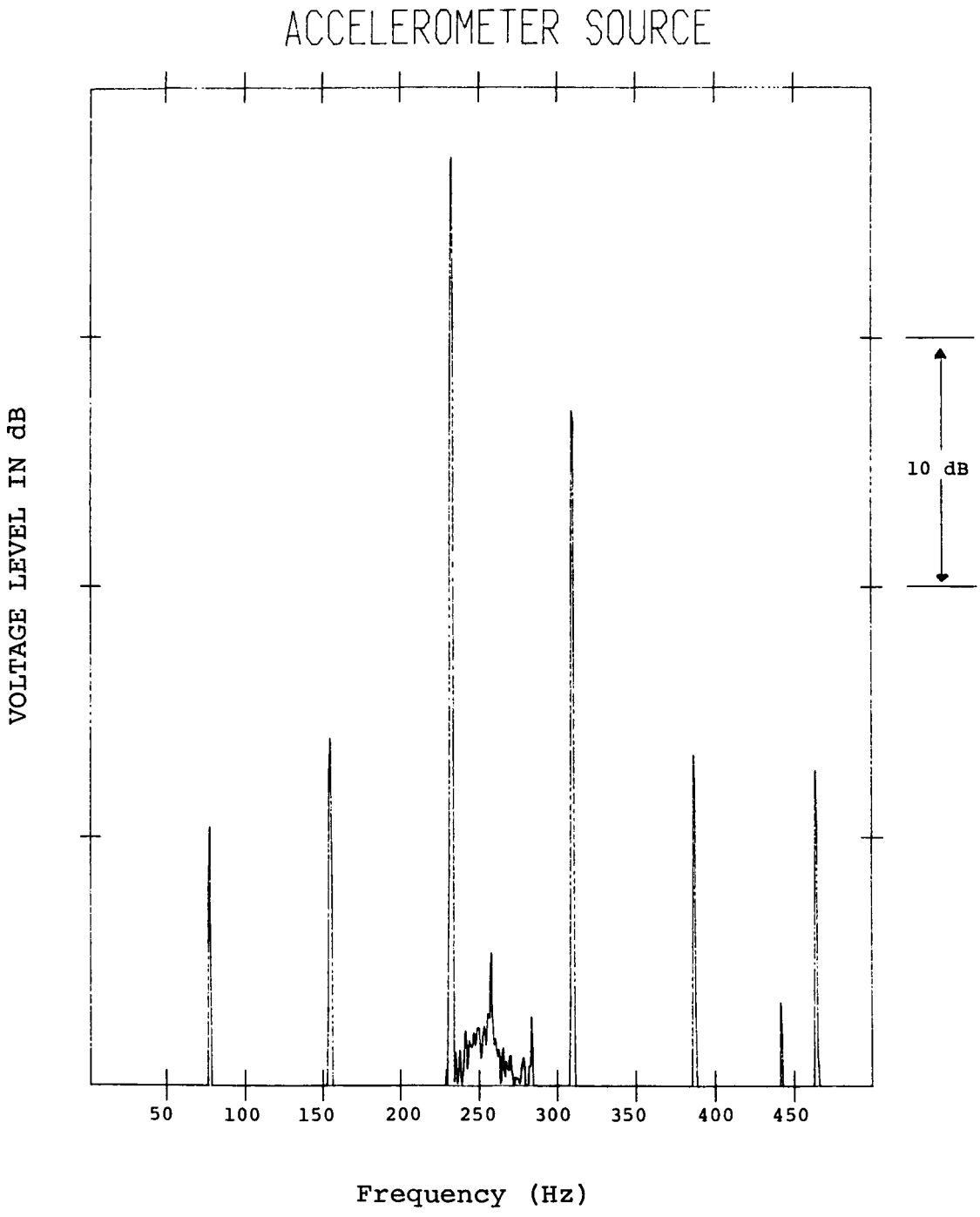

Figure 15: Accelerometer Source Spectrum

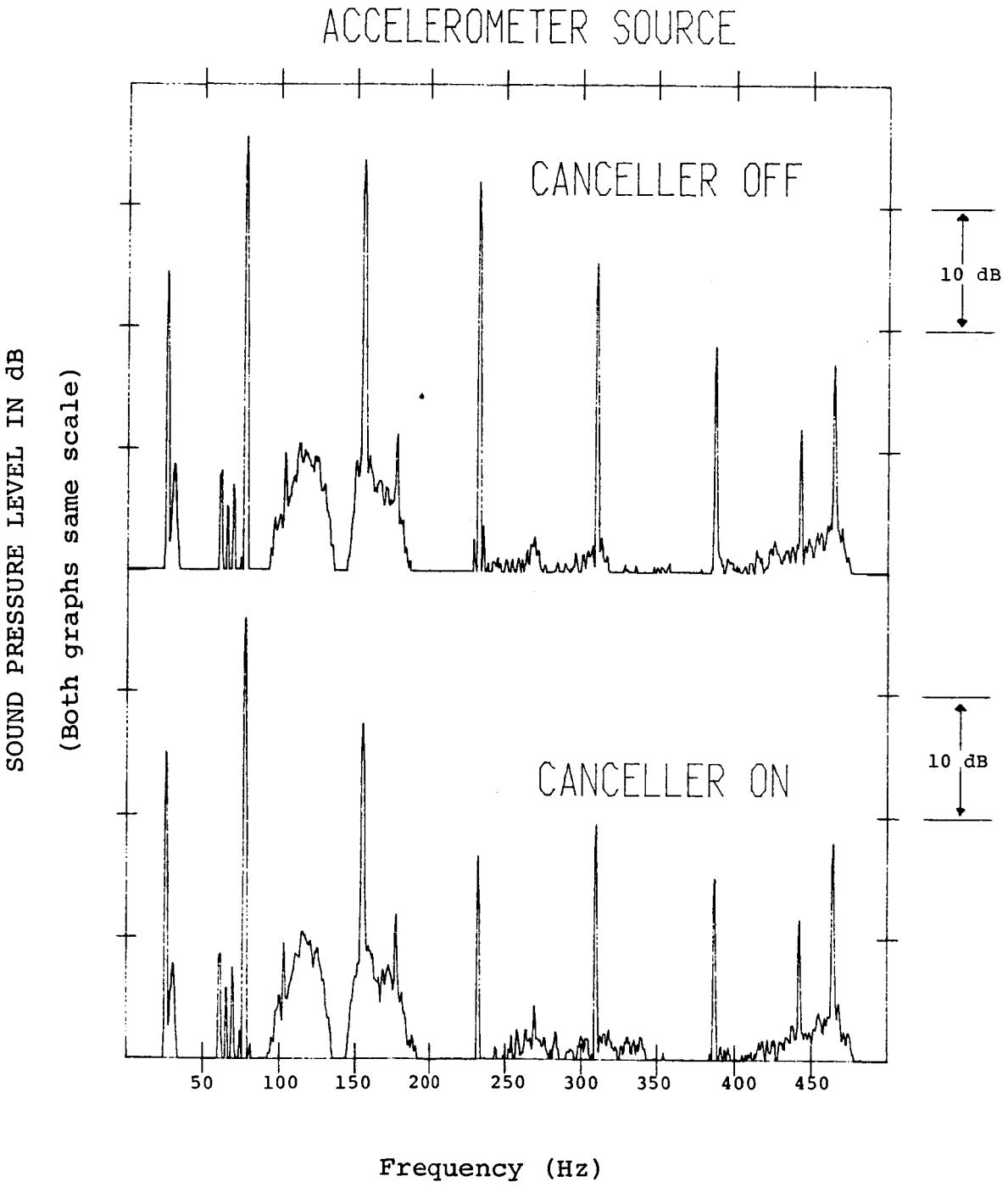

Figure 16: Cancellation Using Accelerometer Source

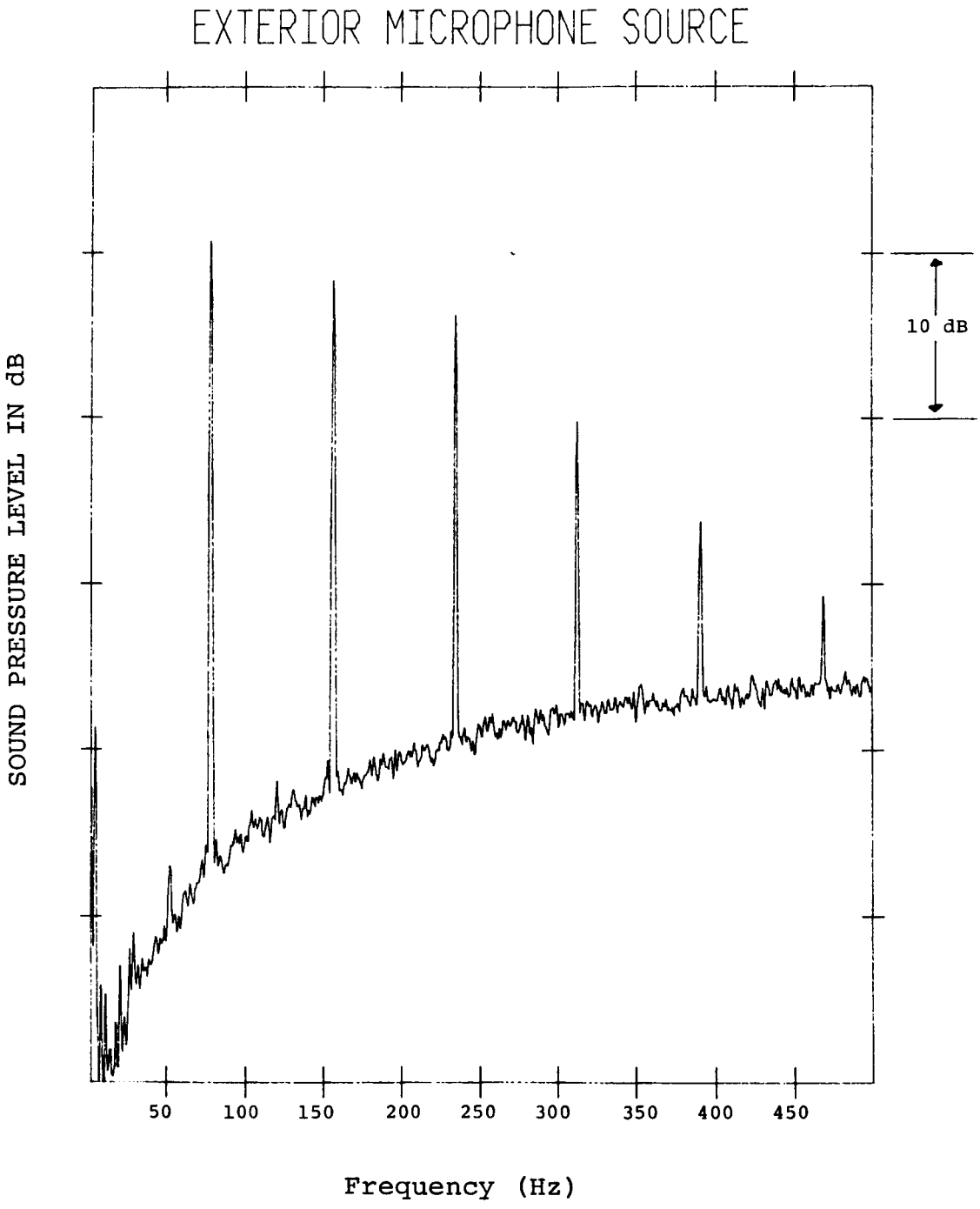

Figure 17: Exterior Microphone Source Spectrum

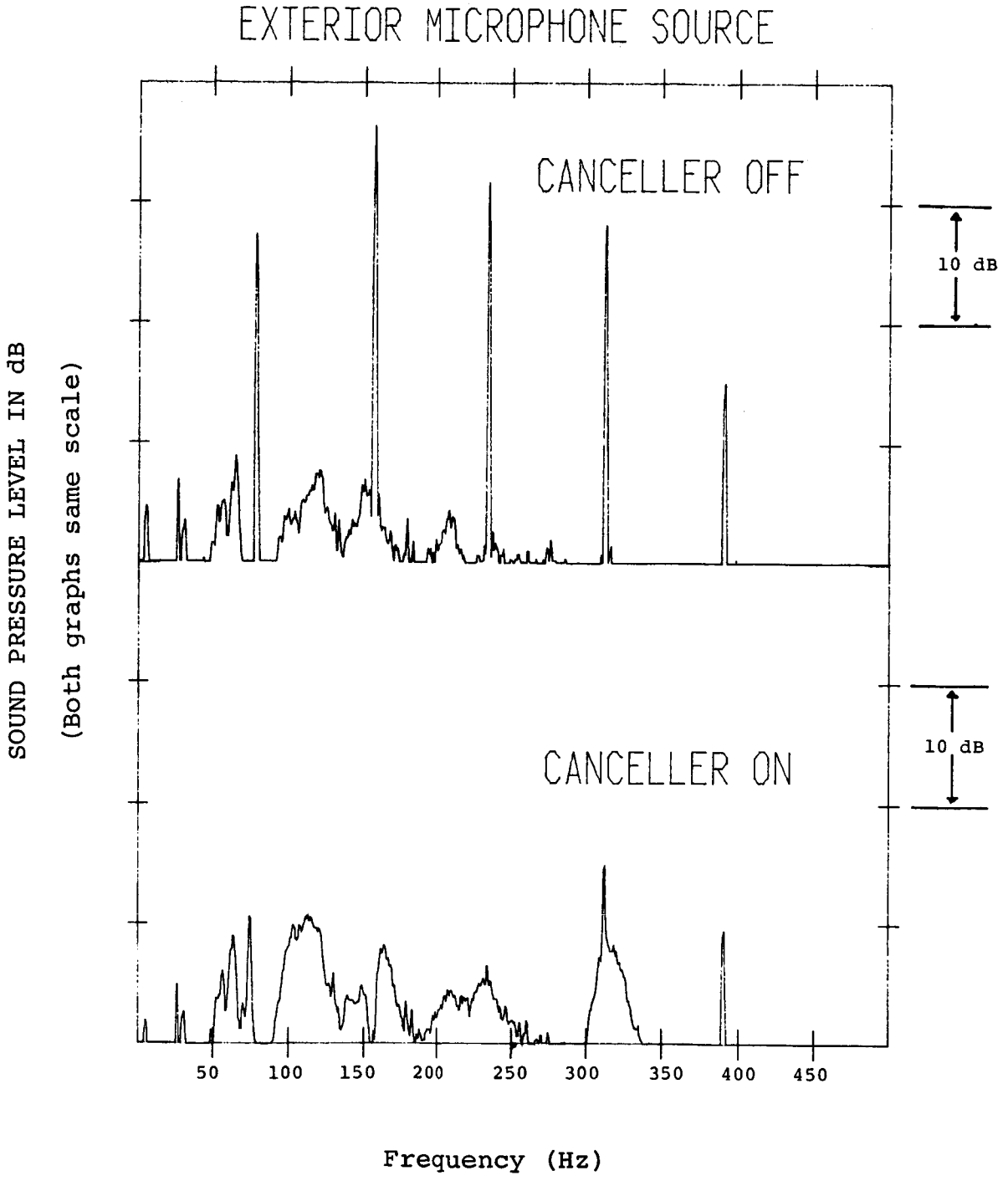

Figure 18: Cancellation Using Exterior Microphone Source

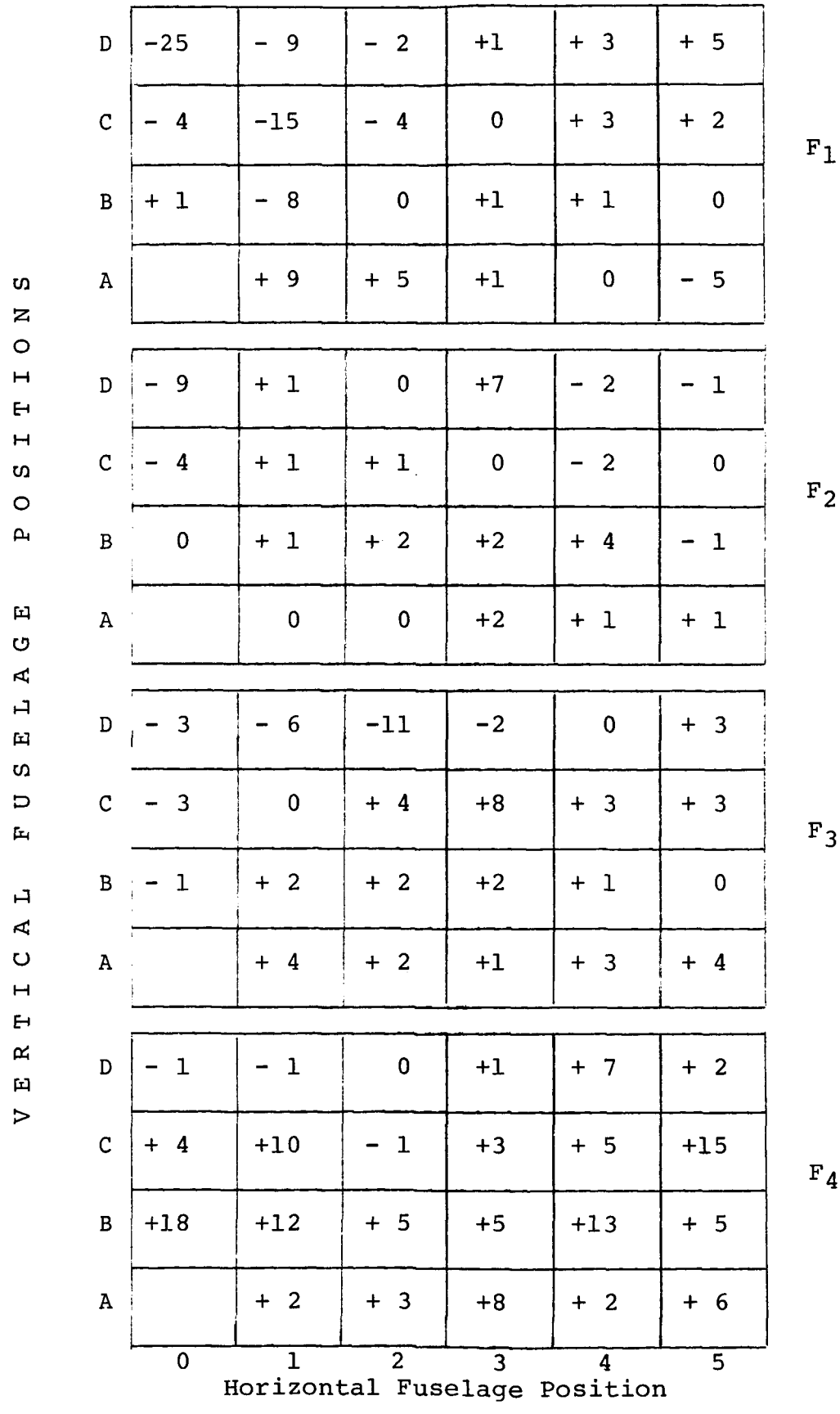

FIGURE 19: AIRCRAFT C, LEFT ENGINE ON, CANCELLATION IN dB

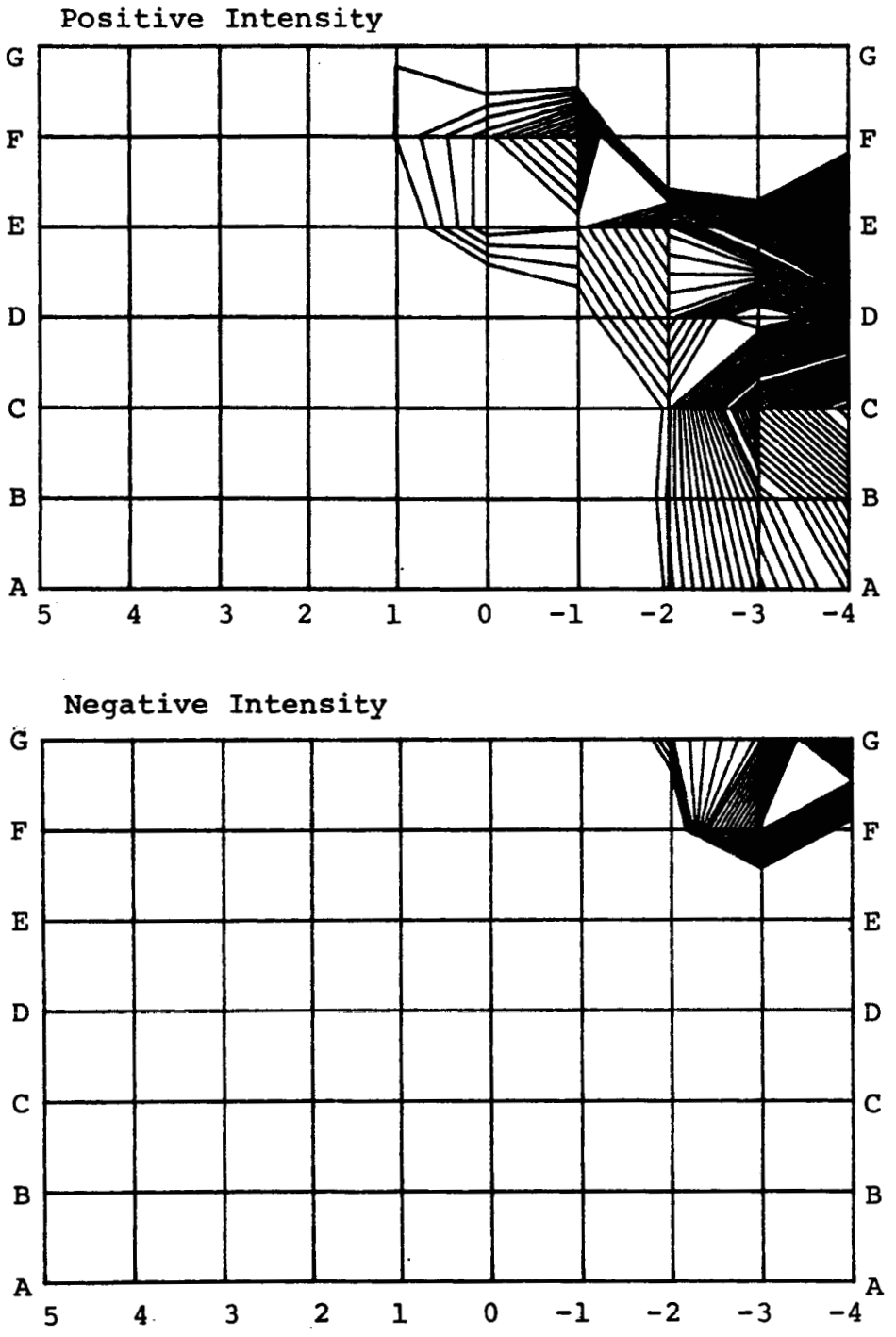

Figure 20: Aircraft B, Left Side
Both engines on
Range: 100-110 dB
Frequency: 77 Hz

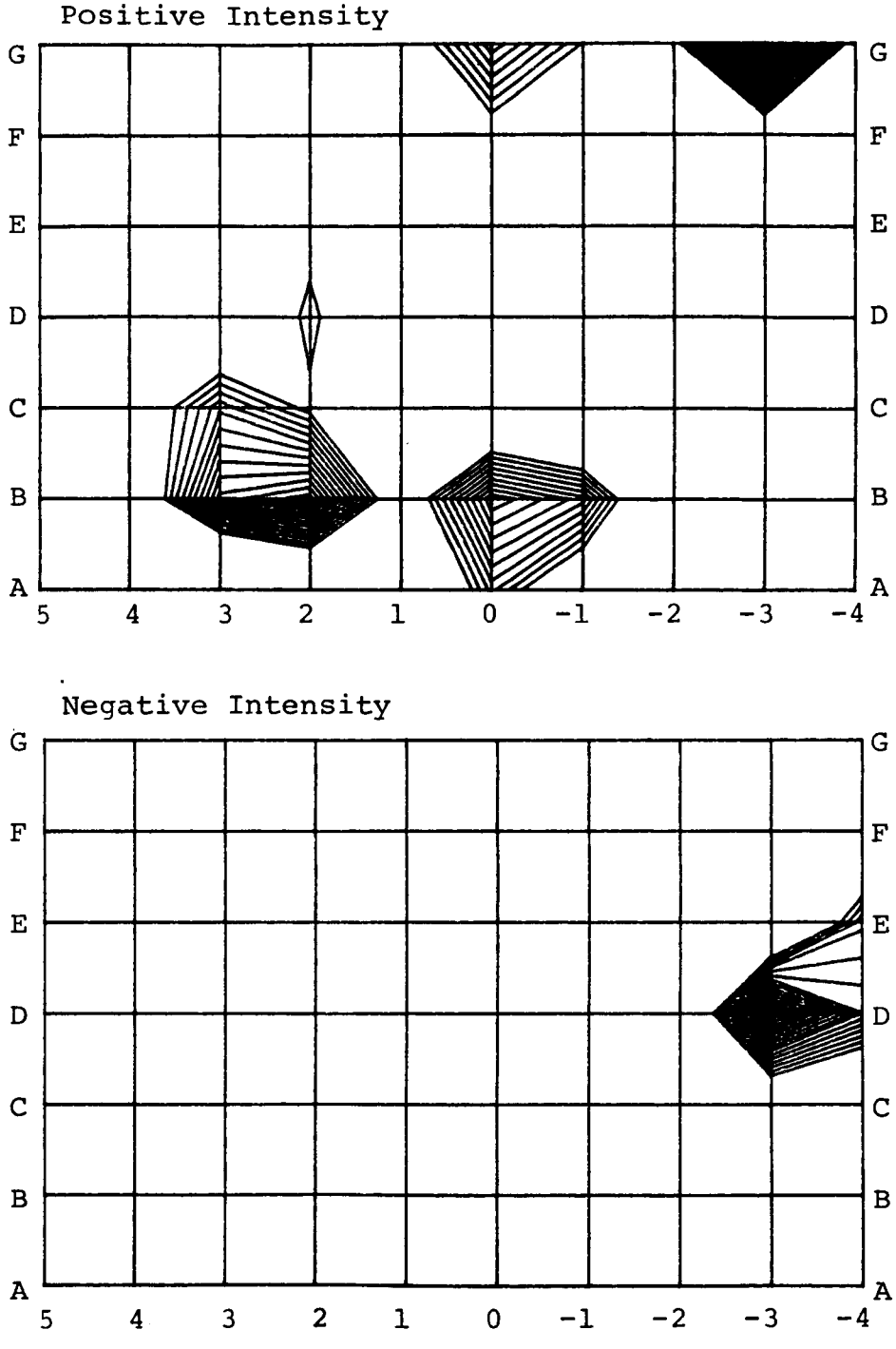

Figure 21: Aircraft B, Left Side
Both Engines On
Range: 100-110 dB
Frequency: 155 Hz

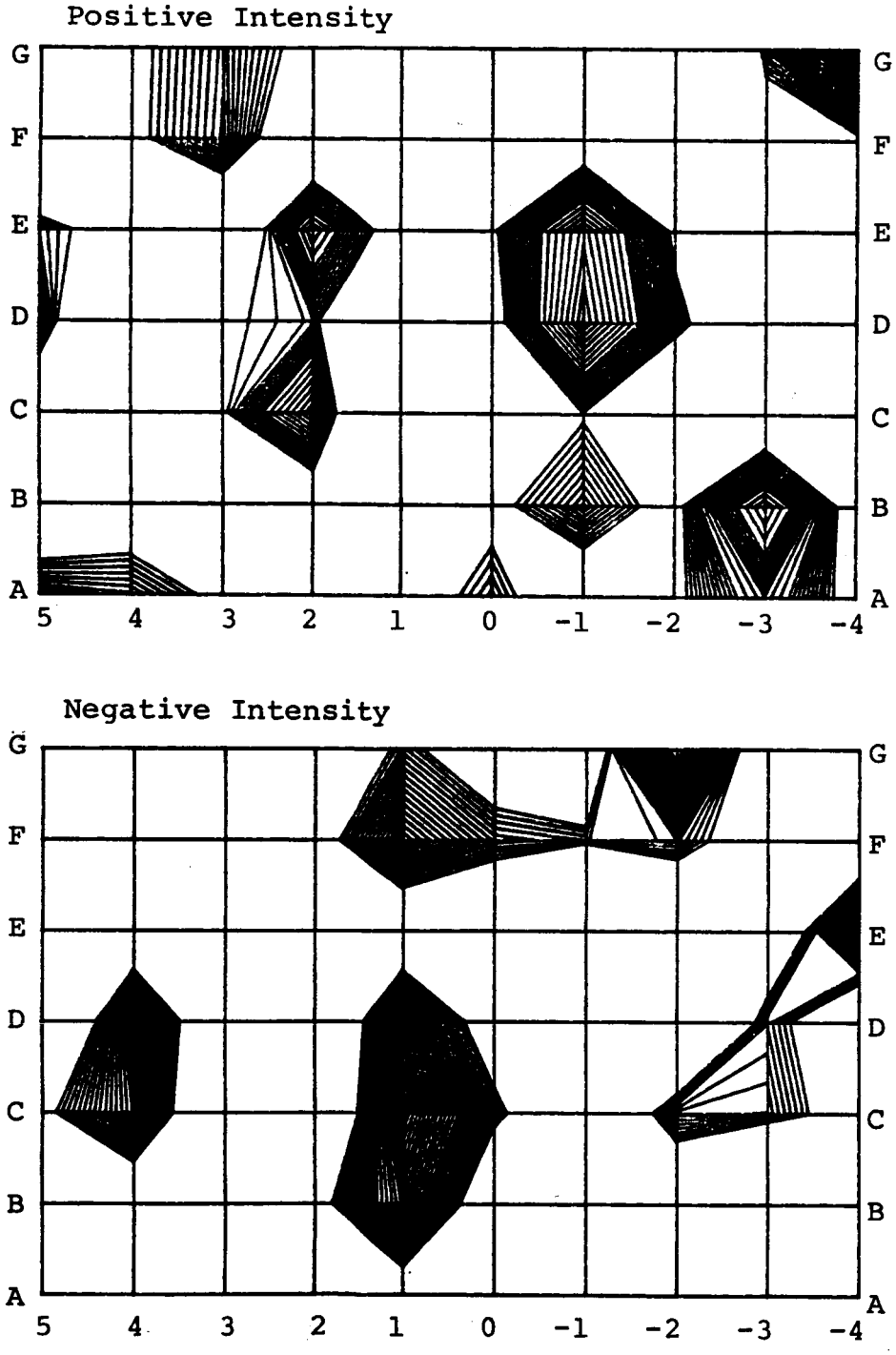

Figure 22: Aircraft B, Left Side
Both Engines On
Range: 90-100 dB
Frequency: 232 Hz

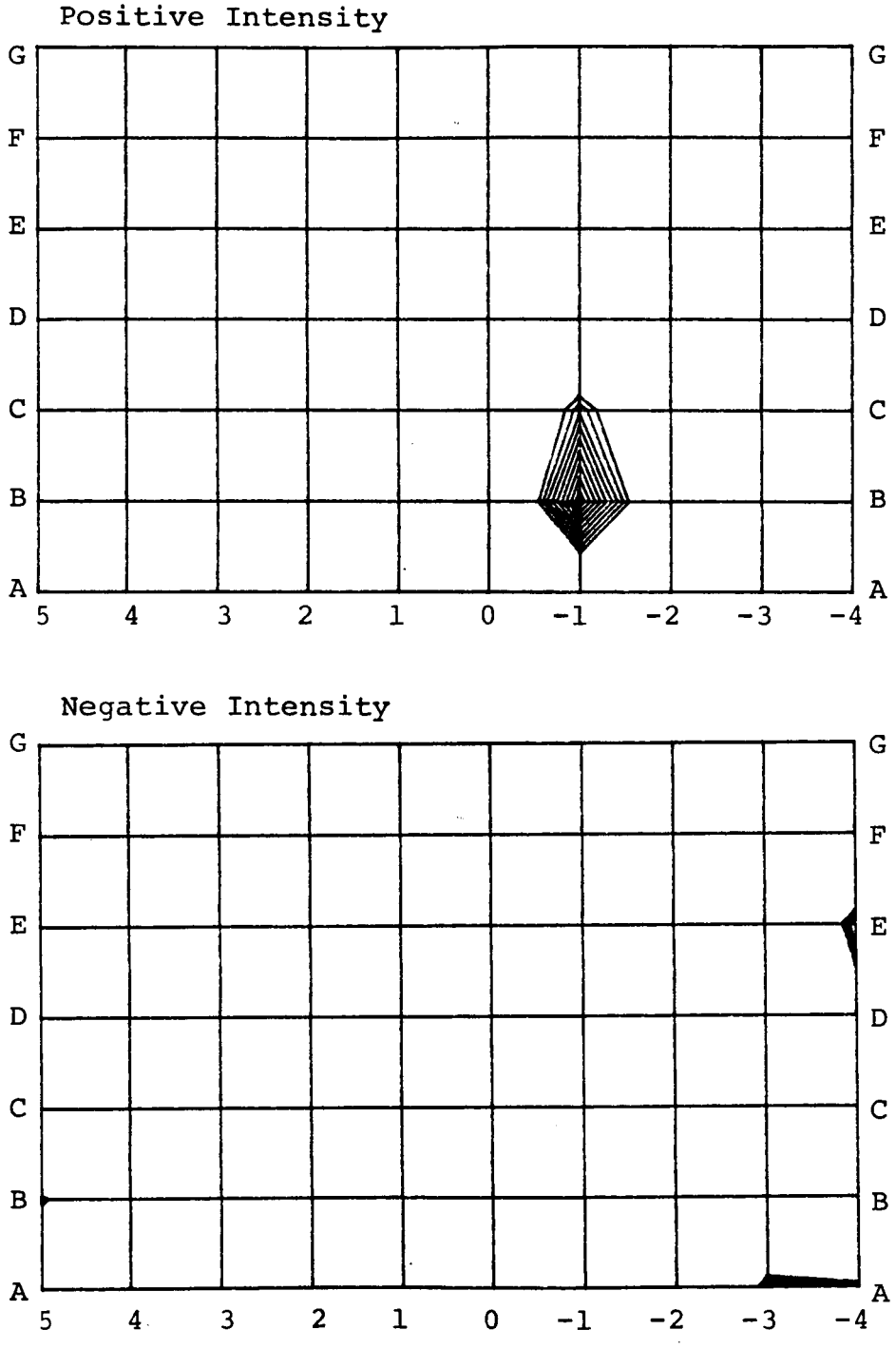

Figure 23: Aircraft B, Left Side
Both Engines On
Range: 100-110 dB
Frequency: 310 Hz

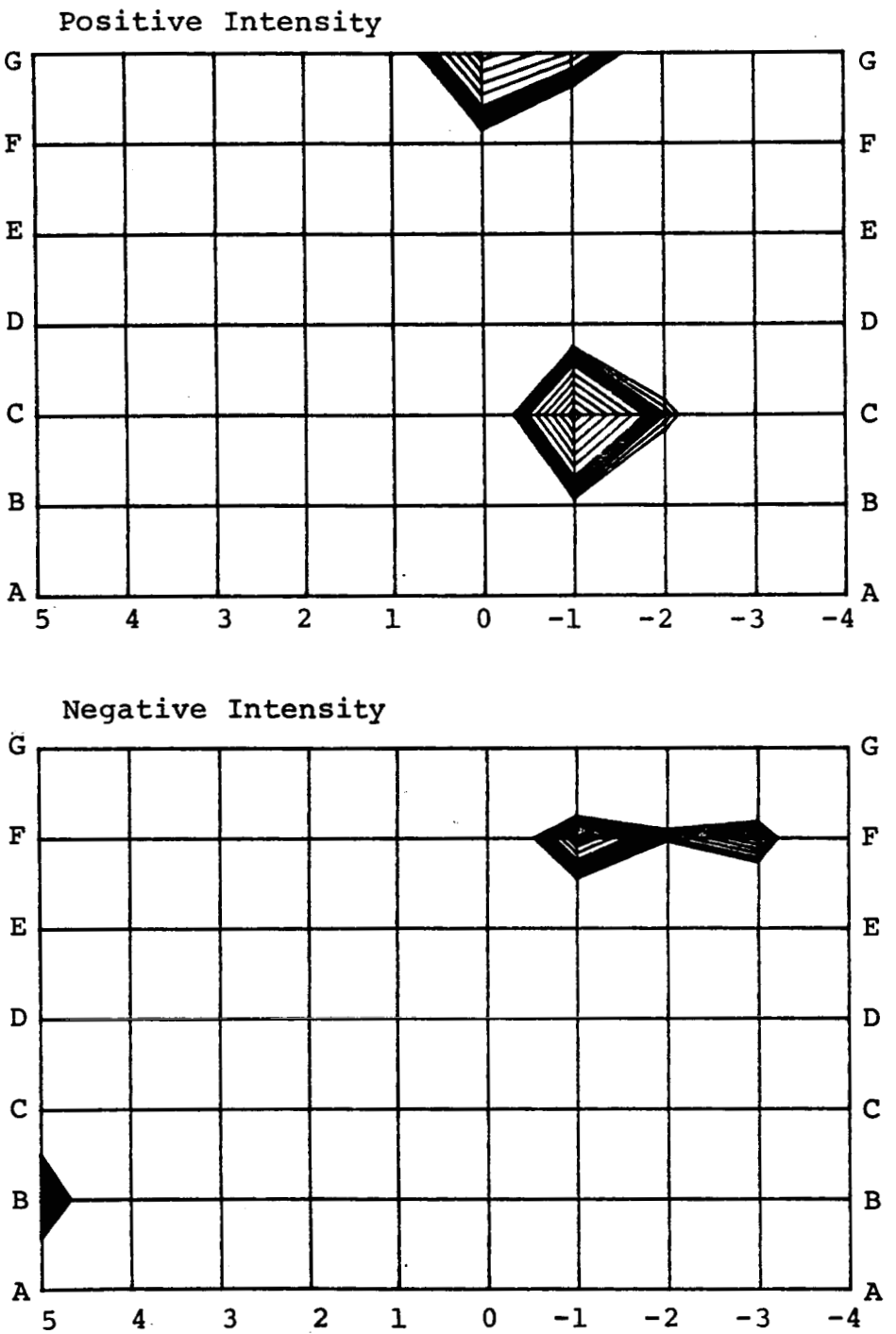

Figure 24: Aircraft B, Left Side
Both Engines On
Range: 90-100 dB
Frequency: 387 Hz

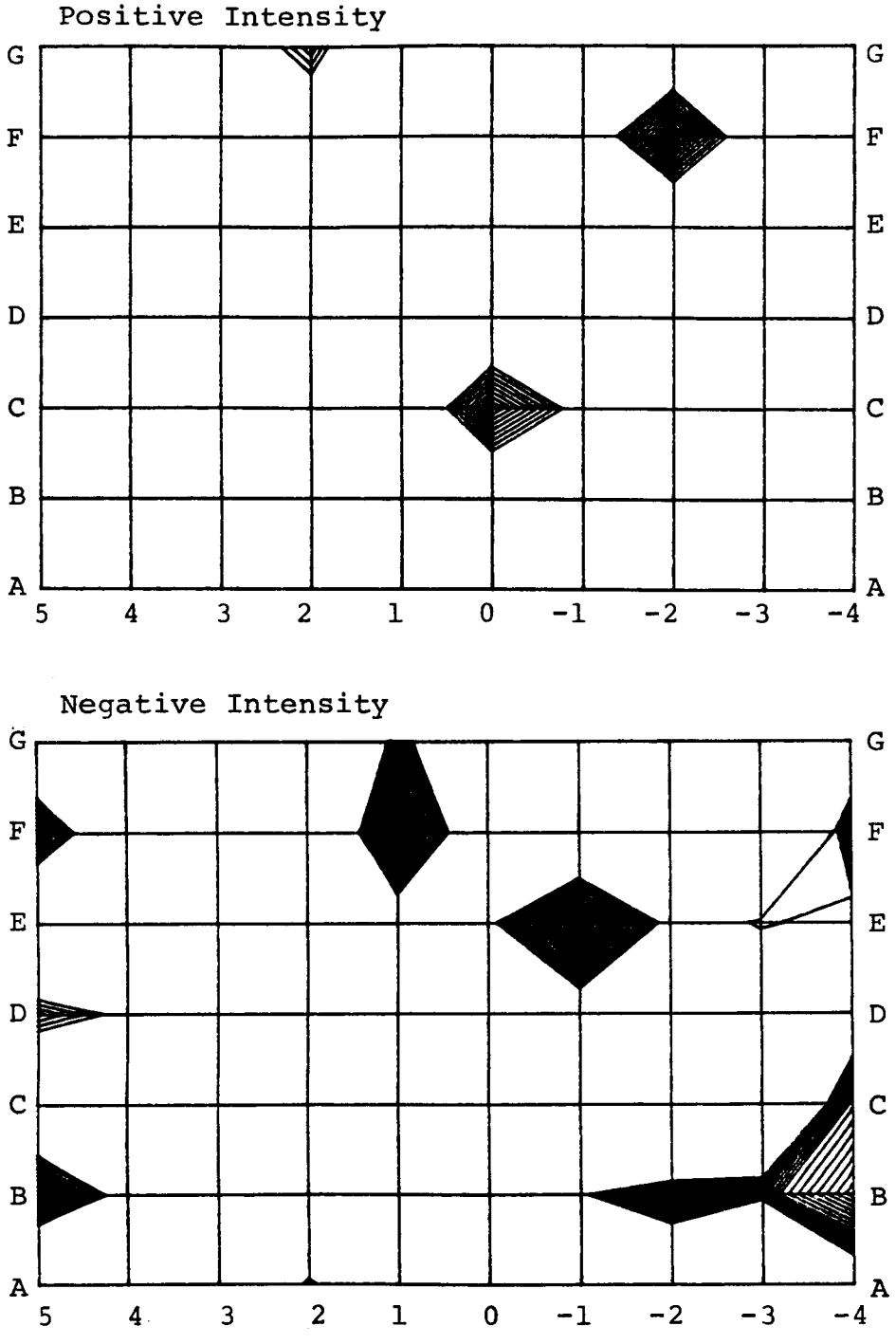

Figure 25: Aircraft B, Left Side
Both Engines On
Range: 90-100 dB
Frequency: 464 Hz

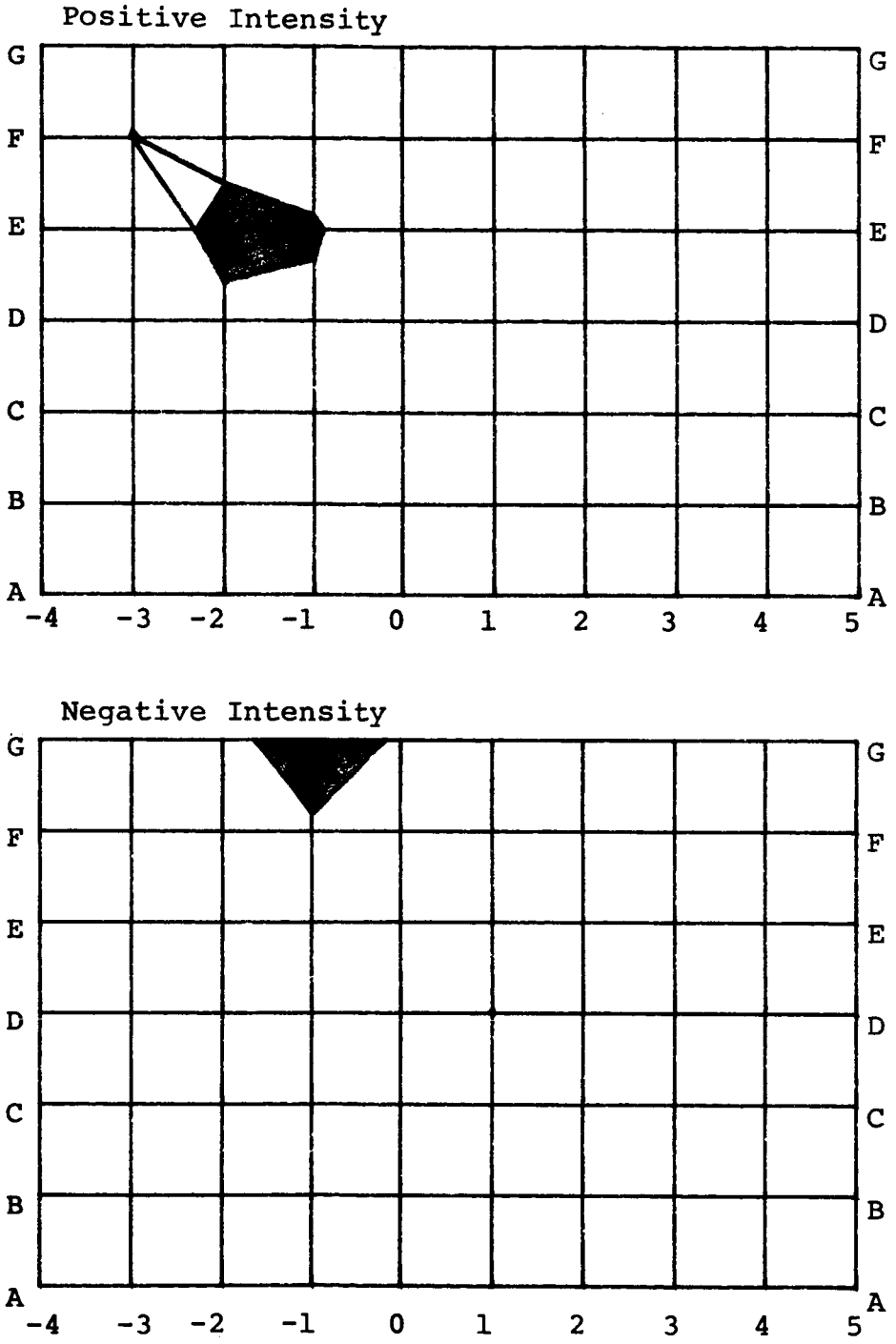

Figure 26: Aircraft B, Right Side
Both Engines On
Range: 100-110 dB
Frequency: 77 Hz

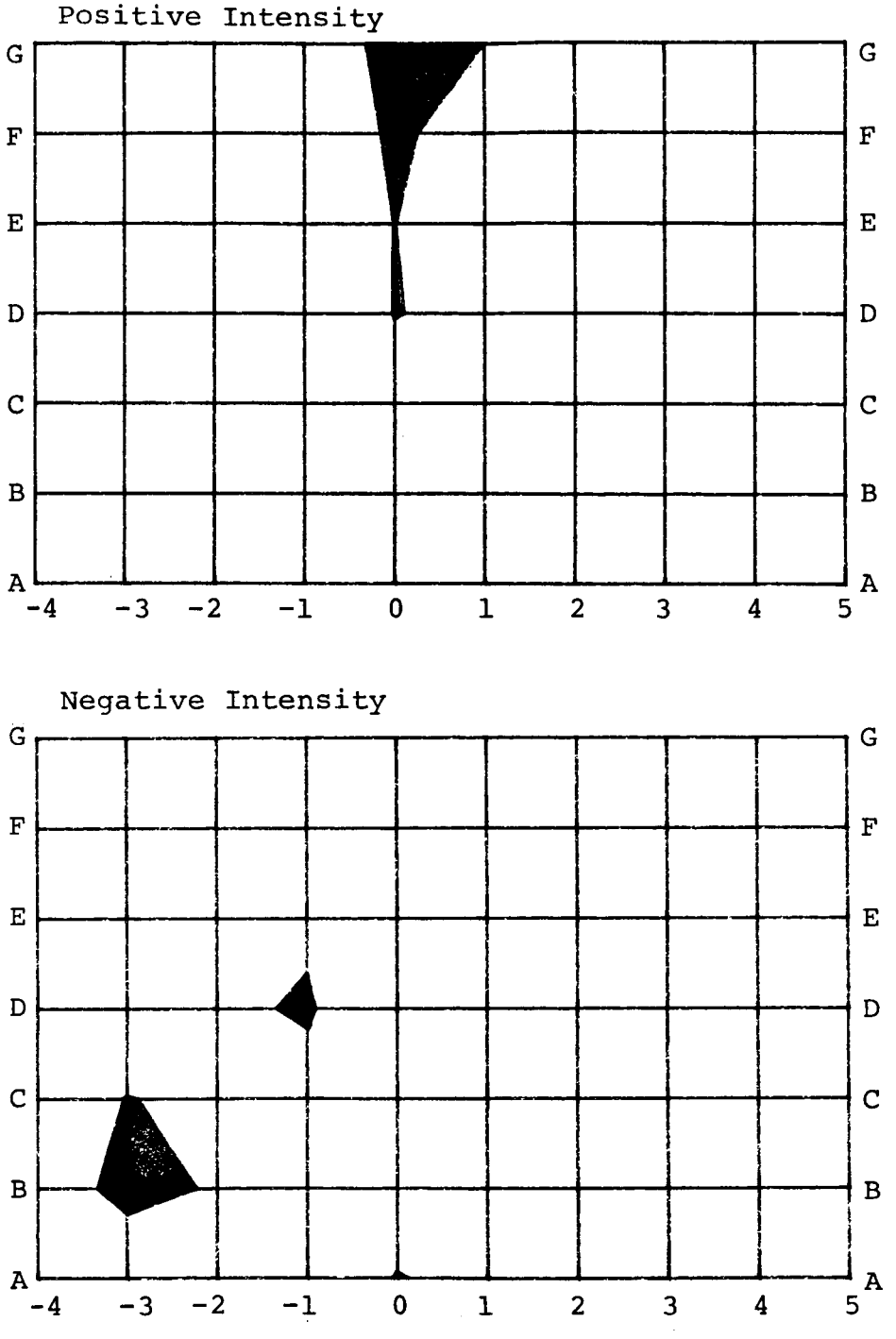

Figure 27: Aircraft B, Right Side
Both Engines On
Range: 100-110 dB
Frequency: 155 Hz

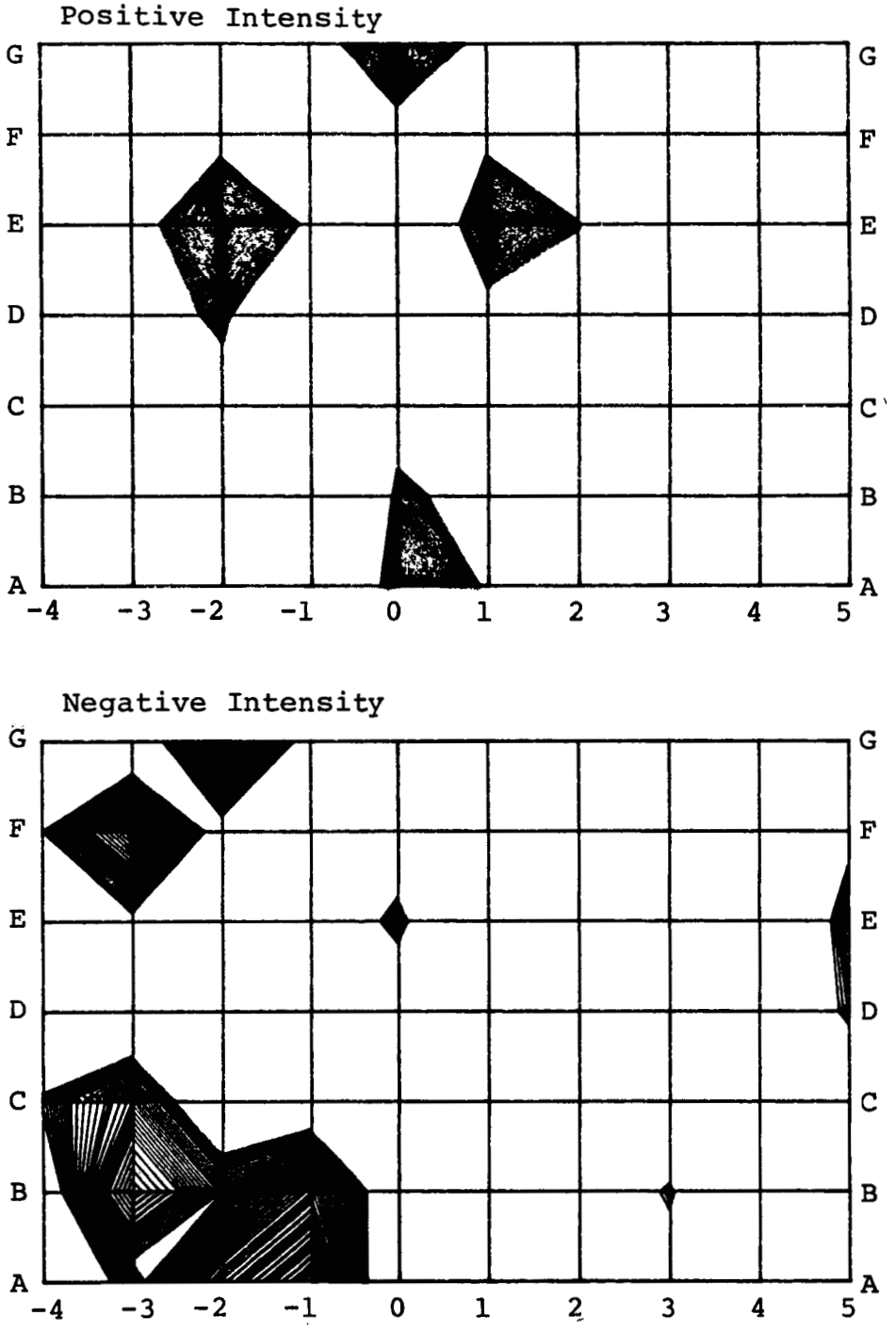

Figure 28: Aircraft B, Right Side
Both Engines On
Range: 90-100 dB
Frequency: 232 Hz

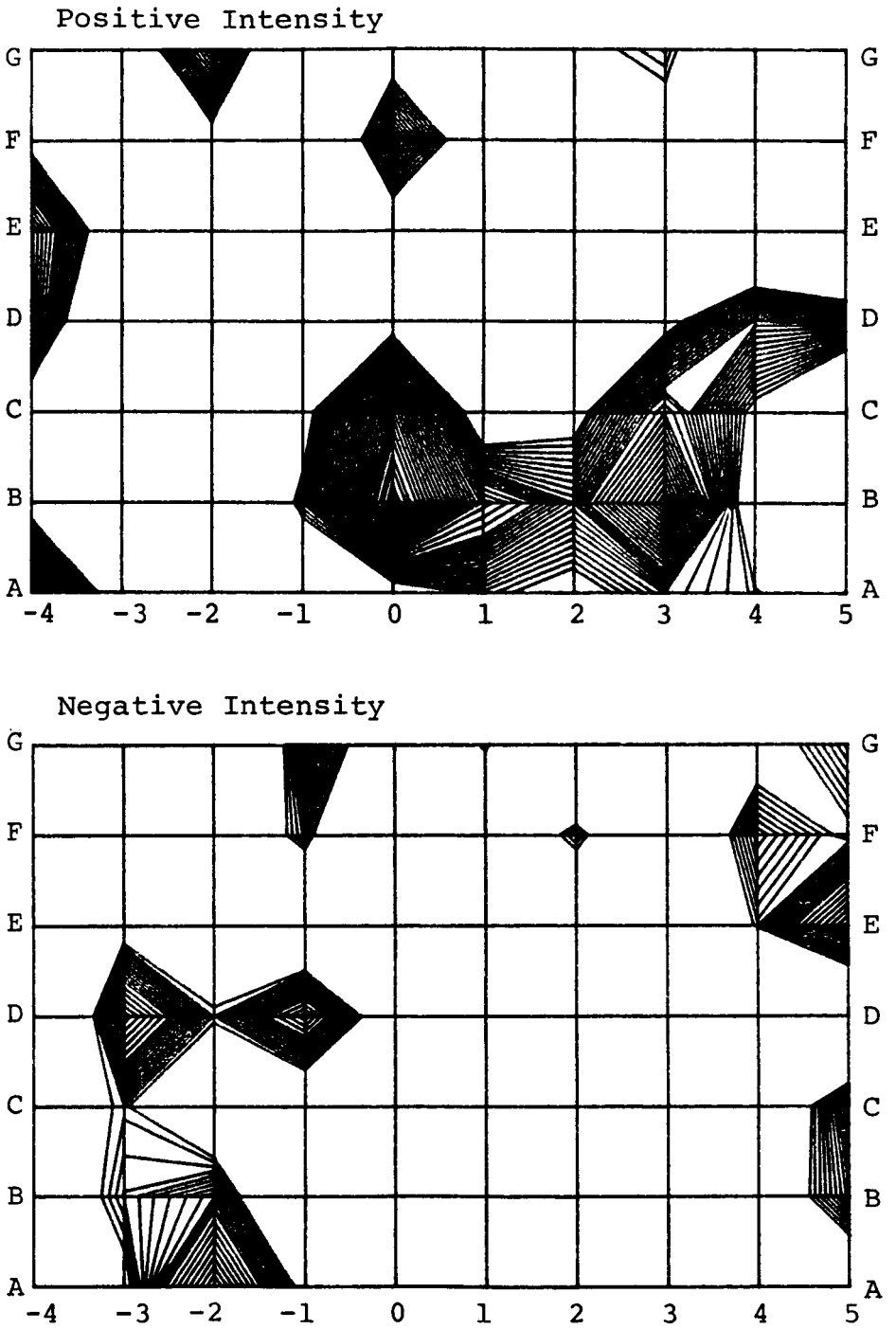

Figure 29: Aircraft B, Right Side
Both Engines On
Range: 90-100 dB
Frequency: 310 Hz

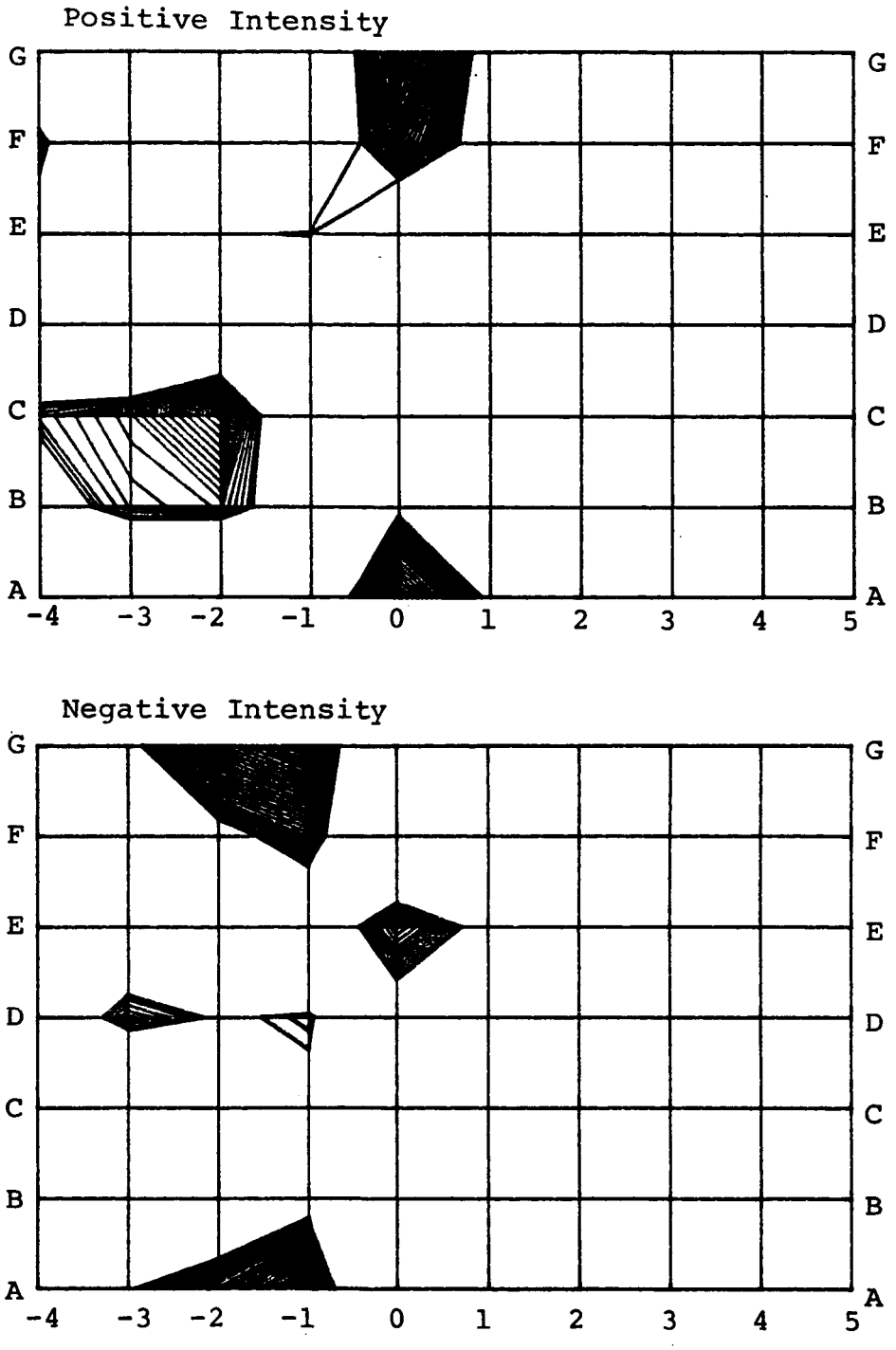

Figure 30: Aircraft B, Right Side
Both Engines On
Range: 90-100 dB
Frequency: 387 Hz

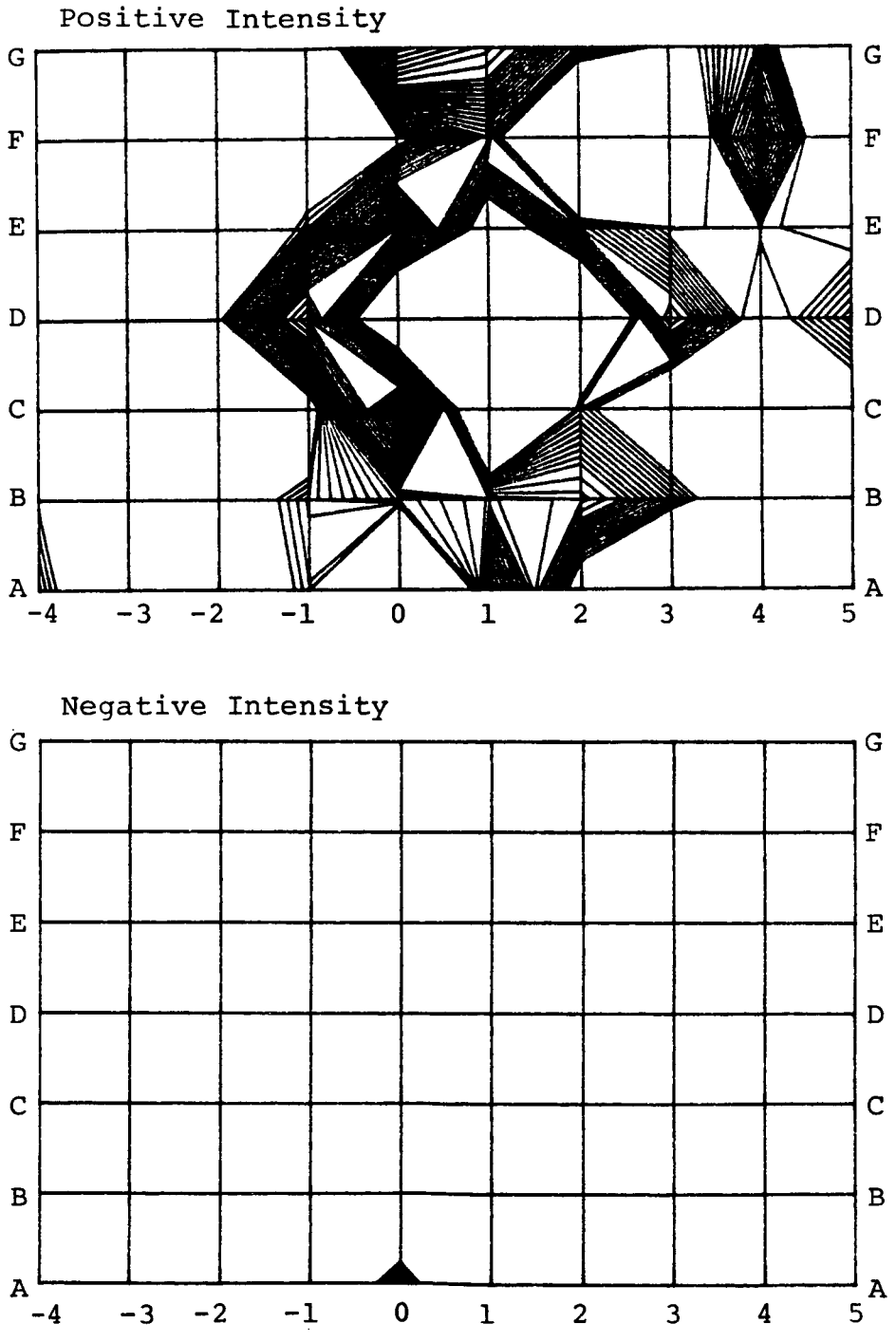

Figure 31: Aircraft B, Right Side
Both Engines On
Range: 80-90 db
Frequency: 465 Hz

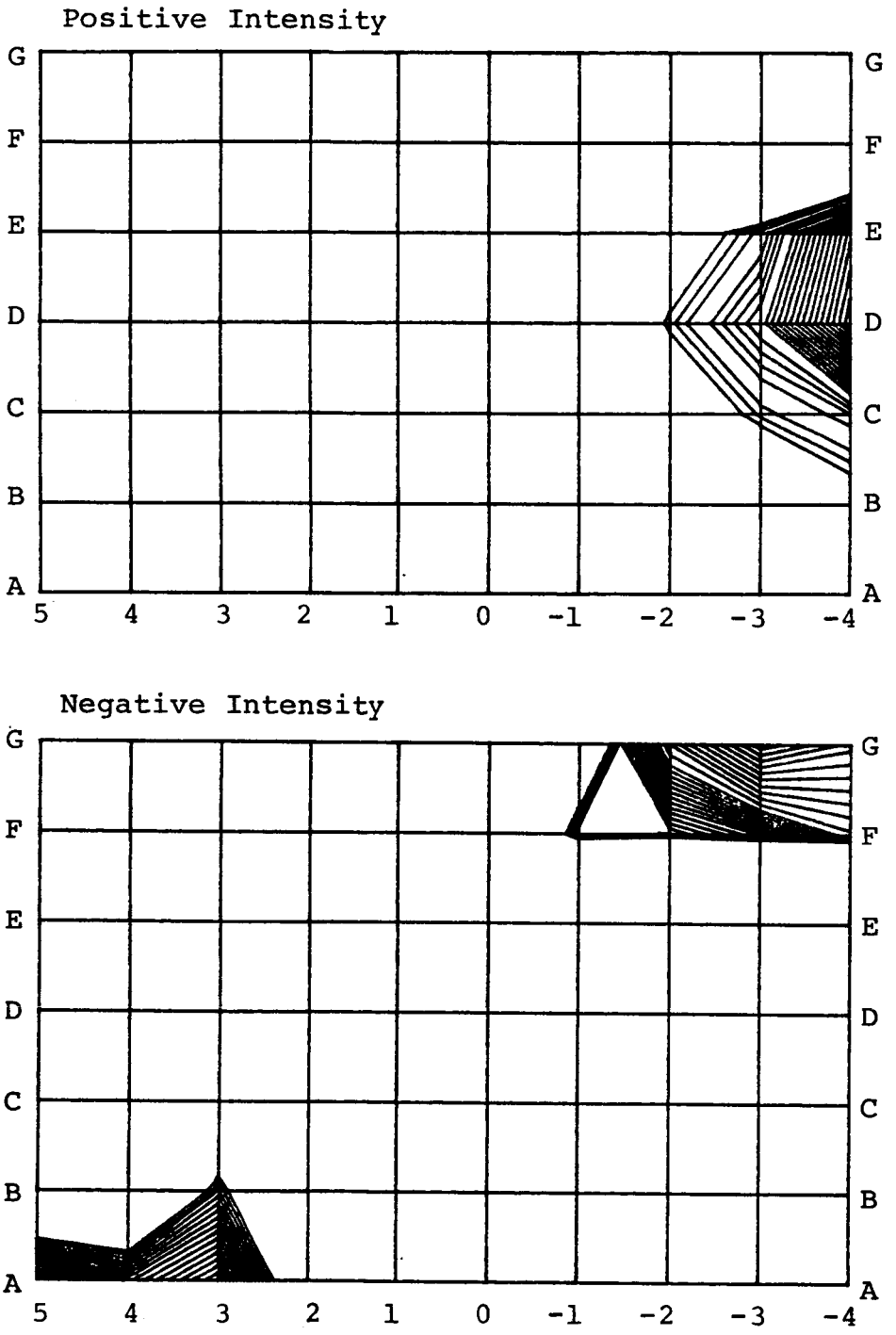

Figure 32: Aircraft B, Left Side
Left Engine On
Range: 100-110 dB
Frequency: 77 Hz

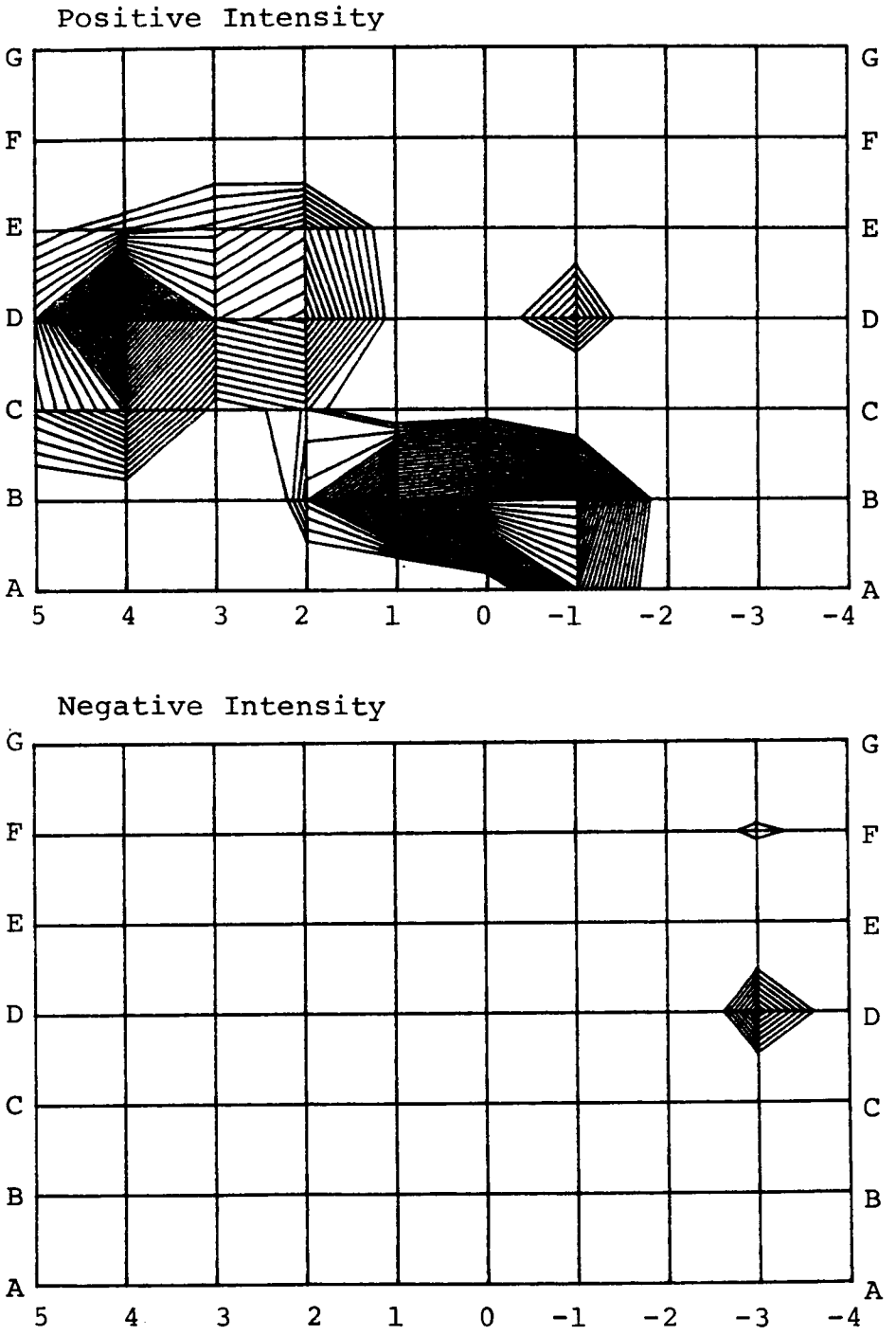

Figure 33: Aircraft B, Left Side
Left Engine On
Range: 90-100 dB
Frequency: 155 Hz

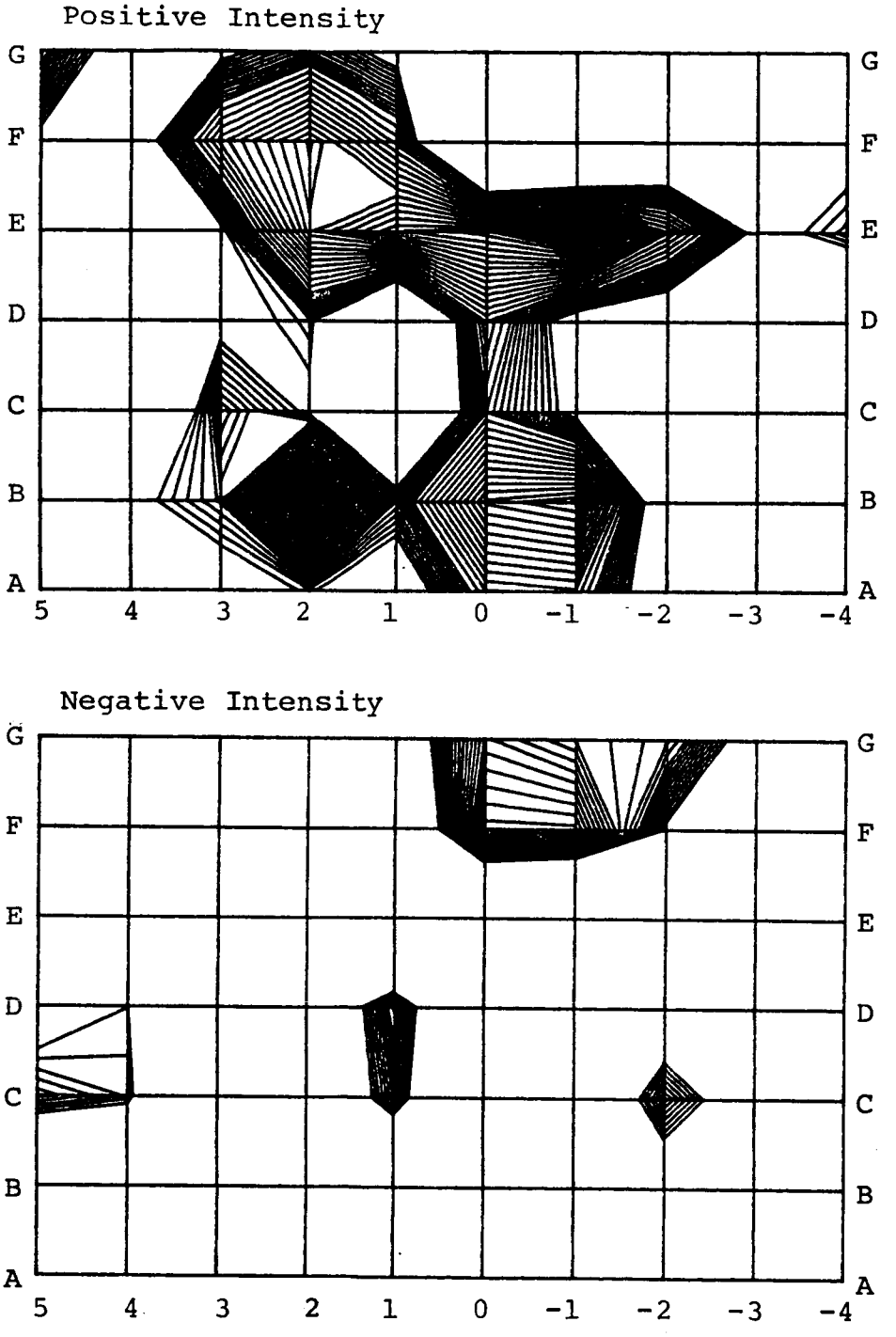

Figure 34: Aircraft B, Left Side
Left Engine On
Range: 80-90 dB
Frequency: 232 Hz

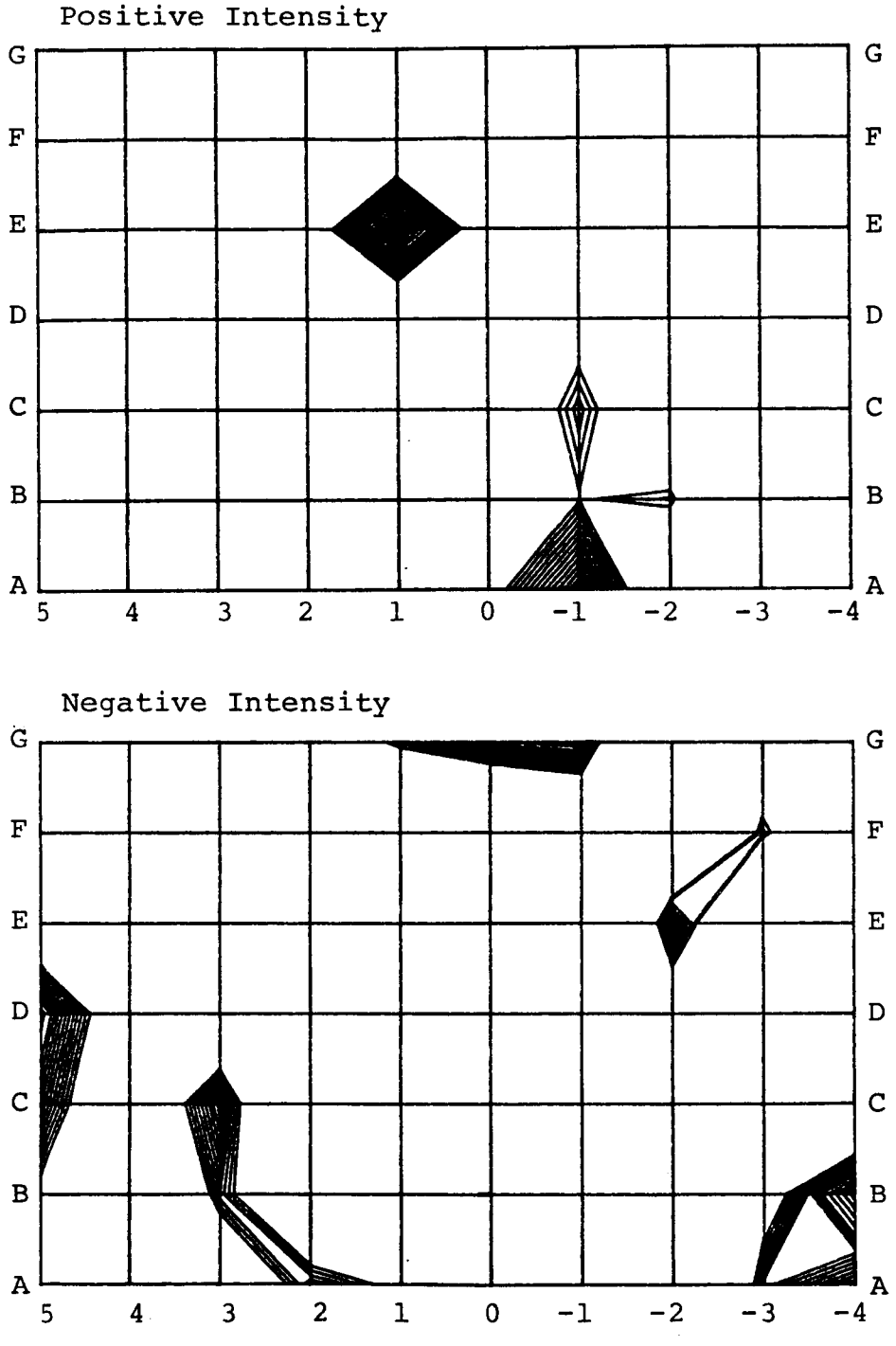

Figure 35: Aircraft B, Left Side
Left Engine On
Range: 80-90 dB
Frequency: 310 Hz

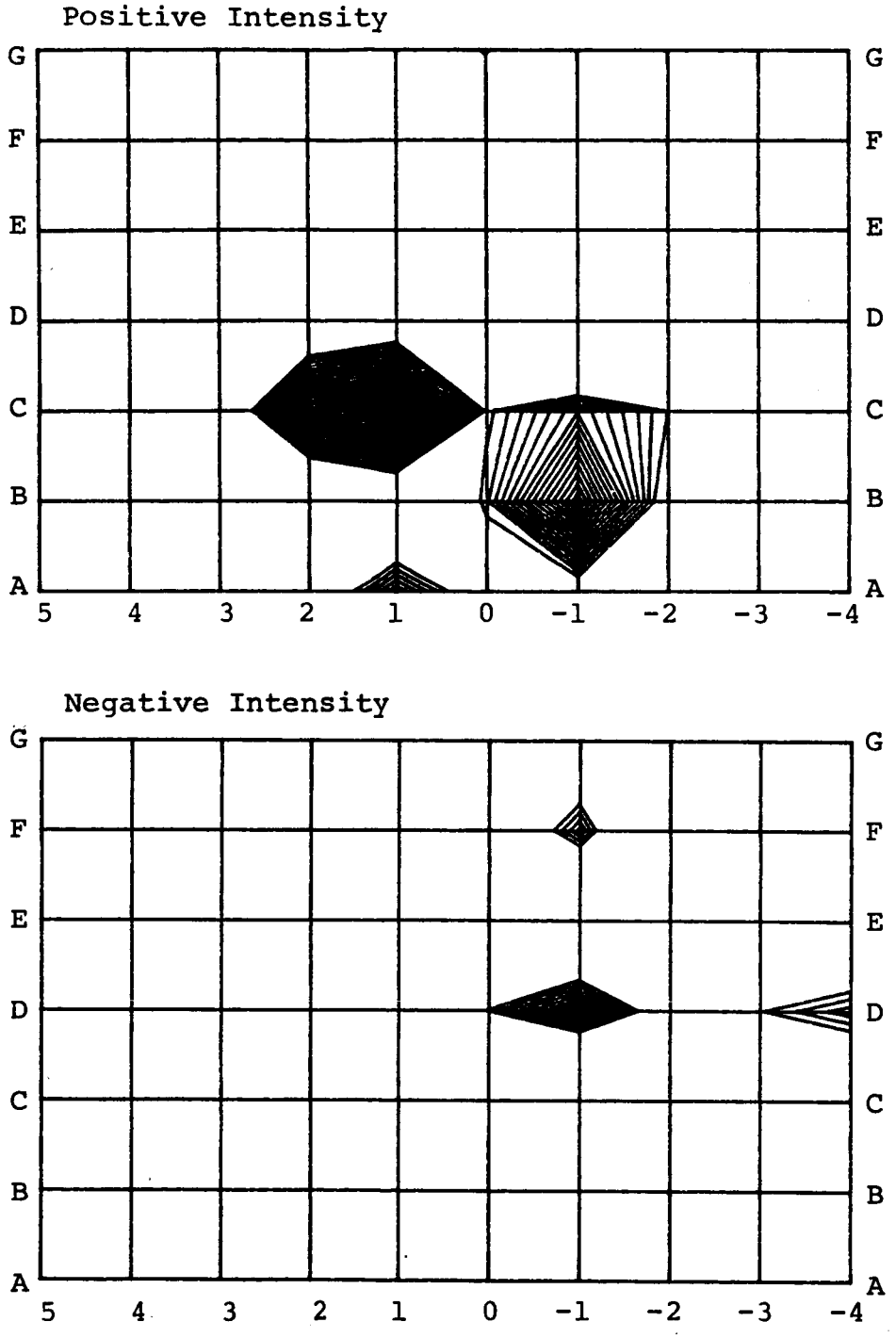

Figure 36: Aircraft B, Left Side
Left Engine On
Range: 80-90 dB
Frequency: 387 Hz

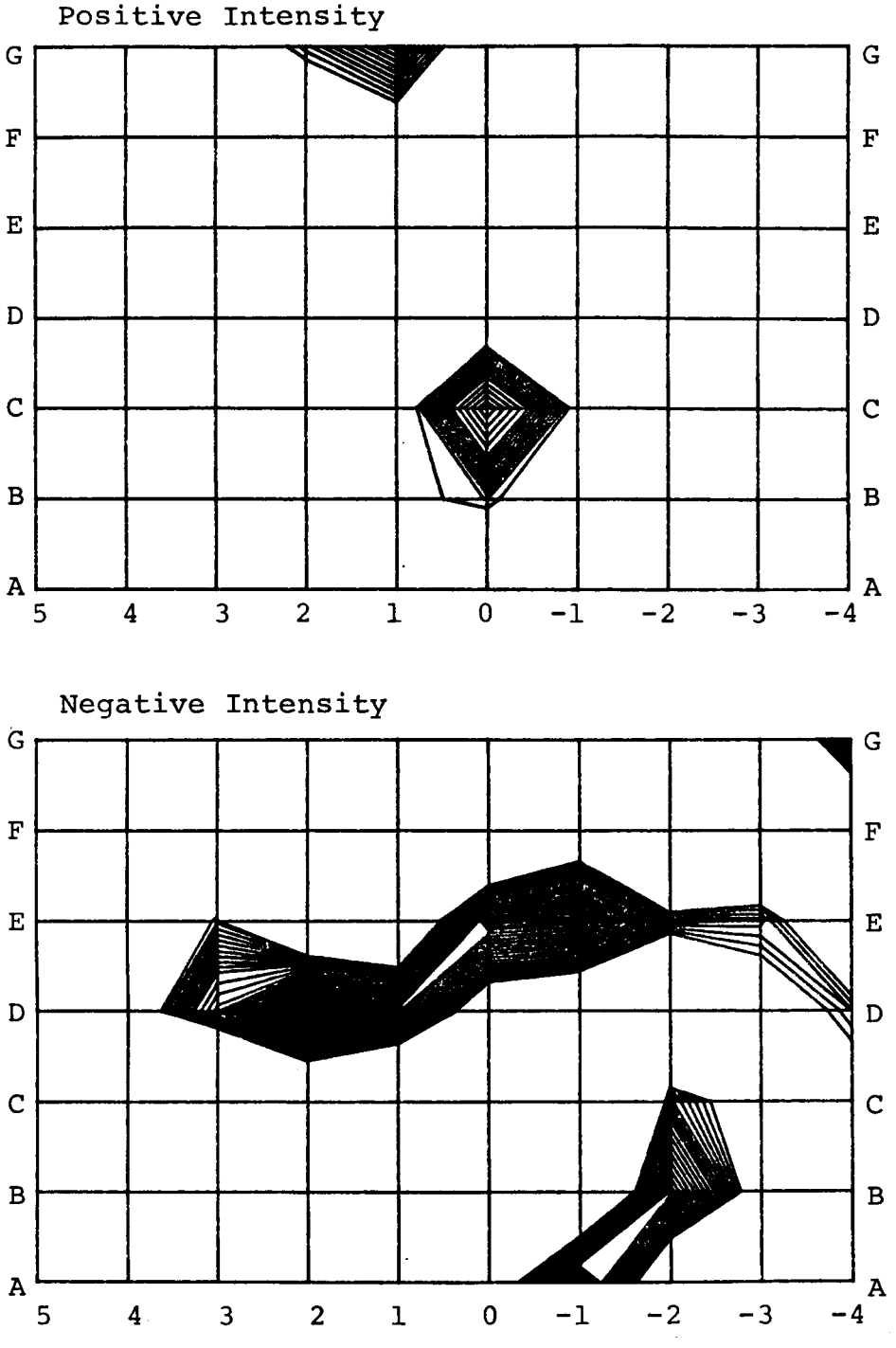

Figure 37: Aircraft B, Left Side
Left Engine On
Range: 80-90 dB
Frequency: 465 Hz

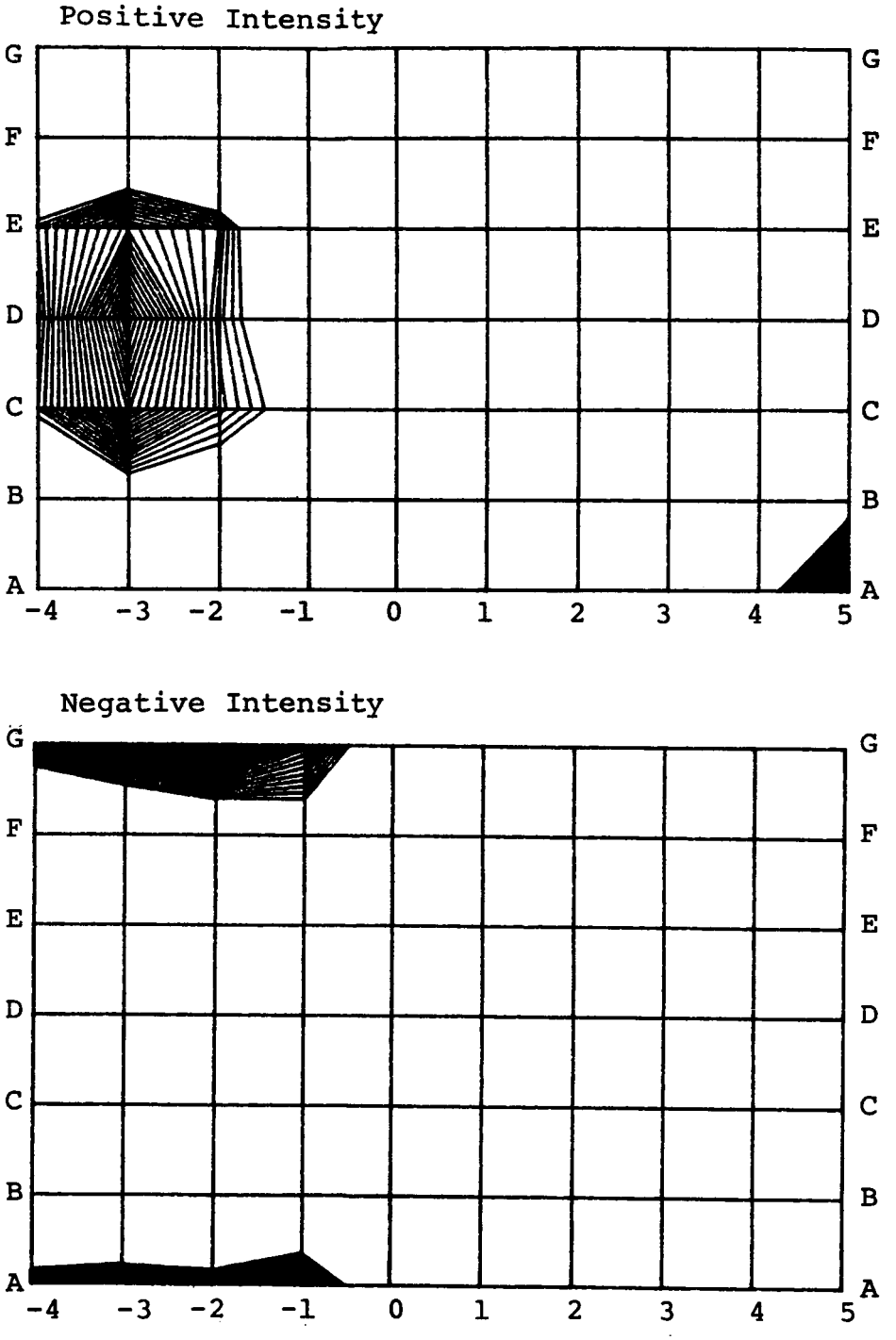

Figure 38: Aircraft B, Right Side
Right Engine On
Range: 100-110 dB
Frequency: 77 Hz

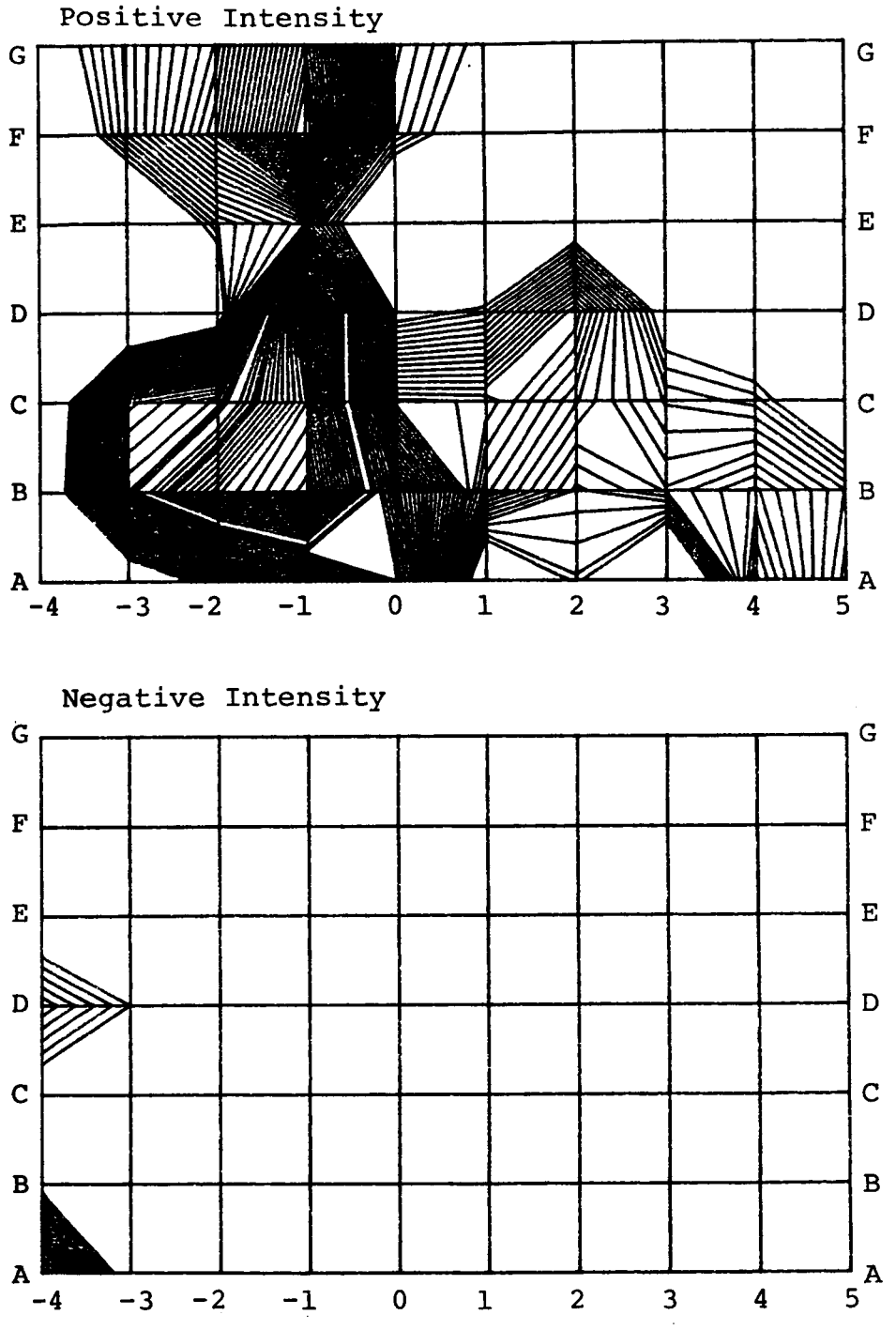

Figure 39: Aircraft B, Right Side
Right Engine On
Range: 90-100 dB
Frequency: 156 Hz

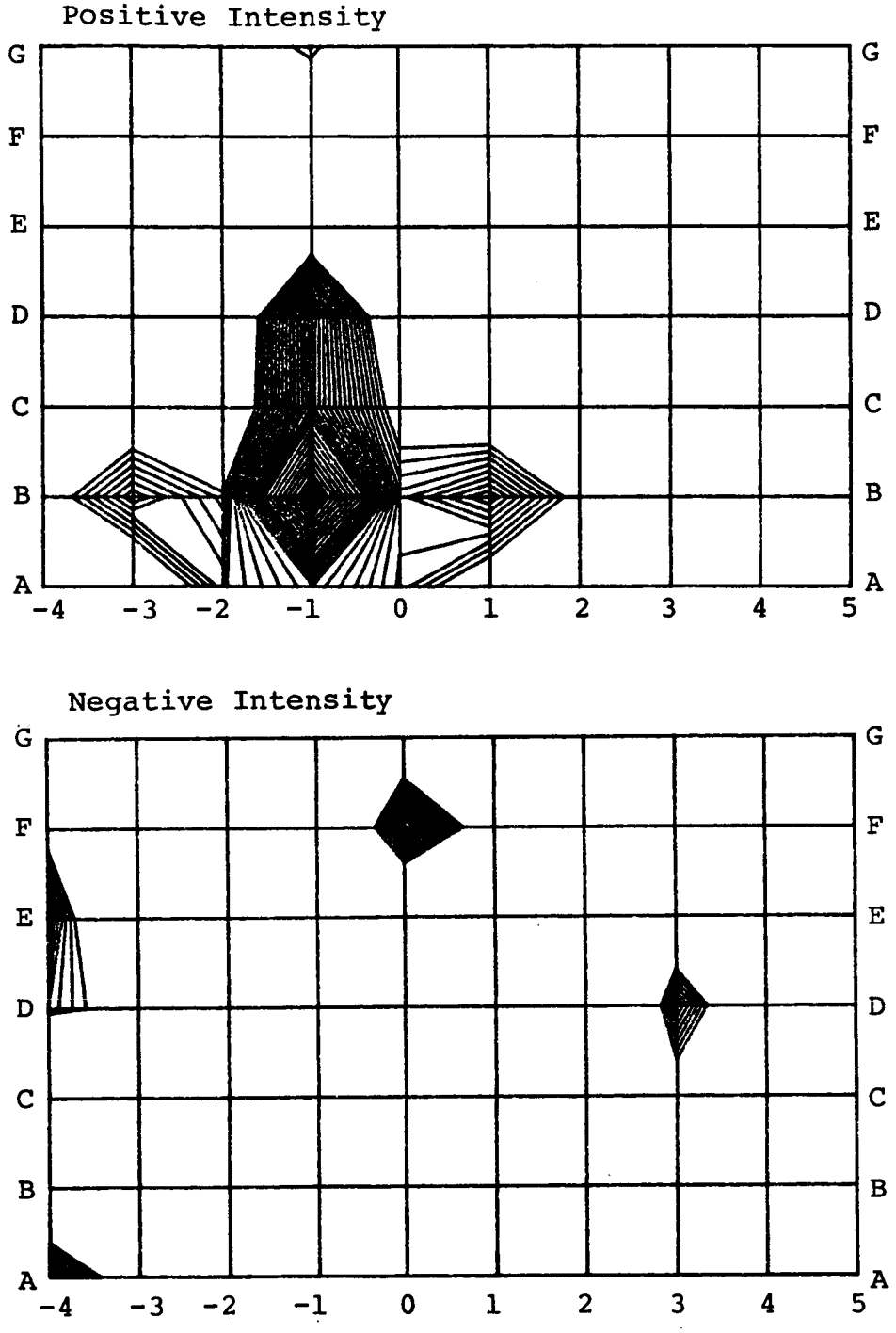

Figure 40: Aircraft B, Right Side
Right Engine On
Range: 90-100 dB
Frequency: 232 Hz

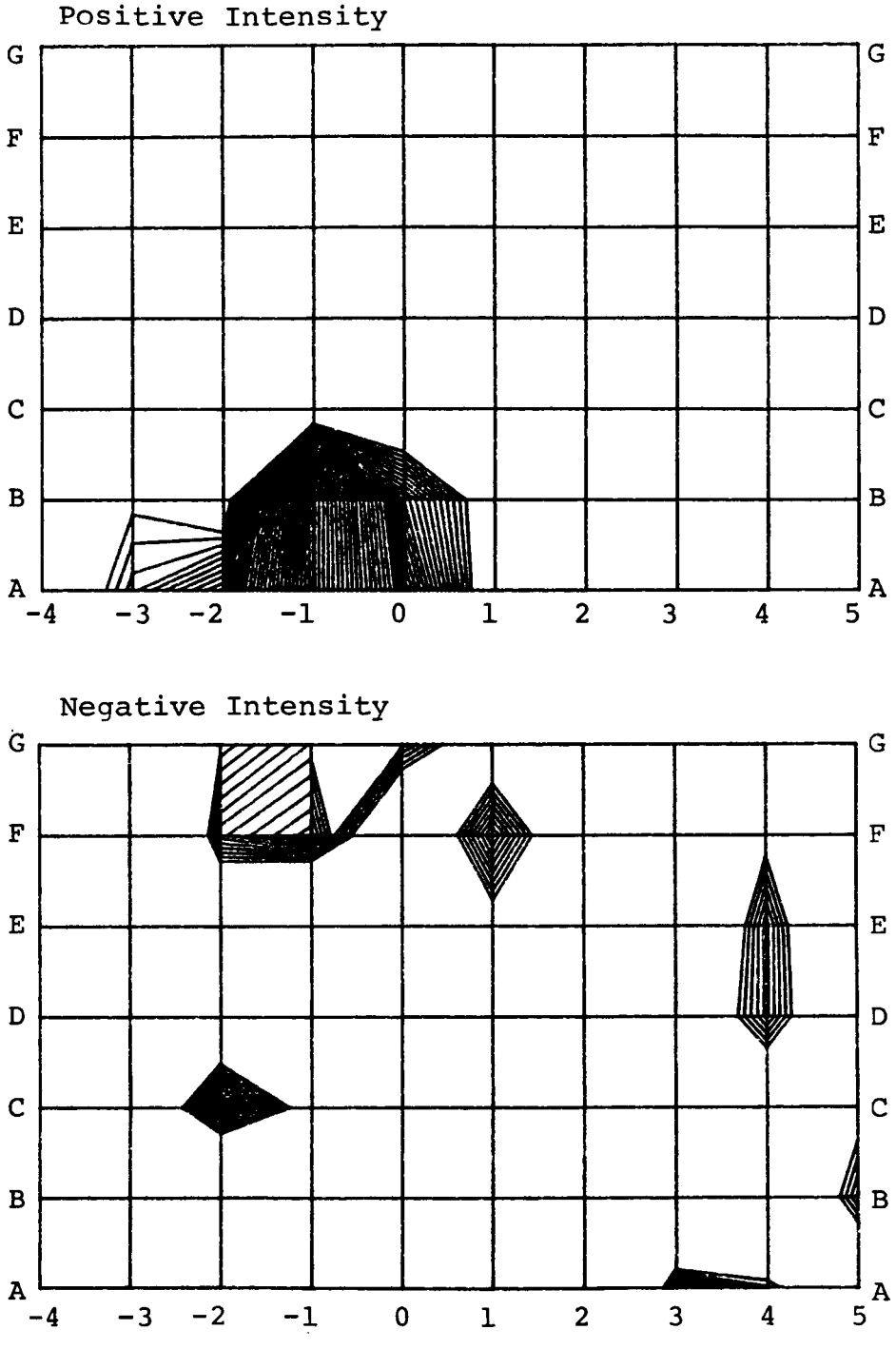

Figure 41: Aircraft B, Right Side
Right Engine On
Range: 90-100 dB
Frequency: 310 Hz

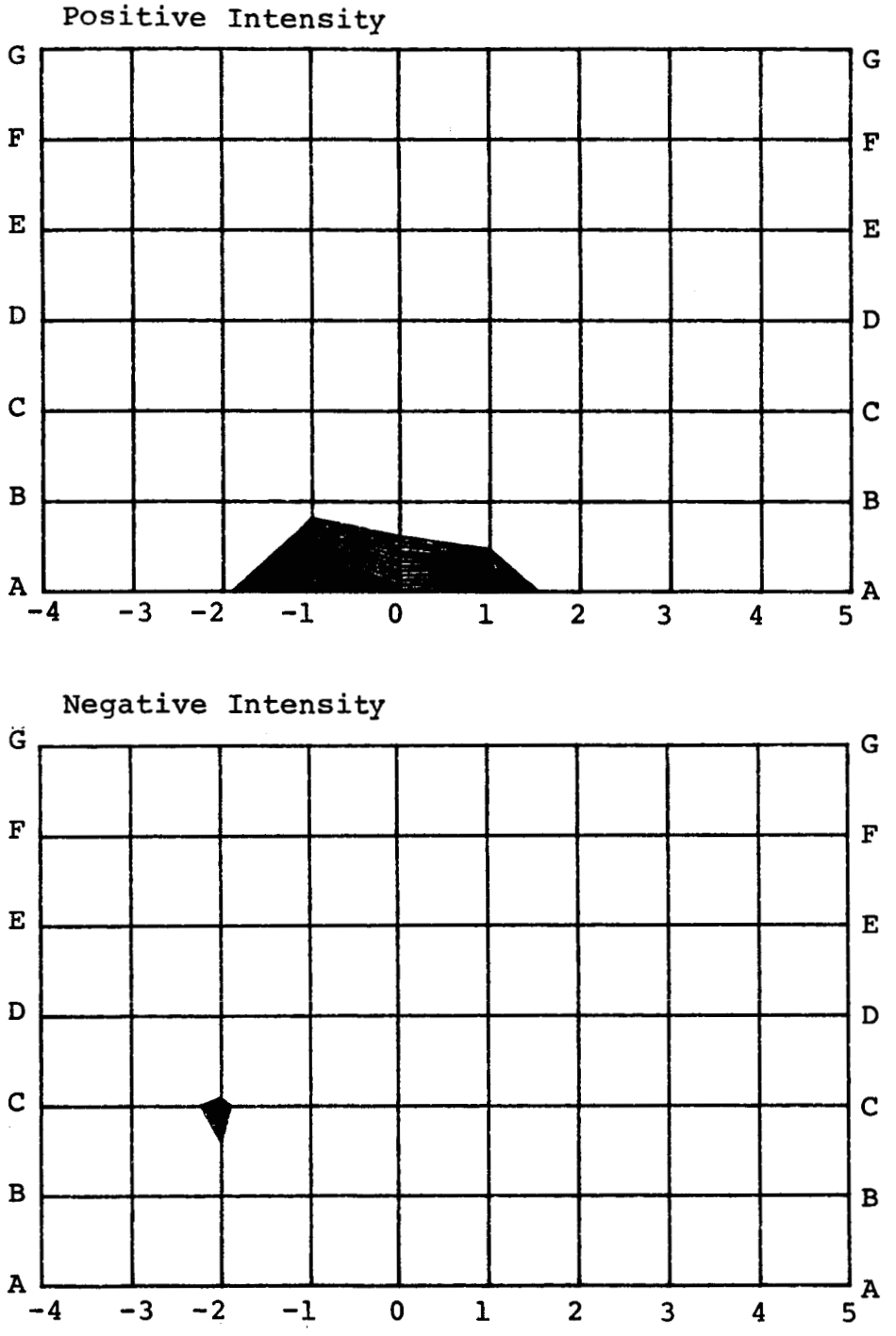

Figure 42: Aircraft B, Right Side
Right Engine On
Range: 90-100 dB
Frequency: 387 Hz

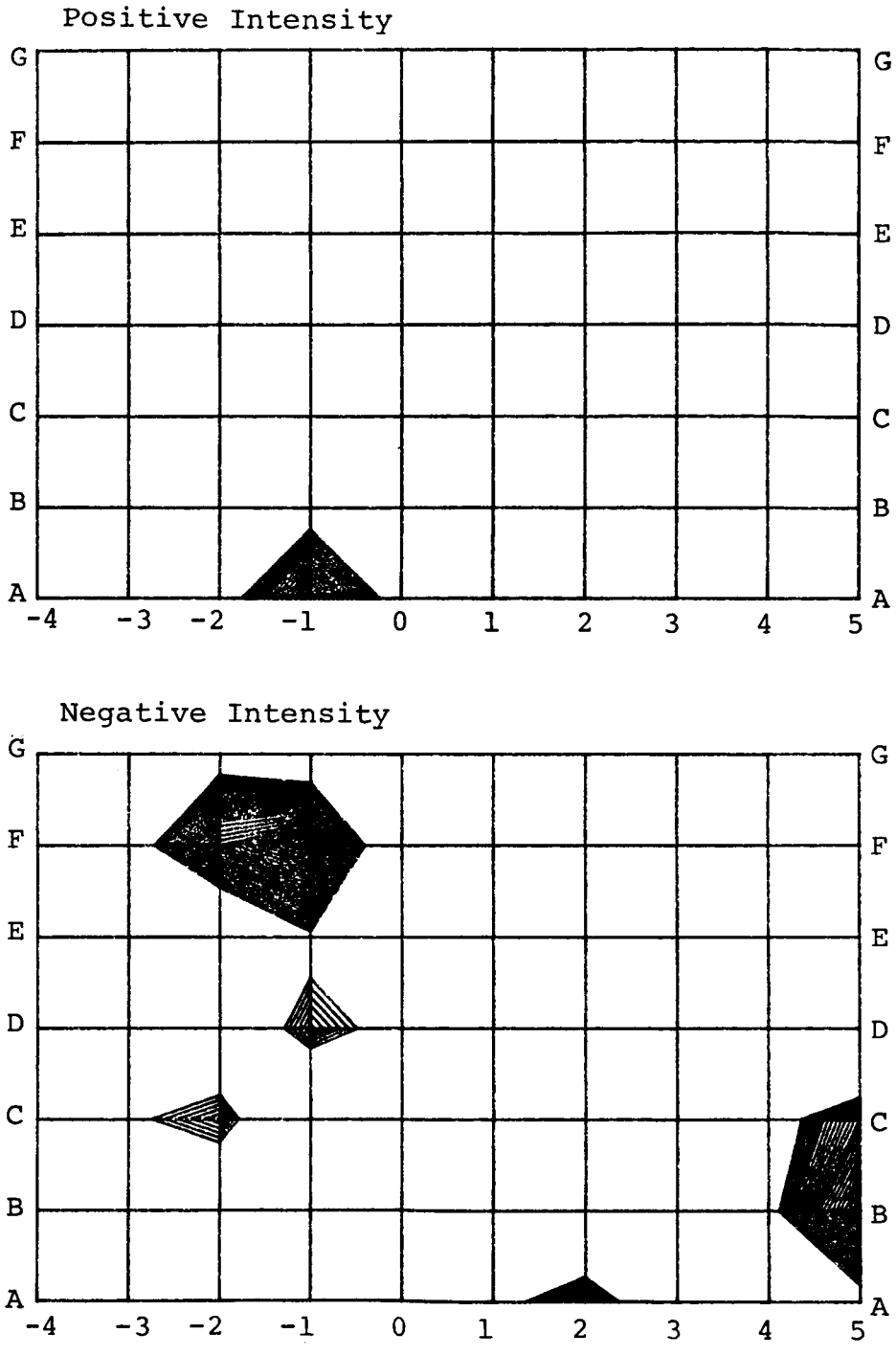

Figure 43: Aircraft B, Right Side
Right Engine On
Range: 90-100 dB
Frequency: 465 Hz

Positive Intensity

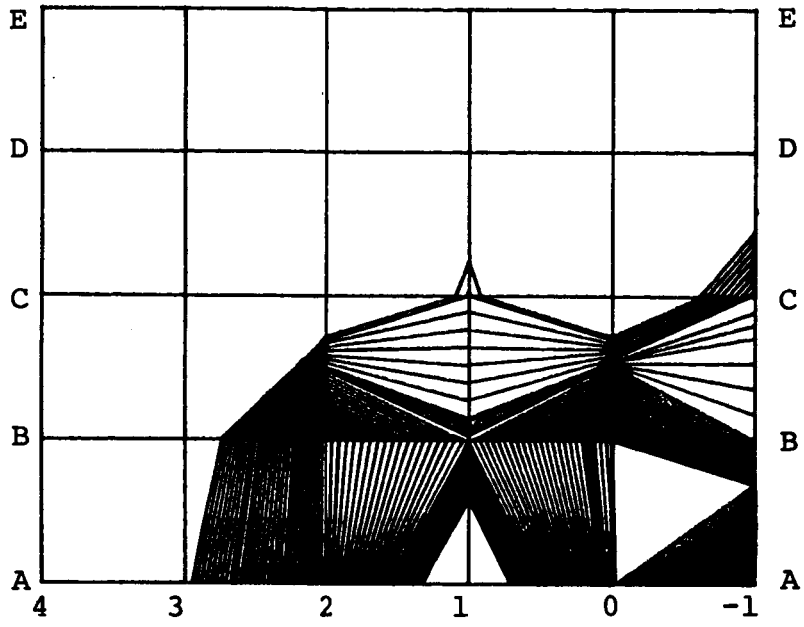

Negative Intensity

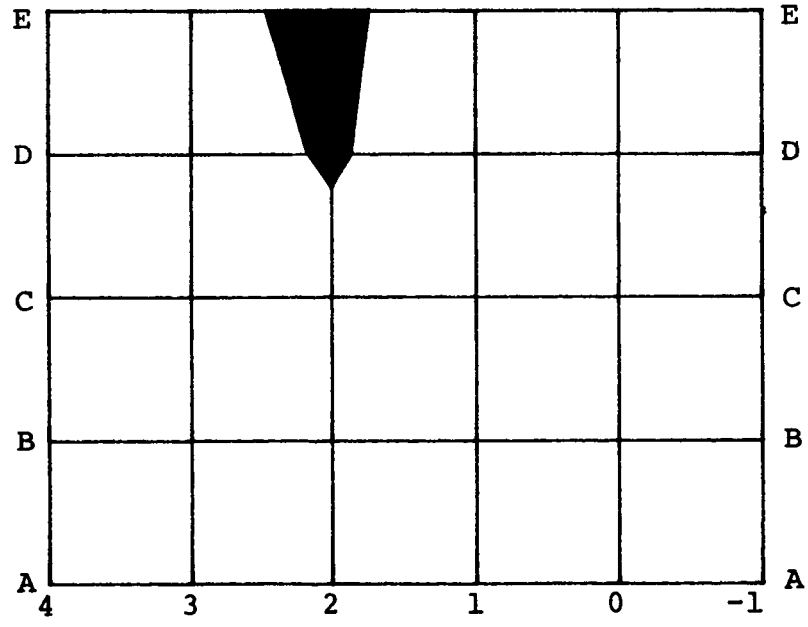

Canceller Off

Figure 44: Aircraft C, Left Side
Left Engine On
Range: 100-110 dB
Frequency: 0-500 Hz

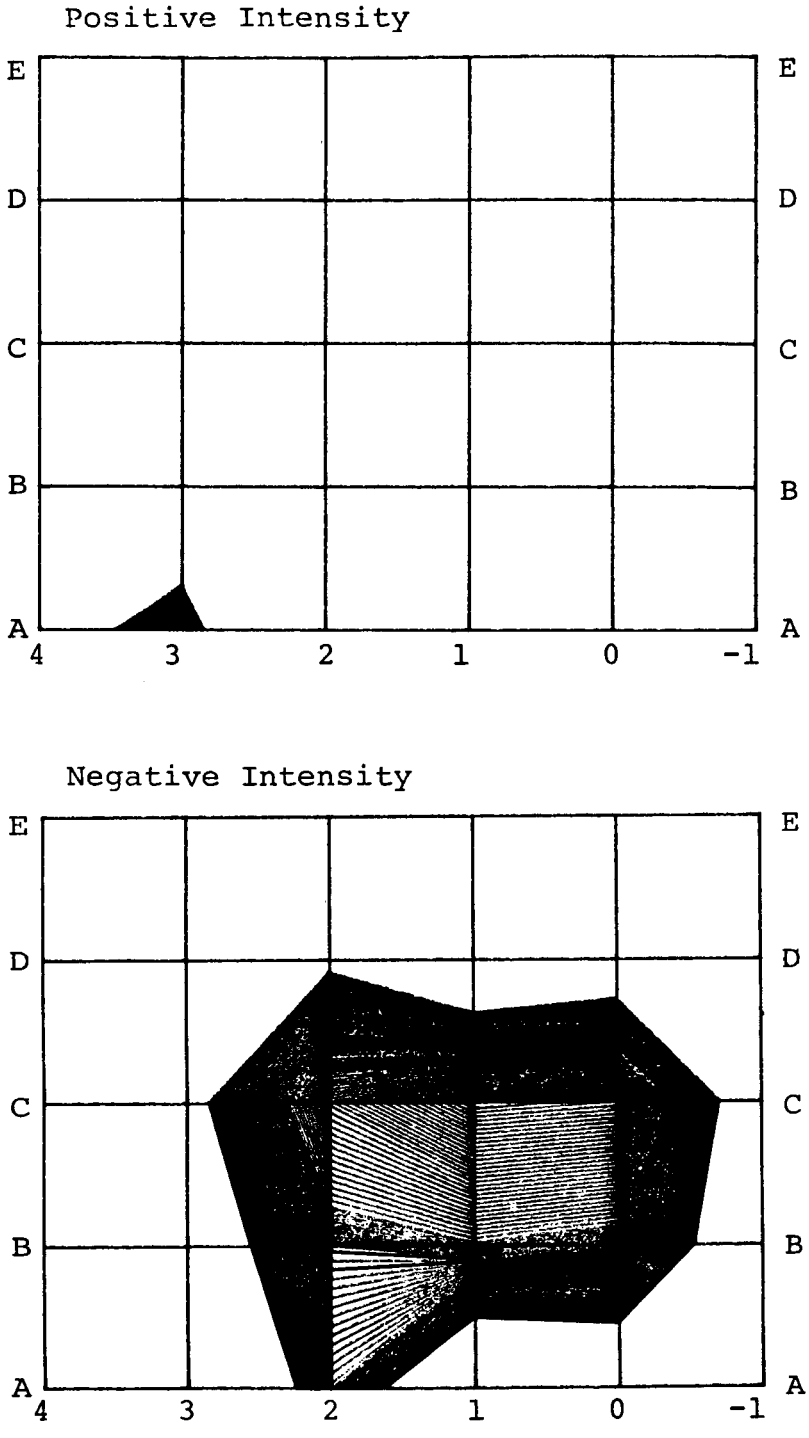

Figure 45: Aircraft C, Left Side
Left Engine On
Range: 100-110 dB
Frequency: 0-500 Hz

Positive Intensity

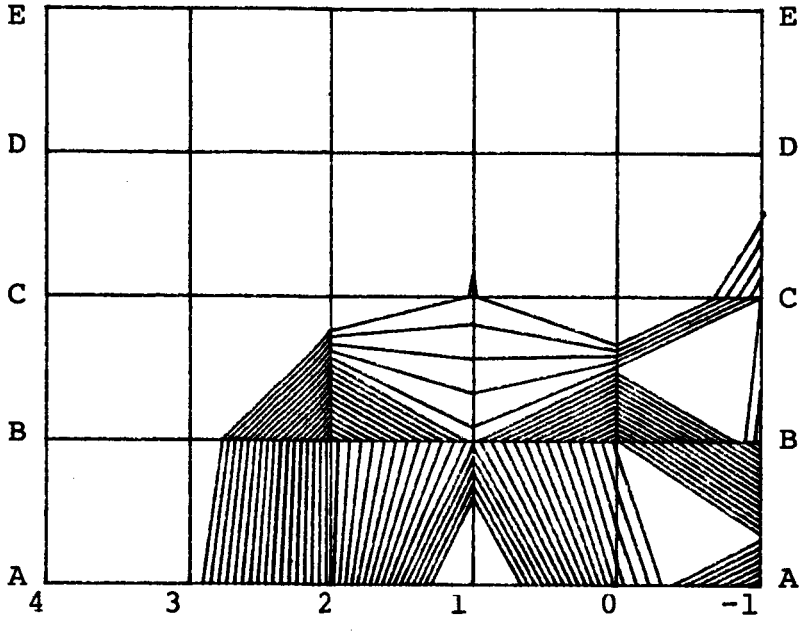

Negative Intensity

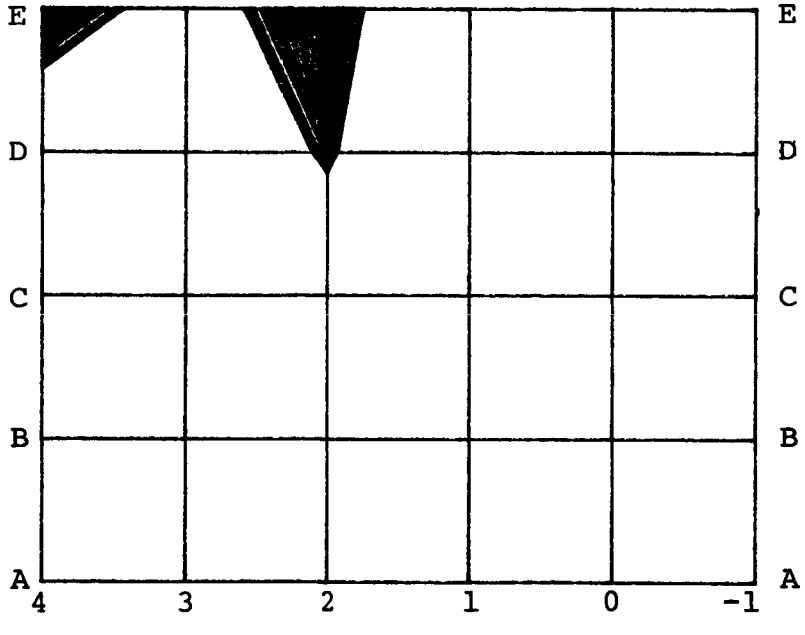

Canceller Off

Figure 46: Aircraft C, Left Side
Left Engine On
Range: 100-110 dB
Frequency: 100 Hz

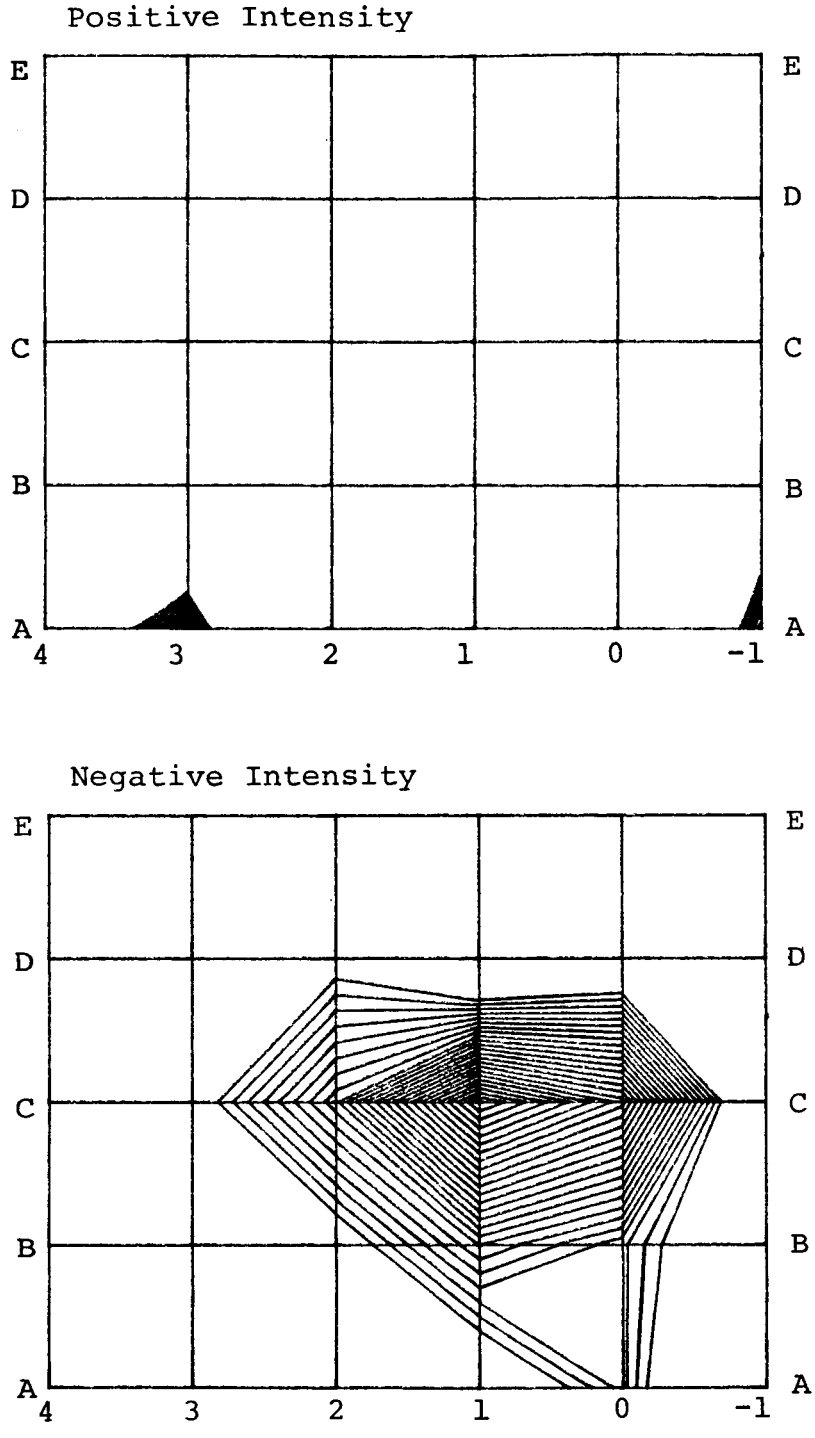

Canceller On

Figure 47: Aircraft C, Left Side
Left Engine On
Range 100-110 dB
Frequency: 100 Hz

Positive Intensity

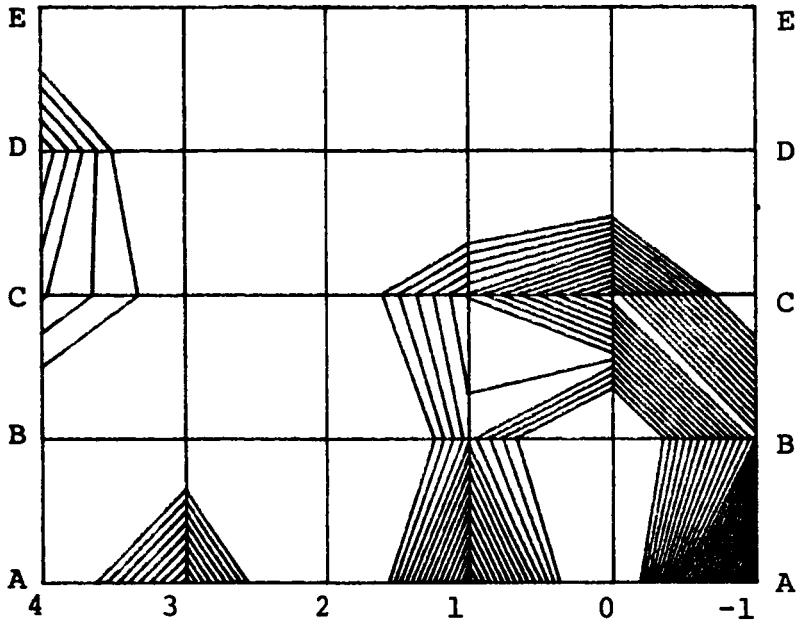

Negative Intensity

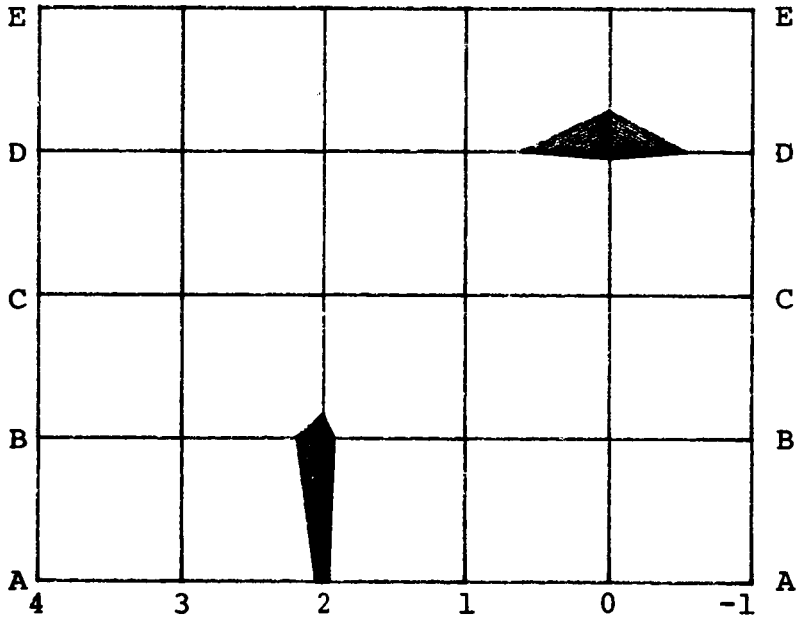

Canceller Off

Figure 48: Aircraft C, Left Side
Left Engine On
Range: 90-100 dB
Frequency: 200 Hz

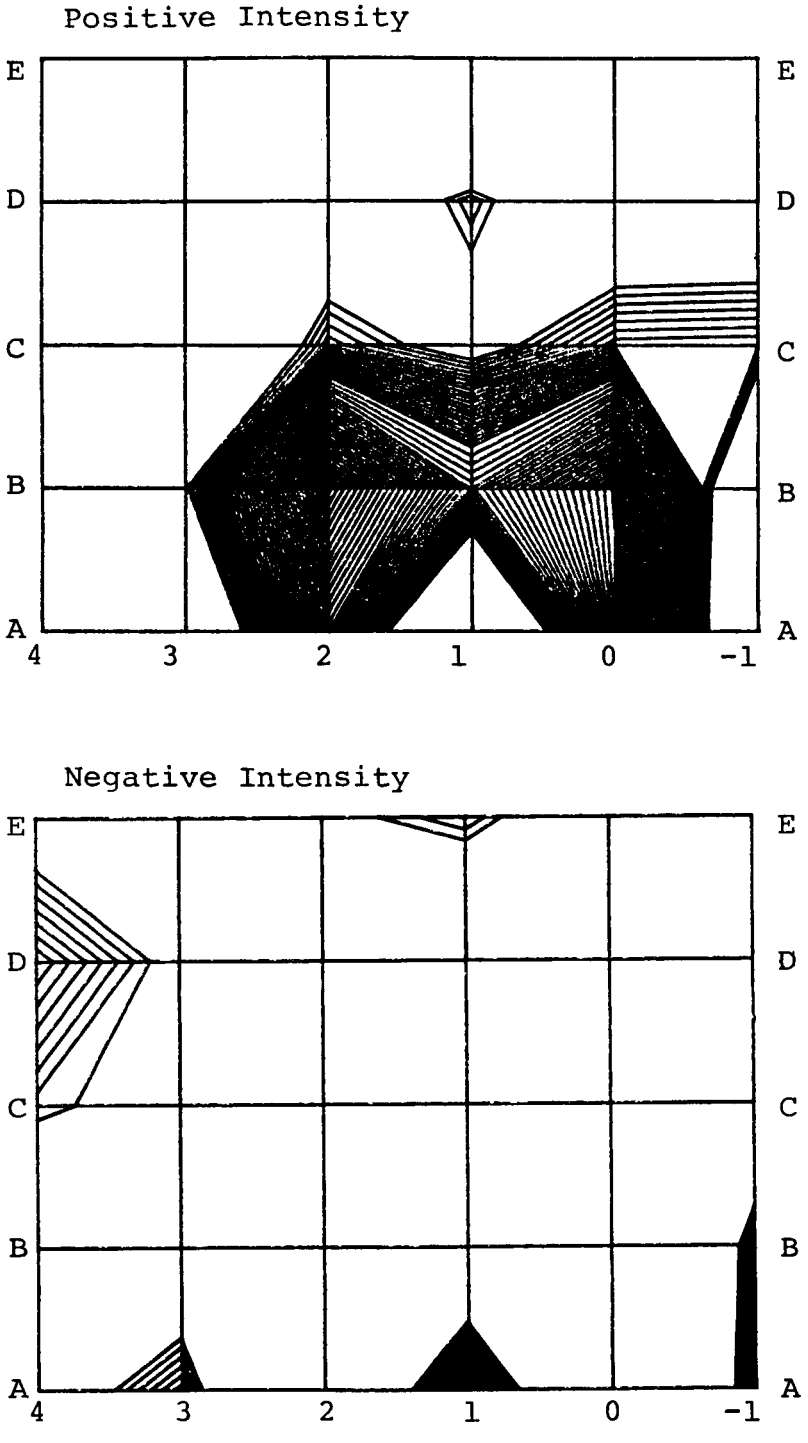

Canceller On

Figure 49: Aircraft C, Left Side
Left Engine On
Range: 90-100 dB
Frequency: 200 Hz

Positive Intensity

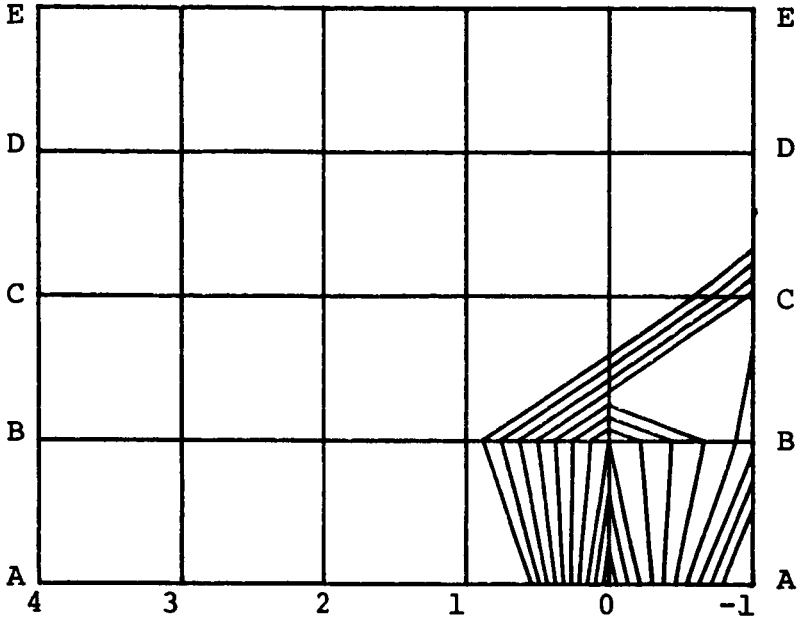

Negative Intensity

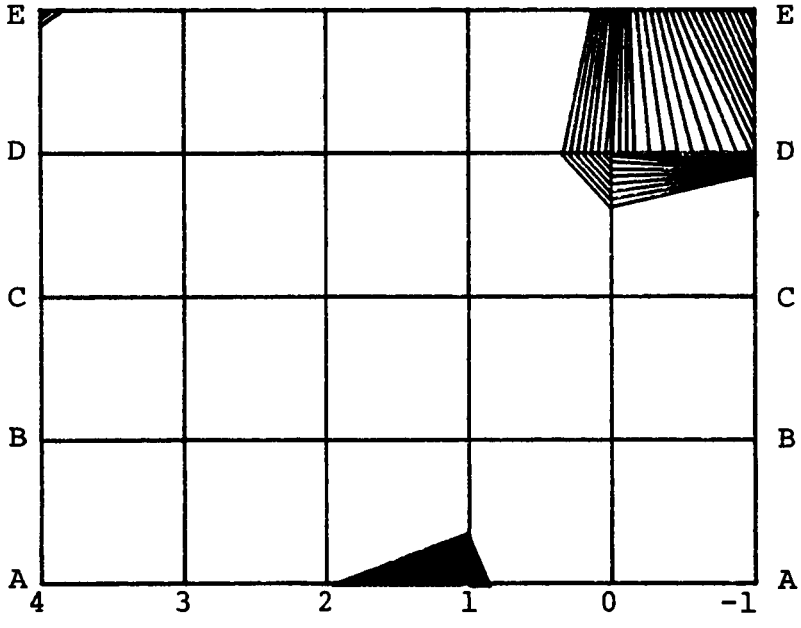

Canceller Off

Figure 50: Aircraft C, Left Side
Left Engine On
Range: 90-100 dB
Frequency: 300 Hz

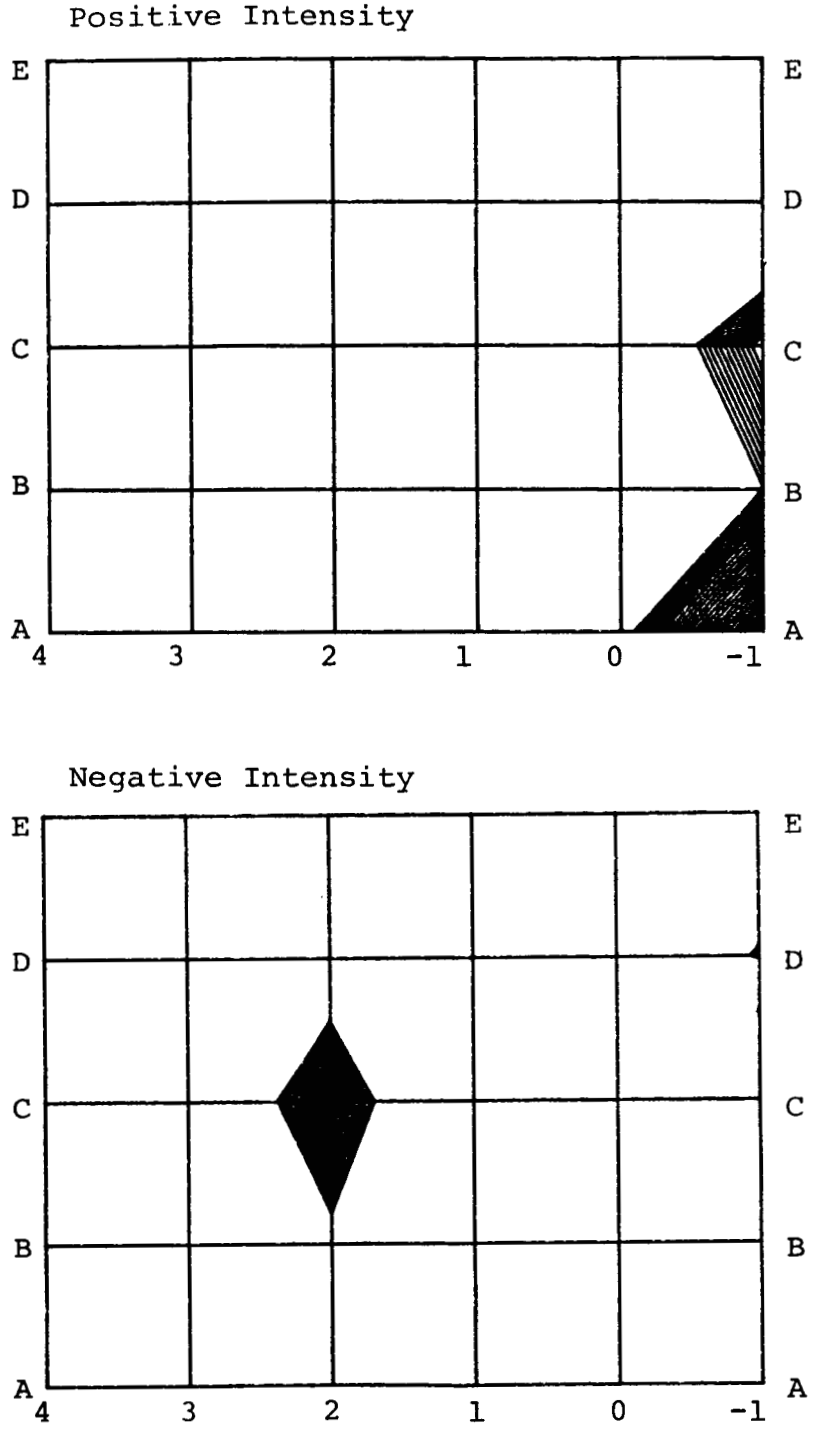

Figure 51: Aircraft C, Left Side
Left Engine On
Range: 90-100 dB
Frequency: 300 Hz

Positive Intensity

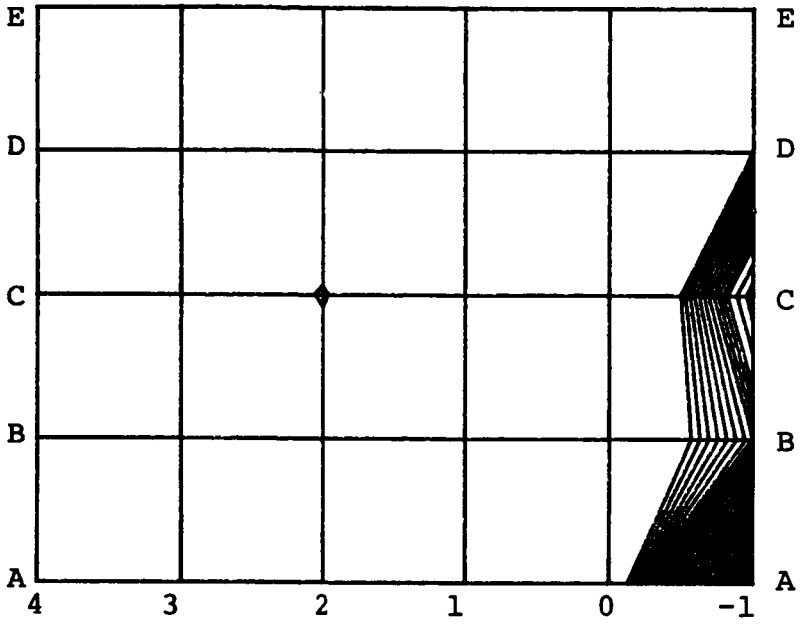

Negative Intensity

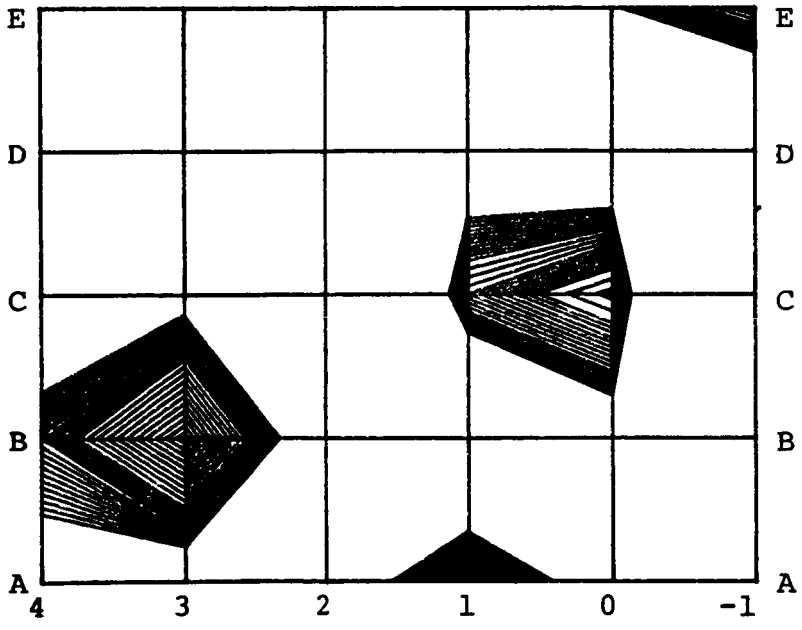

Canceller Off

Figure 52: Aircraft C, Left Side
Left Engine On
Range 80-90 dB
Frequency: 400 Hz

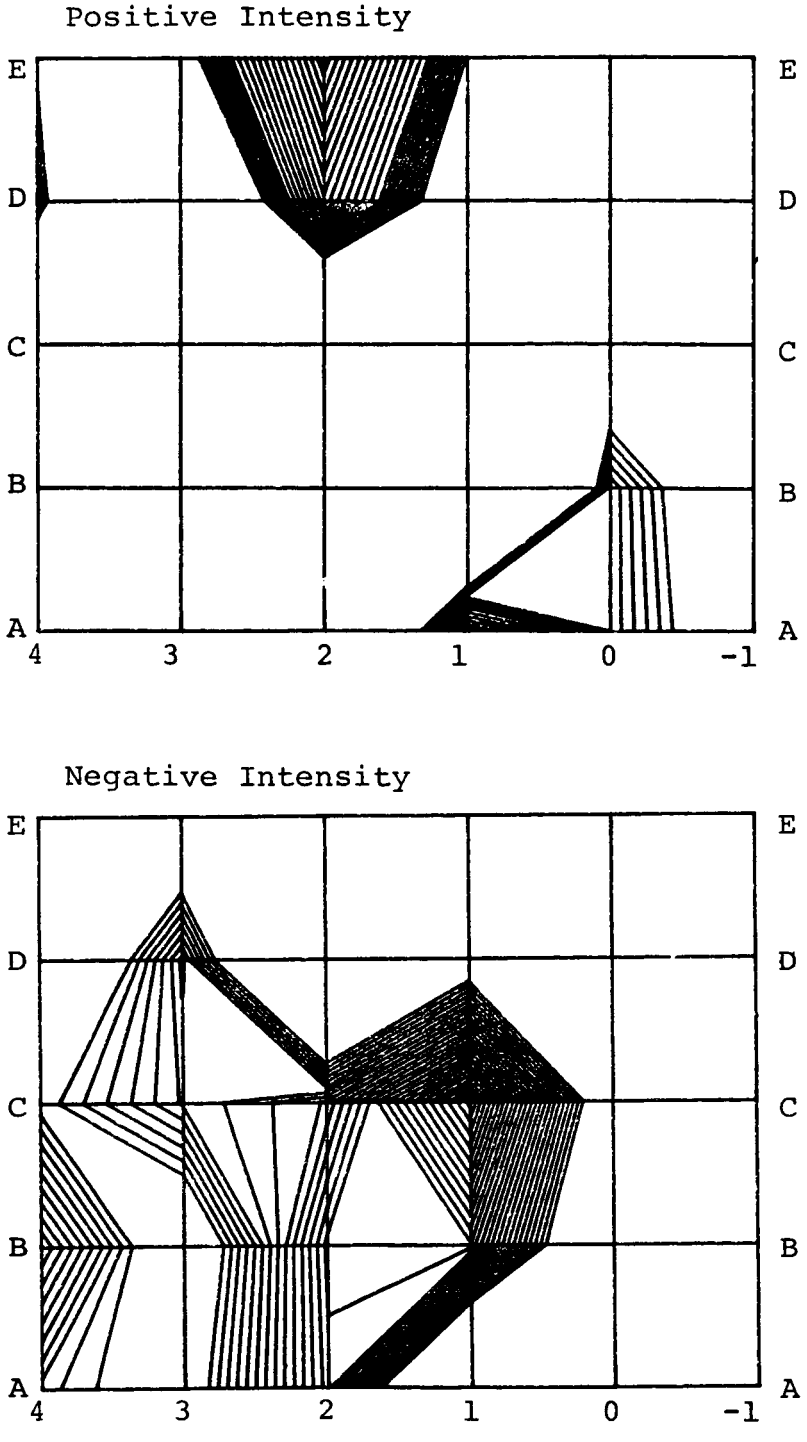

Canceller On

Figure 53: Aircraft C, Left Side
Left Engine On
Range: 80-90 dB
Frequency: 400 Hz

APPENDIX

Basic Approach to Sound Field Control

This section addresses some basic problems of the feedback approach to sound field cancellation in an enclosure. The existing experience with these systems indicates that the degree of sucess and the complexity of these systems depends to a great extent on the way the acoustic energy is injected into the enclosure. If the noise source is small, it is usually feasible to reduce its sound power radiation by placing the cancellation sources in its close vicinity, and to create in this way a higher order source which has a low radiation efficiency at the low frequencies. The control of such a system requires only one microphone and the noise reduction is achieved everywhere in the enclosure.

For large noise sources or multiple sources distributed inside the enclosure or over its walls, such as in an airplane fuselage, the cancellation problems become much more complex and a global cancellation cannot be achieved by a simple system.

So far, a definite scheme for an overall cancellation has not been found. The purpose of this section is to point out some fundamental problems and suggest one possible way to approach this problem.

Any noise reduction scheme based on radiation of sound from suitably located and controlled auxiliary sources represents a feedback system. Therefore, before analyzing more complex systems, the basic function and stability criteria of such a system will be summarized.

The properties of the sound fields, as well as of the electronic systems, can be described in terms of their transfer functions. The basic configuration of the feedback system is shown in Figure 54.

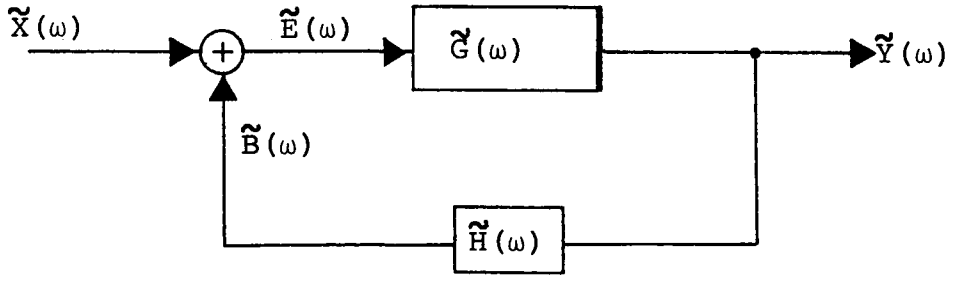

Figure 54: Configuration of Feedback System

A system is described in the frequency domain by its transfer function $\tilde{G}(\omega)$ which will, in the case of a sound field, represent the properties of the sound path between points A and B . Let us assume that a sound source with an output $\tilde{X}(\omega)$ is placed in point A and a microphone in point B . The microphone voltage will be amplified by a system described by $\tilde{H}(\omega)$. The equations describing the system in Figure 54 can be formulated as

$$\left.\begin{aligned} \tilde{E}(\omega) &= \tilde{X}(\omega)+\tilde{B}(\omega) \\ \tilde{Y}(\omega) &= \tilde{G}(\omega)\tilde{E}(\omega) \\ \tilde{B}(\omega) &= \tilde{H}(\omega)\tilde{Y}(\omega) \end{aligned}\right\} \quad . \tag{1}$$

The symbol $\tilde{}$ above a quantity denotes a complex number. However, as most of the quantities are complex, we will use it only when needed to distinguish from the absolute value.

The system response $\tilde{T}(\omega)$ from Equation (1) will be

$$\tilde{T}(\omega) = \frac{\tilde{Y}(\omega)}{\tilde{X}(\omega)} = \frac{\tilde{G}(\omega)}{1 - \tilde{G}(\omega)\tilde{H}(\omega)} \quad . \tag{2}$$

System stability. In general, the transfer functions will be complex. The system will be stable if the Nyquist's criteria for unconditional stability are satisfied. The system will be unstable only if (Reference 7)

$$\left.\begin{aligned} &|\tilde{L}(\omega)| \geq 1.0 \\ &\text{and} \\ &\psi(\omega) = 2\pi n \qquad n = 0,\pm 1,\ldots \end{aligned}\right\} \quad , \tag{3}$$

where

$$\tilde{L}(\omega) = \tilde{G}(\omega)\tilde{H}(\omega) = L(\omega)\, e^{j\psi(\omega)} \quad . \tag{4}$$

As it can be shown, both theoretically and practically, the stability conditions can impose constraints on the actual construction of the controlling electronics and have to be observed in much broader frequency range than the range of our interest.

Sound field in an enclosure. The enclosure of interest to us is an aircraft fuselage, representing very complex sound field boundaries. The walls consist of a heterogeneous structure with wall impedance frequency- and position-dependent. The internal furnishings of the airplane consisting of chairs and other objects is also part of the boundary.

A sound field in an enclosure can be mathematically represented by the eigenfunctions which are obtained by solving the wave equation

for the given boundary conditions. Although we cannot find a closed form solution for the fuselage interior, the eigenfunction concept is very useful to analyze the sound field control, particularly at the low frequency region of our interest. As shown in the literature (Reference 8), the sound field in an aircraft fuselage can be quite often approximated at low frequencies by a field of a mathematically idealized shape.

The eigenfunctions $\psi_N(x,y,z)$ describe the sound field properties at a point (x,y,z). Each mode expressed by an eigenfunction has a specific frequency f_N in a three-dimensional space, where N represents a combination of three integers.

The sound pressure at a point (x,y,z) inside the enclosure can be expressed in terms of the eigenfunction sum

$$p(x,y,z) = \sum_N A_n \psi_N(x,y,z) \quad , \tag{5}$$

where A_N are coefficients dependent upon the spacial distribution of sources and their volume velocities. If the enclosure boundaries can be described by an impedance which is locally reactive (as opposed to an impedance with extended reaction), the eigenfunctions are orthogonal which means that

$$\int_V \psi_N(x,y,z)\psi_M(x,y,z)\,dxdydz = \begin{cases} 0 & N \neq M \\ V\,\Lambda_N & N = M \end{cases} \quad , \tag{6}$$

where the integral is executed over the total enclosure volume V.

Let us examine first a sound field generated in an enclosure by a small source (approximated by a point source) of a uniform surface velocity u_s and an area A_s, so that its volume velocity $Q_s = A_s u_s$. If the source is located at a point $(x_o y_o z_o)$, then the forced sound field at (x,y,z) can be calculated from (Reference 9)

$$p(x,y,z) = \frac{j\omega\rho Q_s}{V} \sum_N \frac{\psi_N(x_o,y_o,z_o)\psi_N(x,y,z)}{\Lambda_N(K_N^2 - k^2)} \quad , \tag{7}$$

where $k = \omega/c$ and $K_N = \omega_N/c$ is the wave number of the N^{th} mode. With a finite wall impedance or any damping of the wave propagation inside the enclosure, K_N is complex:

$$\tilde{K}_N = \beta_N + j2\alpha_N\beta_N \quad , \tag{8}$$

where α_N represents the damping. For α_N small (low damping),

$$\tilde{K}_N^2 \simeq \beta_N^2 + j2\alpha_N\beta_N \quad . \tag{9}$$

If Equation (9) is substituted into Equation (7), the denominator at a resonance for $k = \beta_N$ is finite and the sound pressure has no singularities.

Generally, the noise field in a fuselage is not excited by a single point source because its whole structure vibrates and the sources are distributed all over the fuselage surface. In this case, the source term in Equation (7) is replaced by the summation over the source surface area and

$$p(x,y,z) = j\frac{\omega\rho}{V}\sum_N \frac{\psi_N(x,y,z)}{\Lambda_N(K_N^2 - k^2)}\iint_S u_n(x_o,y_o,z_o)\psi_N(x_o,y_o,z_o)dS_o \quad . \tag{10}$$

The integral is executed over the boundary with a distributed normal component of the velocity u_n .

Although Equation (10) describes the field more generally, Equation (7) for a point source may be useful because quite often the sound penetrates into the airplane through relatively small areas, close to the outside sources, such as a propeller. As shown earlier in the report, the results of the intensity measurements allow this first order approximation.

As has been proven by computer calculations, the convergence of the series of Equation (7) can be very slow if the source and the receiver are very close. This is because the sound field at the observation point is dominated by the direct field which, in the absence of boundaries, would be given by

$$p(R) = j\omega\rho Q_s \frac{e^{-jkR}}{4\pi R} \quad , \tag{11}$$

where R is the distance between the source and the receiver. In order to simplify some calculations, Morse (Reference 9) developed an approximation consisting of the direct field and the reverberant field terms

$$p(x,y,z) = j\frac{\omega\rho Q_s e^{-jk\alpha}}{4\pi a} + jk^3\rho c Q_s \sum_{N=1}^{\infty} \frac{\psi_N(x_o,y_o,z_o)}{V\Lambda_N K_N^2 (K_N^2 - k^2)} \quad . \tag{12}$$

The above equation is valid only for the source-receiver distance a very small compared with the wavelength and low frequencies.

Noise Reduction Systems with One Controller

Before considering more complicated schemes, we will analyze a system with one source and one controller. The arrangement is shown schematically in Figure 55. A small source vibrates with a surface velocity u_s so that the sound pressure p_r is generated at the

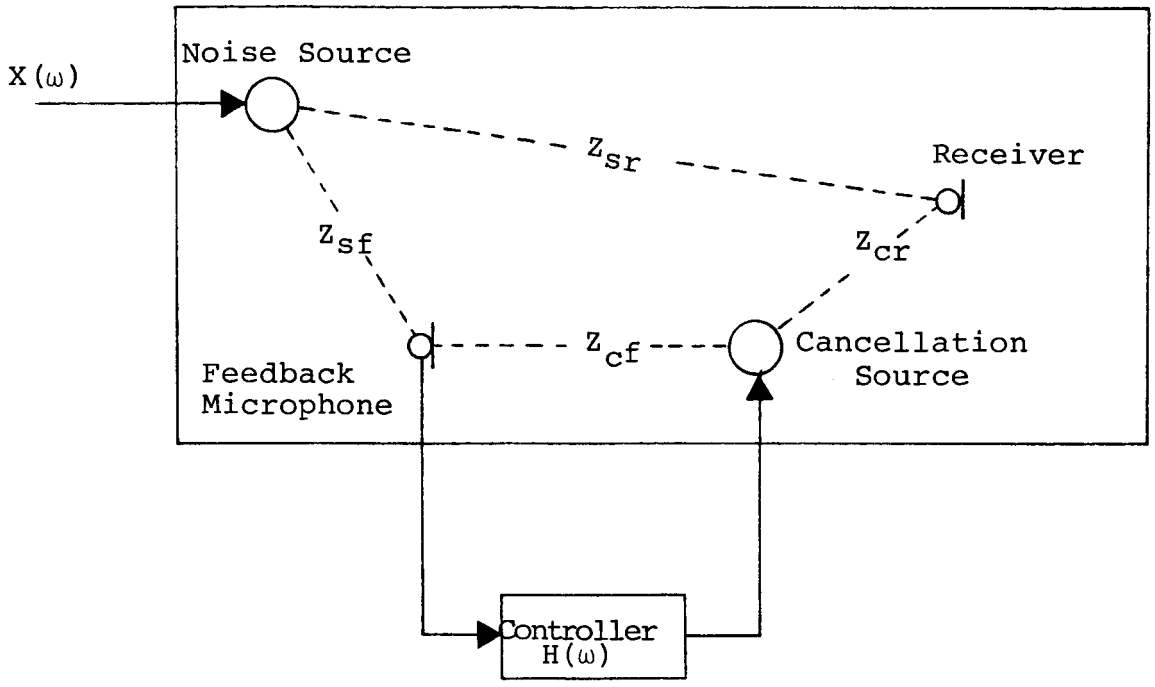

Figure 55: Cancellation System with one Source and one Controller

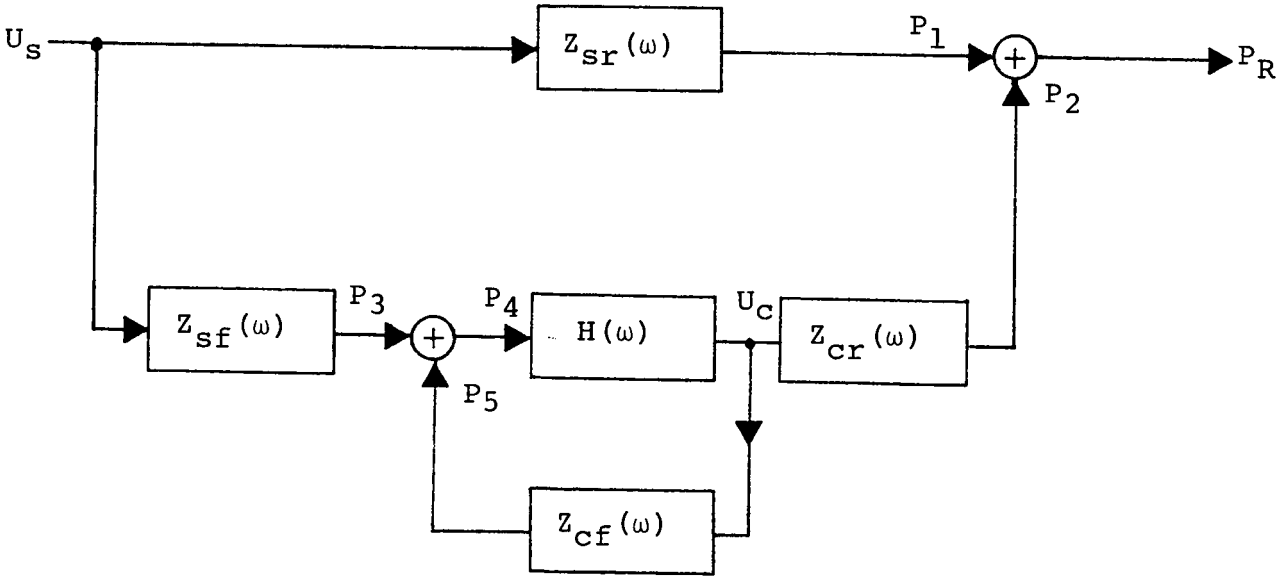

Figure 56: Acoustically Coupled System

receiver (field) point. In the absence of any other sources, p_r is given by

$$p_r = Z_{sr} u_s \quad , \tag{13}$$

where Z_{sr} is the transfer impedance between the points r and s. If we insert the cancellation source, the sound pressure at the receiver is the sum of the sound pressures from both sources:

$$p_r = Z_{sr} u_s + Z_{cr} u_c \quad , \tag{14}$$

where u_c is the surface velocity of the (small) cancellation source and Z_{cr} the transfer impedance between the points c and r.

The controller receives the signal from both the noise source and the cancellation source. The block diagram of the whole acoustically coupled system is shown in Figure 56. The system can be described by the following set of equations:

$$\left.\begin{aligned} p_r &= p_1 + p_2 \\ p_3 &= u_s Z_{sf} \\ p_4 &= p_3 + p_5 = p_3 + U_c Z_{cf} \\ U_c &= H\, p_4 \\ p_2 &= U_c Z_{cr} \\ p_1 &= u_s Z_{sr} \end{aligned}\right\} \quad . \tag{15}$$

A simple manipulation of Equation (15) results in obtaining the total transfer impedance Z_t between the source and the receiver:

$$\tilde{Z}_t = \frac{\tilde{p}_r}{\tilde{u}_s} = \tilde{Z}_{sr} + \frac{\tilde{Z}_{cf}\tilde{Z}_{cr}\tilde{H}}{1 - \tilde{Z}_{cf}\tilde{H}} \quad . \tag{16}$$

Equation (16) allows us to study the effect of the cancellation source, environment and the controller on the transmission of sound from the noise source into the field point. Theoretically, by a proper choice of $\tilde{Z}_{cf}$, $\tilde{Z}_{cr}$ and particularly $\tilde{H}$, any transmission can be achieved, as long as the system can be kept stable. Impedances $\tilde{Z}_{cf}$ and $\tilde{Z}_{cr}$ are given by the positions of the controlling microphone and source and can be considered fixed. Therefore, we will examine the effect of the controller transfer function $\tilde{H}$ on the sound pressure at the receiver point.

We solve Equation (16) for $\tilde{H}$:

$$\tilde{H} = \frac{\tilde{Z}_t - \tilde{Z}_{sr}}{\tilde{Z}_{sf}\tilde{Z}_{cr} - \tilde{Z}_{sr}\tilde{Z}_{cf} + \tilde{Z}_{cf}\tilde{Z}_t} \quad . \tag{17}$$

System stability. Before proceeding with the analysis of Equation (17), we will discuss the stability conditions. Any system is considered stable if its output remains bounded for a bounded input. The stability condition can be stated in different ways. The most common Nyquist formulation (Reference 7) requires studying the location of the poles and zeros of the open loop transfer function given in Equation (16) by the product $\tilde{Z}_{cf}\tilde{H}$. The transmission impedance will generally remain finite if the denominator of Equation (16) will not have zeros, causing poles of $\tilde{Z}_t$.

Because the purpose of this section is to analyze possible noise reduction schemes, we will not concentrate on the details of the stability analysis. Instead of the conventional representations of the functions in the s-plane, we will use the frequency representation by substituting $s = j\omega$, resulting in a straightforward understanding of the stability formulations. The transfer functions and gains are generally complex, expressed as

$$\left.\begin{aligned} \tilde{H}(\omega) &= H(\omega)e^{j\theta(\omega)} \\ \tilde{Z}_{cf}(\omega) &= Z_{cf}(\omega)e^{j\theta_{cf}(\omega)} \end{aligned}\right\} \quad . \tag{19}$$

For the system to be unstable, the denominator of Equation (16) must be zero, which requires that $\tilde{H}\,\tilde{Z}_{cf}$ be real and equal to one. Therefore, to keep the system stable,

$$\theta_{cf} + \theta \neq 2\pi n \qquad n = 0, \pm 1, \pm 2 \tag{20}$$

and

$$H\,Z_{cf} < 1 \quad . \tag{21}$$

If we define $\tilde{L} = \tilde{H}\,\tilde{Z}_{cf}$ and substitute for $\tilde{H}$ from Equation (17), we obtain

$$\tilde{L} = Le^{j\phi} = \frac{\tilde{Z}_{cf}\tilde{Z}_t - \tilde{Z}_{sr}\tilde{Z}_{cf}}{\tilde{Z}_{sf}\tilde{Z}_{cr} - \tilde{Z}_{sr}\tilde{Z}_{cf} + \tilde{Z}_{cf}\tilde{Z}_t} \quad . \tag{22}$$

To determine the stability, the magnitude and phase of $\tilde{L}$ have to be calculated. Executing a tedious algebra, we obtain

$$L = \left\{ [Z_{cf}^2 Z_t^2 + Z_{sr}^2 Z_{cf}^2 - 2Z_{sr}Z_{cf}^2 Z_t \cos(\theta_{sr} - \theta)] \; / \right.$$

$$[Z_{sf}^2 Z_{cr}^2 + Z_{sr}^2 Z_{cf}^2 + Z_{cf}^2 Z_t^2 + 2Z_{sf}Z_{cf}Z_{cr}C$$

$$\left. - 2Z_{sr}Z_{cf}^2 Z_t \cos(\theta_{sr} - \theta)] \right\}^{1/2} \qquad (23)$$

and

$$\phi = \tan^{-1} \left\{ [Z_{sf}Z_{cf}Z_{cr}Z_t \sin(\theta_{cf} + \theta - \theta_{sf} - \theta_{cr}) \right.$$

$$- Z_{sr}Z_{sf}Z_{cf}Z_{cr} \sin(\theta_{sr} + \theta_{cf} - \theta_{sf} - \theta_{cr})] \; /$$

$$[Z_{cf}^2 Z_t^2 + Z_{cf}^2 Z_{sr}^2 - 2Z_{sr}^2 Z_{cf}^2 Z_t \cos(\theta_{sr} - \theta)$$

$$\left. + Z_{sf}Z_{cf}Z_{cr}C] \right\} \quad , \qquad (24)$$

where

$$C = Z_t \cos(\theta_{sf} + \theta_{cr} - \theta_{cf} - \theta) - Z_{sr} \cos(\theta_{sf} + \theta_{cr} - \theta_{sr} - \theta_{cf}) \; . \qquad (25)$$

To simplify the notation, we will substitute

$$\left. \begin{aligned} \gamma &= \theta_{sf} + \theta_{cr} - \theta_{sr} - \theta_{cf} \\ \theta &= \theta_{sr} + \delta \end{aligned} \right\} \; . \qquad (26)$$

The instability can occur only if $\phi = 0$ [see Equation (20)] which is satisfied by the numerator of Equation (24) if

$$Z_t \sin(\gamma - \delta) - Z_{sr} \sin\gamma = 0 \quad . \qquad (27)$$

Also, the denominator of Equation (24) must not be zero when the numerator vanishes. To avoid this, for any value of $\cos\delta$,

$$C < - \frac{Z_{cf}}{Z_{sf}Z_{cr}} [Z_t^2 + Z_{sr}^2 - 2Z_{sr}Z_t \cos\delta] \quad . \qquad (28)$$

The angle γ depends upon the source and receiver positions and, therefore, we will search for an optimum value of δ to guarantee stability. The extreme values for $C = Z_t \cos(\gamma + \delta) - Z_{sr} \cos\delta$ are

$$\left.\begin{aligned} C_{max} &= Z_t + Z_{sr} \quad \text{if} \quad \gamma = \pi \quad \text{and} \quad \delta = \pi \\ \text{and} & \\ C_{min} &= -[Z_t + Z_{sr}] \quad \text{if} \quad \gamma = 0 \quad \text{and} \quad \delta = \pi \end{aligned}\right\} . \tag{29}$$

Because we want C to be a large negative number to satisfy Equation (28), the choice of $\delta = \pi$ is not optimal because, for $\gamma = \pi$, we would obtain C_{max}. Therefore, we will consider $\delta = 0$. The requirements for ϕ to vanish and cause instability will now be

$$\sin\gamma(Z_{sr} - Z_t) = 0 \tag{30}$$

and

$$C > -\frac{Z_{cf}}{Z_{sf}Z_{cr}}\left[Z_t^2 + Z_{sr}^2 - 2Z_{sr}Z_t\right] . \tag{31}$$

In this case, the extremes for C are obtained if Equation (30) is valid. Then,

$$\left.\begin{aligned} C_{min} &= Z_{sr} - Z_t \;,\; C_{max} = Z_t - Z_{sr} \quad \text{if} \quad Z_t > Z_{sr} \\ \text{and} & \\ C_{min} &= Z_t - Z_{sr} \;,\; C_{max} = Z_{sr} - Z_t \quad \text{if} \quad Z_t < Z_{sr} \end{aligned}\right\} . \tag{32}$$

The examination of Equation (25) reveals that any value $\delta > 0$ will increase the range $C_{max} - C_{min}$ and therefore, $\delta = 0$ represents an optimum value.

Let us consider now $Z_t > Z_{sr}$. Inserting the extremes into Equation (31) results in

$$C_{max} = Z_t - Z_{sr} > -\frac{Z_{cf}}{Z_{sf}Z_{cr}}\left[Z_t^2 - Z_{sr}^2\right] \tag{33}$$

for $\delta = 0$, and

$$C_{min} = Z_{sr} - Z_t > -\frac{Z_{cf}}{Z_{sf}Z_{cr}}\left[Z_{sr}^2 - Z_t^2\right] \tag{34}$$

for $\delta = \pi$. Both preceding equations can be modified to

$$1 > -\frac{Z_{cf}}{Z_{sf}Z_{cr}}\left[Z_t - Z_{sr}\right] \tag{35}$$

and

$$1 < -\frac{Z_{cf}}{Z_{sf}Z_{cr}}\left[Z_{sr} - Z_t\right] . \tag{36}$$

Recalling our assumptions on ϕ, we conclude that Equation (35) is always valid, which implies that $\phi = 0$ for $\gamma = 0$, $\gamma = 0$ and $Z_t > Z_{sr}$. However, Equation (36) is invalid whenever

$$Z_t - Z_{sr} < \frac{Z_{sf}Z_{cr}}{Z_{cf}} \quad . \tag{37}$$

Thus, when $\delta = 0$, $\gamma = \pi$ and $Z_t > Z_{sr}$, $\phi = \pi$ as long as Equation (37) is valid.

If we consider $Z_{sr} < Z_t$, the extreme values of Equation (32) can be inserted into Equation (31) yielding

$$C_{max} \rightarrow 1 > -\frac{Z_{cf}}{Z_{sf}Z_{cr}} [Z_{sr} - Z_t] \tag{38}$$

when $\gamma = \pi$, and

$$C_{min} \rightarrow 1 > -\frac{Z_{cf}}{Z_{sf}Z_{cr}} [Z_t - Z_{sr}] \tag{39}$$

when $\gamma = 0$. Equation (38) is always valid and therefore, $\phi = 0$ when $\gamma = \pi$. Also, Equation (39) is invalid whenever

$$Z_{sr} - Z_t < \frac{Z_{sf}Z_{cr}}{Z_{cf}} \quad . \tag{40}$$

Thus, when $\delta = 0$, $\gamma = 0$ and $Z_t < Z_{sr}$, $\phi = \pi$ if Equation (40) is valid.

In summary, $\phi = 0$ only if:

(a) $Z_t > Z_{sr}$ and $\gamma = 0$

(b) $Z_t > Z_{sr}$ and $\gamma = \pi$ and $Z_t - Z_{sr} > \frac{Z_{sf}Z_{cr}}{Z_{cf}}$

(c) $Z_t < Z_{sr}$ and $\gamma = \pi$

(d) $Z_t < Z_{sr}$ and $\gamma = 0$ and $Z_{sr} - Z_t > \frac{Z_{sf}Z_{cr}}{Z_{cf}}$

The stability condition requires $L < 1$. Using Equation (23), we find that in Case (a), L is always less than unity since $Z_t - Z_{sr}$ is positive.

In Case (b), L can be greater than unity only if

$$Z_t - Z_{sr} > \frac{Z_{sf}Z_{cr}}{Z_{cf}} \quad .$$

Cases (c) and (d) yield similar results. Therefore, if H is given by Equation (17), the system will be stable unless, at some point,

$$\left.\begin{array}{l} Z_t > Z_{sr}\,,\ \gamma = \pi \ \text{ and } \ Z_{cf} > \dfrac{Z_{sf}Z_{cr}}{Z_{sr} - Z_t} \\ \text{or} \\ Z_t < Z_{sr}\,,\ \gamma = 0 \ \text{ and } \ Z_{cf} > \dfrac{Z_{sf}Z_{cr}}{Z_t - Z_{sr}} \end{array}\right\} \quad . \tag{41}$$

To achieve a stable system, we must secure that Equation (41) is never valid. This can be accomplished by restricting Z_t by the condition

$$Z_{sr} - \frac{Z_{sf}Z_{cr}}{2Z_{cf}} < Z_t < \frac{Z_{sf}Z_{cr}}{2Z_{cf}} + Z_{sr} \quad . \tag{42}$$

The magnitude and phase of $\tilde{H} = He^{j\theta}$ are given by

$$H(\omega) = \Big\{ [Z_t^2 + Z_{sr}^2 - 2Z_{sr}Z_t] \Big/ [Z_{sf}^2 Z_{cr}^2 + Z_{cf}^2 (Z_t^2 + Z_{sr}^2 - 2Z_{sr}Z_t) + 2Z_{sf}Z_{cf}Z_{cr}\cos\gamma(Z_t - Z_{sr})] \Big\}^{1/2} \tag{43}$$

and

$$\theta(\omega) = \tan^{-1} \Big\{ [Z_{sf}Z_{cr}\sin(\theta_{sr} - \theta_{sf} - \theta_{cr})(Z_t - Z_{sr}) + 2Z_{sr}Z_{cf}Z_t\sin\theta_{cf} - Z_{cf}\sin\theta_{cf}(Z_t^2 + Z_{sr}^2)] \Big/ [Z_{sf}Z_{cf}\cos(\theta_{sr} - \theta_{sf} - \theta_{cr})(Z_t - Z_{sr}) - 2Z_{sr}Z_{cf}Z_t\cos\theta_{cf} + Z_{cf}\cos\theta_{cf}(Z_t^2 + Z_{sr}^2)] \Big\} \quad . \tag{44}$$

Cancellation condition. Equations (16) - (26) have general validity because any value of Z_t can be considered. Our main interest is in the cancellation of the sound field at the receiver point r. This can be determined by setting $Z_t = 0$. From Equation (17),

$$\tilde{H} = \frac{\tilde{Z}_{sr}}{\tilde{Z}_{sr}\tilde{Z}_{cf} - \tilde{Z}_{sf}\tilde{Z}_{cr}} \quad . \tag{46}$$

Similarly, Equations (23) and (24) simplify to

$$L = \left[\frac{Z_{sr}^2 Z_{cf}^2}{Z_{sf}^2 Z_{cr}^2 + Z_{sr}^2 Z_{cf}^2 - 2Z_{sr}Z_{cf}Z_{cr}Z_{sr}\cos\gamma} \right]^{1/2} \tag{47}$$

and

$$\phi = \tan^{-1}\left[\frac{- Z_{sr}Z_{sf}Z_{cf}Z_{cr}\sin\gamma}{Z_{cf}^2 Z_{cr}^2 - Z_{sf}Z_{cf}Z_{cr}Z_{sr}\cos\gamma} \right] \quad . \tag{48}$$

To maintain the stability $\phi \neq 0$ so that it follows from the preceding equation that neither of the transfer impedances should be zero or

$$\sin\gamma \neq 0 \quad . \tag{49}$$

The consideration similar to formulation of Equation (28) requires that, to avoid the possibility of ϕ to vanish,

$$Z_{sf}Z_{cr} < Z_{cf}Z_{cr} \quad . \tag{50}$$

After modifying Equation (23) for $Z_t = 0$, we obtain, requiring that $L < 1$,

$$\cos\gamma < \frac{Z_{sf}Z_{cr}}{2Z_{sr}Z_{cf}} \quad . \tag{51}$$

Equation (42) has a general validity for any transfer impedance Z_t. Therefore, for $Z_t = 0$, the stability condition is given by

$$Z_{sr} - \frac{Z_{sf}Z_{cr}}{2Z_{cf}} < 0 < \frac{Z_{sf}Z_{cr}}{2Z_{cf}} + Z_{sr} \quad . \tag{52}$$

The transfer function $\tilde{Z}_{sr}$ can be obtained from Equation (7) substituting for $Q_s = A_s u_s$ so that if the receiver point coordinates are $r \equiv (x,y,z)$ and the noise source is at $r_o \equiv (x_o,y_o,z_o)$. To remove the effects of the source areas, we will define Z_{sr} as

$$Z_{sr} = \frac{p_r}{Q_s} = \frac{j\omega\xi}{V} \sum_N \frac{\psi_N(r)\psi_N(r_o)}{\Lambda_N(K_N^2 - k^2)} \quad . \tag{53}$$

The other impedances will be given by similar expressions, substituting for the feedback microphone position $r_f \equiv (x_f,y_f,z_f)$ and the controller source position $r_c \equiv (x_c,y_c,z_c)$.

Using Equation (16), we will calculate the transmission impedance between the noise source and the receiving point.

$$Z_t = \frac{j\omega\rho}{V} \sum_N \frac{\psi_N(r)[\psi_N(r_o) + K\psi_N(r_c)]}{\Lambda_N(K_N^2 - k^2)} \quad , \tag{54}$$

where

$$\tilde{K} = \frac{\tilde{Z}_{sf}\tilde{H}}{1 - \tilde{Z}_{cf}\tilde{H}} \tag{55}$$

and

$$Z_{sf} = \frac{j\omega\rho}{V} \sum_N \frac{\psi_N(r_s)\psi_N(r_f)}{\Lambda_N(K_N^2 - k^2)} \quad . \tag{56}$$

The impedance Z_{cf} will be given by an expression similar to Equation (56), using r_c and r_f.

We can see from Equation (54) that the expression for the transmission impedance Z_t is similar to Equation (53) and that the change introduced by the feedback channel consists of replacing the eigenfunctions $\psi_N(r_o)$ with a more complex effective eigenfunction $\psi_N(r_o) + K\psi_N(r_c)$.

The effect of the feedback on the spatial response is determined for a given r_c and r_f by the factor K. If, for instance, H becomes very small, K will also be small, and in Equation (54), $\psi_N(r_o)$ will become dominant over $K\psi_N(r_c)$ and Z_t will not differ too much from Z_{sr}. On the other hand, a strong feedback with H very large can result in the second term in Equation (54) to be dominant over $\psi_N(r_o)$.

The aforementioned considerations on the effect of various terms have to be done in context with the magnitudes of the impedance terms, which will have maxima at the modal frequencies. The effect of damping which modifies the denominator of Equation (56) can be quite significant.

The stability of the system is determined entirely by the expression for K. We will solve Equation (55) for $\tilde{H}$ to determine the possible values of K for the system to remain stable.

$$\tilde{H} = \frac{\tilde{K}}{\tilde{Z}_{sf} + \tilde{K}\tilde{Z}_{cf}} \quad . \tag{57}$$

As before, in Equation (22), we will calculate $\tilde{L} = \tilde{H}\tilde{Z}_{cf}$ and substituting for K, we find

$$\tilde{L} = \frac{1}{1 + \frac{\tilde{Z}_{cf}}{\tilde{Z}_{cf}\tilde{K}}} = Le^{j\phi} \quad . \tag{58}$$

Equation (58) is analogous to Equation (22) except for expressing L in terms of K rather than of Z_t. The magnitude of L can be obtained as

$$L = \left[1 + \frac{Z_{sf}^2}{Z_{cf}^2 K^2} + \frac{2Z_{sf}}{Z_{cf}K} \cos(\theta_{sf} - \theta_{cf} - \zeta) \right]^{-1/2} \tag{59}$$

where ζ is the phase angle of K defined from

$$\tilde{K} = Ke^{j\zeta} \quad . \tag{60}$$

The phase of L is

$$\phi = \tan^{-1} \left[\frac{-\frac{Z_{sf}}{Z_{cf}K} \sin(\theta_{sf} - \theta_{cf} - \zeta)}{1 + \frac{Z_{sf}}{Z_{cf}K} \cos(\theta_{sf} - \theta_{cf} - \zeta)} \right] \quad . \tag{61}$$

To determine the system stability, we examine Equation (61) for possible values of $\phi = 0 \pm 2\pi n$. This would occur if

$$\zeta = \theta_{sf} - \theta_{cf} \pm 2\pi n \quad . \tag{62}$$

We can also obtain $\phi = 0$ for

$$\zeta = \theta_2 - \theta_3 \pm (2n - 1)\pi \quad \text{and} \quad \frac{G_{sf}}{G_{cf}K} < 1 \quad . \tag{63}$$

If Equation (62) is satisfied, L is always less than unity and, therefore, stability is assured. In the second case, L is always greater than unity and, therefore, we can obtain any value of K by choosing H as long as

$$\left.\begin{aligned} &\zeta \neq \theta_2 - \theta_3 \pm (2n-1)\pi \\ &\text{or} \\ &K < \frac{G_{sf}}{G_{cf}} \end{aligned}\right\} \quad . \tag{64}$$

Therefore, if, for instance, θ_3 could be restricted for all frequencies so that ζ would always satisfy Equation (64), we would choose any value of K and thus achieve any desired degree of regulation.

The condition for a complete sound cancellation in point $r \equiv (x,y,z)$ can be obtained by substituting $Z_t = 0$ in Equation (54) so that

$$\zeta = \theta_{sf} - \theta_{cf} \pm 2n\pi \quad . \tag{62}$$

If

$$\zeta = \theta_{sf} - \theta_{cf} \pm (2n-1)\pi \quad \text{and} \quad \frac{Z_{sf}}{Z_{cf}K} = 1 \quad , \tag{65}$$

the limit of the argument of $\tan^{-1}$ in Equation (61) will result in a nonzero value, so that $\phi \neq 0$.

The other stability condition requires that $L < 1$ if $\phi = 0$, which is satisfied for $\cos(\theta_{sf} - \theta_{cf} - \zeta) = 1$ for any value of $Z_{sf}/Z_{cf}K$.

The conditions for a complete cancellation of sound in point $r \equiv (x,y,z)$ can be formulated by substituting $Z_t = 0$ in Equation (54) so that

$$\sum_N \frac{\psi_N(r)[\psi_N(r_o) + K\psi_N(r_c)]}{\Lambda_N(K_N^2 - k^2)} = 0 \quad . \tag{66}$$

Solving for K results in

$$K(\omega) = -\frac{G_{sr}(\omega)}{G_{cr}(\omega)} \quad . \tag{67}$$

The feedback function $\tilde{H}$ will be the same as Equation (46),

$$\tilde{H} = \frac{\tilde{Z}_{sr}}{\tilde{Z}_{sr}\tilde{Z}_{cf} - \tilde{Z}_{sf}\tilde{Z}_{cr}} \quad . \tag{68}$$

The actual choice and usability of $\tilde{H}$ is generally limited by the stability conditions.

Adaptive systems. As discussed earlier in this report, the actual physical systems consist of adaptive filters which adjust the controller gain $\tilde{H}(\omega)$ for a minimum sound pressure at the receiver point. The system is more complicated than the scheme presented in Figure 55. To remove possible instabilities, the feedback microphone is removed and the feeding of the filter is arranged from a point unaffected by the radiation from the cancellation source.

The above analysis resulted in stating the conditions to achieve a complete cancellation in a spatial point anywhere in the enclosure. To achieve this goal, we must know the transfer functions between the points of the source and the microphone locations. These can be obtained from measurements to obtain $H(\omega)$. Such a procedure is not too practical, particularly in view of the possible time changes of the transfer functions due to the temperature dependent changes of the sound speed. A system using adaptive filtering overcomes this problem, but requires placing a sensing microphone in the area of desired cancellation.

The mathematical technique developed in this section can be modified to obtain a zero sound pressure by controlling the field at a point different than zero. Such an arrangement requires modifying the value of $H(\omega)$ by a precalculated function and, therefore, requires fairly detailed knowledge of the sound field descriptors, such as transfer functions, and, therefore, the problems of the temporal changes mentioned before cannot be avoided.

Effect of noise source distribution. The preceding analysis assumed that the noise source was small and located in the point $r_o(x_o,y_o,z_o)$. In most real situations, the noise sources are distributed. The examination of Equation (10) shows that the point source eigenfunction $\psi_N(r_o)$ of Equation (7) is equal to the surface integral of u_n over the source area. This means that Equation (66) has to be modified accordingly. Although we cannot determine the transfer function between the noise source and other points of interest, there will be a certain value of $K(\omega)$ to satisfy Equation (66) and achieve the cancellation. This is exactly what a canceller based on an adaptive process will do, if we can keep the system stable.

Multiple Feedback Systems

As shown in the previous section, by means of a suitable feedback arrangement, it is possible to control the sound pressure at a point. In most applications, the interest is in controlling sufficiently large regions or in achieving an overall reduction of the sound levels within the enclosure.

Size of the controlled region. Let us first analyze the size of the controlled region. The sound field in an enclosure can be represented by the modes, determined by the boundary conditions. Because of the mode interference, the spatial distribution of the sound pressure is nonuniform. If the analytical expression for the eigenfunctions is known, the sound field becomes deterministic and the sound pressure around a minimum can be calculated, provided the positions of the sources are known. For a point source, Equation (7) can be utilized, while a continuous source distribution over the boundaries requires application of Equation (10):

$$p(x,y,z) = j\frac{\omega\rho}{V}\sum_N \frac{\psi_N(x,y,z)}{\Lambda_N(K_N^2 - k^2)} \iint_S u_n(x_o,y_o,z_o)\psi_N(x_o,y_o,z_o)dS_o \,. \tag{69}$$

The analysis of the above equation reveals that, for a given frequency, the integral representing the source term represents a numerical value as well as the denominator, and that the spatial distribution of the sound pressure depends only on the summation over the eigenfunctions $\psi_N(x,y,z)$ of the receiver point position.

In most situations of practical interest, the analytical form of the eigenfunctions is not known. However, we can benefit from the statistical approach to the sound properties in enclosures which can, for our purpose, be summarized in the following way:

1. The spatial distribution of the minima and maxima is irregular and depends very little on damping (as opposed to frequency distributions).

2. Above a certain frequency, $f_c \simeq 2000\sqrt{T/V}$, where T is the reverberation time, and V is the volume in m^3, the spatial sound pressure distributions can be described by statistical laws.

3. The average distance of two adjacent maxima or minima above the critical frequency f_c is approximately 0.7λ.

4. At the frequency region below f_c, the pressure distributions have to be either calculated exactly from the known eigenfunctions or boundary conditions, or adequate sound pressure statistics have to be determined either experimentally or by approximating the eigenfunctions.

5. Above the critical frequency, the spatial distribution of p^2 normalized to the spatial average $\overline{p^2}$ is exponential with the probability density function

$$f(p^2/\overline{p^2}) = e^{-p^2/\overline{p^2}} \tag{70}$$

and the distribution function

$$F(p^2/\overline{p^2}) = 1 - e^{-p^2/\overline{p^2}} \quad . \tag{71}$$

The knowledge of the spatial distributions of p^2 can be used to develop an approximate statistical estimate of the size of the minima region. Let us assume a regular distribution of the maxima and minima so that, in a cube with the side equal to the average distance of two maxima 0.7λ, the pressure distribution in all points of the volume $V = (0.7\lambda)^3$ will be exponential. The positioning of the cube is such that the pressure maximum will be on its surface, and the pressure minimum will be in the center of the cube. The magnitude of the volume in which the points have p^2 values between zero and certain upper limits can be determined from the probability function $F(p^2/\overline{p^2})$. All these points would be inside the sphere of volume V_o centered at the cube center. It can be determined from Equation (71) that, for $p^2/\overline{p^2}$, the value of the distribution function is $F = 0.63$, which means that the points with $p^2/\overline{p^2} \leq 1$ will occupy $0.63\ V$. Therefore, the points with the sound pressure value $p^2/\overline{p^2} < a$ will occupy the volume

$$V_o = F(a)(0.70\lambda)^3 \quad . \tag{72}$$

If, for instance, we choose $a = 0.1$ which corresponds to sound pressure level values lower by at least 10 dB than the sound pressure level corresponding to p^2, the points will occupy volume V_o,

$$V_o = F(0.1)(0.7\lambda)^3 = 0.0326\ \lambda^3$$

and the corresponding sphere radius is

$$r_o = \sqrt[3]{\frac{3}{4\pi}\ V_o} = 0.198\ \lambda \quad .$$

The magnitude of the volume V_o, as obtained from Equation (72), has to be understood in the statistical sense. The presented example shows that the sphere radius depends linearly on the wavelength, which makes the low sound pressure region decrease with increasing frequency, as it corresponds to decreasing distances between pressure maxima or minima.

Global cancellation with one system. An overall cancellation inside the enclosure at one frequency or over a broad frequency range would require implementing one or more of the following steps:

1. An overall reduction of the sound field can be achieved by reducing the power injected into the enclosure. If we assume that the wall vibrations are unaffected by the enclosure response, then the radiated power can be reduced by decreasing the radiation impedance of the radiating wall area. Any additional sound radiation inside the enclosure

will affect the wall radiation. However, a randomly positioned source at a large distance having a low spatial correlation with the wall points is not going to affect the total power radiation as, in some areas, the power will be increased and, in other areas, decreased.

2. The amplitude of the modes of interest are reduced by increasing their damping either passively or by affecting the modal coefficients by the cancellation source. This procedure would require first to identify the modes by finding their characteristic vectors and then by solving the appropriate set of equations to determine the position and the volume velocity of the cancellation source. This step has to be studied further. It is unlikely that a single cancellation source position would be sufficient to radiate adequate power to achieve this goal.

Use of multiple source-microphone configurations. A single system with one feedback loop can force a pressure minimum at a spatial point. The conducted experiments have shown that moving the zero microphone can relocate the pressure minimum by changing the standing wave pattern in the enclosure without any appreciable effect on the overall cancellation. There are situations where this solution is adequate, particularly at the low frequencies where the low pressure region is relatively high.

A multiple feedback system consisting of two cancellation sources will not result in sound pressure reduction over a larger space. The transfer impedance function as defined by Equation (16) will consist of the Z_{sr} term plus another term containing both transmission impedances between the field point and the two cancellation sources. However, the spatial range of cancellation will be given by Equation (66) with a different K. Generally, this route does not lead to adjusting the bracket in Equation (66) to zero or a low value for all frequencies.

To achieve a large area cancellation requires a broad study of the modal structure of the field to adjust the radiation of the cancellation source to reduce the amplitude of many modes. Evidently, this can be achieved by approximations only.

Another situation of interest may be the sound field reduction in relatively small areas. A system consisting of several microphones with the sum of the output voltage representing the error signal of the canceller may be a good way to start the experiments. It can be expected that, by imposing low values at relatively close points, an overall region of low sound pressure levels can be achieved. However, the presence of the microphones may limit the applications.

1. Report No.	2. Government Accession No.	3. Recipient's Catalog No.
NASA CR-172386		

4. Title and Subtitle	5. Report Date
ACTIVE ATTENUATION OF PROPELLER BLADE PASSAGE NOISE	July 1984
	6. Performing Organization Code

7. Author(s)	8. Performing Organization Report No.
J. M. Zalas and J. Tichy	
	10. Work Unit No.

9. Performing Organization Name and Address	11. Contract or Grant No.
Lord Corporation P. O. Box 10038 Erie, PA 16514-0038	NAS1 - 17231
	13. Type of Report and Period Covered
12. Sponsoring Agency Name and Address	Contractor Report
	14. Sponsoring Agency Code

15. Supplementary Notes

Langley Technical Monitor: Tony Parrott

16. Abstract

Acoustic measurements are presented to show that active cancellation can be used to achieve significant reduction of blade passage noise in a turboprop cabin. Simultaneous suppression of all blade passage frequencies was attained. The spatial volume over which cancellation occurred, however, is limited. Acoustic intensity maps are presented to show that the acoustic input to the fuselage was sufficiently non-localized so as to require more judicious selection of cancellation speaker location.

17. Key Words (Suggested by Author(s))	18. Distribution Statement
Active Noise Control Turboprop Noise Acoustic Intensity	Unclassified - Unlimited

19. Security Classif. (of this report)	20. Security Classif. (of this page)	21. No. of Pages	22. Price
Unclassified	Unclassified	81	

For sale by the National Technical Information Service, Springfield, Virginia 22161